Synthesis and Electrochemical Studies of Titanium Dioxide Based Nanostructured Catalysts for Environmental Applications

By

Xin Chang

A thesis submitted in conformity with the requirements for the degree of

Doctor of Philosophy in Chemistry and Materials Science

Faculty of Science and Environmental Studies

Department of Chemistry

Lakehead University

Abstract

Nanomaterials are playing an increasingly important role toward addressing emerging environmental challenges. Heterogeneous catalysis is the best option available for the elimination of environmentally incompatible compounds that reside within contaminated water sources. Among all investigated nanomaterials, TiO_2 has proven itself as optimal for various applications such as photocatalysis, electrochromic devices, dye sensitized solar cells, hydrogen production, and sensing. TiO_2 is impressive due to its low cost, non-toxicity, chemical inertness, and high efficiency. In spite of having all these excellent properties, the efficient utilization of TiO_2 for various applications is limited by its inability to absorb visible light. Due to large band gap, only UV light may be absorbed by TiO_2, thus making it minimally efficient when exposed to sunlight, which contains only about 4% in the UV spectrum. An enormous amount of research has been focused on decreasing the band gap of TiO_2 in order to increase its efficiency under sunlight. The present research is focused on the development of new techniques to increase the conductivity of TiO_2 nanomaterials as well as to decrease its band gap to make it an efficient photoelectrocatalyst.

During my PhD study, TiO_2 nanostructured materials were fabricated using a facile anodization method. TiO_2 nanotubes were synthesized by employing DMSO + 2% HF as an electrolyte. An electrochemical (EC) reduction method was employed to reduce the TiO_2 nanotubes, which were subsequently employed as a novel and efficient catalyst for the oxidation of salicylic acid (SA) for the first time. The effects of the cathodic current and reduction time on the electrocatalytic activity of the reduced TiO_2 were investigated, and the results revealed that the optimal electrochemical treatment conditions were -5 mA cm^{-2} for 10 min. The electrochemically treated TiO_2 nanotubes possessed a much higher overpotential for oxygen evolution than a commercial Pt electrode, and exhibited a high electrocatalytic activity in the oxidation of SA. When compared with a Pt electrode, the electrochemically treated TiO_2 nanotubes exhibited ca. 6 times higher activity toward the oxidation of SA. The high electrocatalytic activity and stability of the treated TiO_2 nanotubes enabled by the facile electrochemical reduction may be attributed to the decrease of Ti(IV), the increase of Ti(II) and Ti(III), and the increase of oxygen vacancies, as well as a significant improvement in the donor density.

The effects of TiO_2 nanotube length on its activity in the electrocatalytic oxidation of lignin were also studied. The TiO_2 nanotubes were grown in a DMSO and 2% HF solution, where a

constant potential was applied for different time intervals. A very uniform increase in the lengths of the nanotubes was observed when the anodization time interval was increased. The increase in the nanotube length had a very significant effect on the electrochemical oxidation of lignin. The rate of lignin oxidation continued to increase until an optimal length was achieved. Impedance studies revealed that there was an optimal length of nanotube that demonstrated the least charge transfer resistance; if longer nanotubes were grown a higher resistant was obtained. The fabricated electrode also showed a very high level of stability.

Nanoporous TiO_2 was directly grown employing a three-step electrochemical anodization process in ethylene glycol + 0.3 wt% NH_4F + 2 wt% H_2O. A significant enhancement in the photocatalytic activity of nanoporous TiO_2 was achieved via a facile electrochemical reduction. Subsequently, the treated nanoporous TiO_2 was investigated as a catalyst for photoelectrochemical water splitting and the photoelectrochemical oxidation of Rhodamine B (Rh B), which is an organic dye pollutant. Due to the presence of higher degree of ordering and a larger surface area, the nanoporous TiO_2 electrode showed a much higher photocurrent under UV light in contrast to TiO_2 nanotubes. The photocurrent of the as-prepared nanoporous TiO_2 was 7.70 mA cm^{-2} at 1.5 V, and it was significantly increased to 46.23 mA cm^{-2} following additional electrochemical treatment. The electron donor density of the electrochemically treated nanoporous TiO_2 was four orders of magnitude higher than that of the untreated nanoporous TiO_2. The treated nanoporous TiO_2 also demonstrated six times more rapid photoelectrochemical degradation of Rh B, as well as remarkable stability.

The high surface area of electrochemically reduced nanoporous TiO_2 may be used as a substrate to synthesize a Pt and Pb co-deposited bifunctional electrode (PtPb/EC-TiO_2) to enable photo-assisted methanol oxidation in a direct methanol fuel cell (DMFC). Photochemical deposition was employed to introduce Pt and Pb onto the nanoporous TiO_2 surface at an equimolar ratio. Mott-Shottky plots and Nyquist plots revealed that the PtPb/EC-TiO_2 bifunctional electrode showed a higher electron donor density and a much lower charge transfer resistance as compared to the Pt/EC-TiO_2, whether in the dark or under solar light irradiation. PtPb/EC-TiO_2 exhibited a further enhancement in activity when solar light irradiation is applied to the electrode thus making it an efficient bifunctional electrode.

The simplicity and efficacy of the novel electrochemical reduction approach developed in this study facilitates the integration of TiO_2 nanostructured materials into the design of high-performance energy harvesting and water purification technologies.

This thesis is dedicated to my loving parents *Yongqing Chang* and *Qifeng Xu* for years of unconditional love, support and encouragement.

Acknowledgements

First and foremost I want to give my sincere gratitude to my supervisor Dr. Aicheng Chen for his guidance, help, efforts and precious time he has put on me. He has enlightened me through his immense knowledge in electrochemistry and materials science and developed my interest in related research work. I highly appreciate all his contributions ideas, and funding to make my Ph.D. experience as fruitful and smooth as possible. Besides my supervisor, I would like to thank the rest of my thesis committee: Dr. Baoqiang Liao and Dr. Mark Gallagher for their encouragement and insightful comments. Thanks also go to Dr. Robert Mawhinney, the coordinator of PhD Chemistry and Materials Science program for his great help.

I would also like to extend my thanks to all the current and former members of Dr. Aicheng Chen's research group, Dr. Guosheng Wu, Dr. Sapanbir Thind, Dr. Min Tian, Jiali Wen, Zhaoyang Zhang, Dr. Guohong Xie, Shuai Chen, Xiao Qu, Dr. Zhonggang Liu, Suresh Konda, Mona Amiri, Congmin Wang, Dr Maduraiveeran Govindhan for their friendship and collaborations. I also want to take this opportunity to thank both faculty and the staff members of Department of Chemistry, Instrument Lab and Graduate Studies for their support and encouragement.

My biggest thanks to my ever loving parents. They are the ones whose unconditional love and support kept me going during my Ph.D. There are no words that can truly express the level of gratitude and appreciation I have for them.

List of Figures

List of Tables

List of Abbreviations and Symbols

Ar	Argon
AOPs	Advanced oxidation processes
CA	Chronoamperometry
CB	Conduction band
CV	Cyclic Voltammetry
DMFC	Direct methanol fuel cell
DSSC	Dye sensitized solar cell
DMSO	Dimethyl sulfoxide
EC	Electrochemical
EDS	Energy-dispersive X-ray spectroscopy
EIS	Electrochemical impedance spectroscopy
E_g	Band gap
EPR	Electron paramagnetic resonance spectroscopy
LV	Linear voltammetry
N	Nitrogen
ORR	Oxygen reduction reaction
PEMFCs	Proton exchange membrane fuel cells
Rh B	Rhodamine B
SA	Salicylic acid
SEM	Scanning electron microscopy

T	Temperature
TEM	Transmission electron microscopy
TOC	Total organic carbon
UV	Ultraviolet
UV-Vis	Ultraviolet-Visible
VB	Valence band
XRD	X-ray diffraction spectroscopy
XPS	X-ray photoelectron spectroscopy

Table of Contents

Chapter 1: Introduction

Over the last few decades, researchers have become increasingly engrossed in the exploration of functional semiconductor based nanomaterials for environmental remediation and energy-related applications.[1] TiO_2 is unquestionably one of the most intensely studied semiconductors in materials science, due to its unique combination of outstanding properties, such as biological and chemical inertness, low cost, high efficiency, environmental tolerance, and high stability.[2] Further, TiO_2 nanomaterials may be fabricated with various morphologies and dimensions to obtain specific optical and electronic properties. Owing to this, TiO_2 is being extensively studied toward the development of high efficiency photocatalysts, hydrogen production, dye sensitized solar cells, and fuel cells. A brief description of nanomaterials and their importance in environmental and energy applications is provided in the following sections.

1.1 Development of nanotechnology and nanomaterials

In 1959, Nobel laureate Richard P. Feynman introduced the concept of nanotechnology during his lecture "There's Plenty of Room at the Bottom".[3] Since then, enormous efforts have been invested in the development of nanotechnology. In general, nanotechnology may be defined as the study, design, and fabrication of extremely small constituents of matter (at the atomic and/or molecular scale), with at least one characteristic dimension that is typically measured from 1 to 100 nm.[4] Materials at nanometric scales exhibit numerous advantageous properties: 1) provision of a large surface area to boost the reactions that take place at surfaces of the nanomaterials; 2) bringing about exceptional or novel size-dependent properties, such as enhanced mechanical strength and surface plasma resonance. For instance, the color of gold may be tuned to purple, pink, and even transparent by altering the dimensions of gold nanoparticles, from a few nanometers to a few tens of nanometers.[5] Generally, there are two methodologies by which nanoparticles may

be fabricated: 1) bottom-up, where atoms or molecules are assembled together to form nanoparticles, 2) top-down, in which bigger structures are dissociated into smaller nanoparticles while maintaining the original properties.[6] Among these two techniques, the bottom-up method is the most promising, and is garnering significant attention from the research community. Using this strategy, atoms or molecules may be arranged in various configurations to synthesize nanomaterials with different morphologies and new properties. Owing to this, nanomaterials offer many new possibilities spanning a wide variety of applications; thereby contributing to the potential resolution of many of the challenges that human society faces today.

Since the early 2000's, nanotechnology and nanomaterials based research and development have undergone tremendous exponential growth spanning medicine, healthcare, energy, electronics, textiles, etc.[7-9] For instance, nanotherapeutics is a state-of-the-art application of nanotechnology, which has become more realistic over the last few years. In 2010, the first clinical evidence of gene silencing was obtained by systemically-administered targeted nanoparticles, which delivered siRNA therapeutics.[10] Subsequently, increasing numbers of nanotherapeutic and nanodiagnostic platforms have been commercialized, or have progressed to clinical trials.[11]

It is well known that most disease processes occur at the molecular and cellular levels, which has led to challenges in viewing and understanding these processes precisely and in real time. Thanks to their small dimensions and size-dependent properties, nanoparticles have emerged as viable imaging agents for the non-invasive probing of such biological events. Many types of nanoparticles have been utilized for bioimaging, including metals (Au, Ag), metal oxide (Fe_3O_4), and semiconductor nanocrystals.[12-13] Biodegradable polymeric nanoparticles are also being studied for their utility in drug delivery. Once the drug molecule payloads of these nanoparticles have been successfully delivered they may be degraded in vivo for subsequent excretion.[14]

Nanomaterials are also gaining substantial attention in the form of nanofilms, as they may be endowed with unique attributes such as water repellency, anti-reflectivity, self-cleaning, ultraviolet or infrared-resistance, anti-fogging, anti-microbial, scratch resistance, or electric conductivity. Nanomaterials can also be used in the purification of water through their integration into membranes to filter and purify water.[15] Nanomaterials can play an important role in the development of electronic devices as well. For example, electrical conductivity might be significantly enhanced when the materials are formed as nanowires or nanotubes, which could likely reduce the power consumption, dimensions, or weight of the devices.[16] Meanwhile, nanomaterials may provide multiple advantages in energy conversion and storage applications, such as dye-sensitized and quantum dot-sensitized solar cells. This is because nanomaterials offer extensive surface areas, thus sufficient dye molecules and quantum dots may be adsorbed onto the materials, which further enhance optical absorption.[17-18]

1.2 Nanotechnology in environmental applications

Currently, rapid environmental deterioration and global warming constitute the most serious challenges that human civilization has yet had to face. With the rapid development of industrialization and population growth, the accumulation of myriad organic contaminants in natural water sources has become a critical issue worldwide.[19] This situation is exacerbated by the fact that most of refractory organic contaminants cannot be completely removed through conventional wastewater treatment technologies (physical, chemical, and biological methods), due to their complex structures and persistent character.[20] Therefore, enormous efforts have been devoted to the development of advanced oxidation processes (AOPs), which are proposed as the most promising alternative to address this issue.[21] AOPs (including Fenton's process[22-24], ozonation[25-26], sonolysis[27-28], photocatalysis[29-30], electrochemical oxidation[31-33], etc.) are based on

the generation of highly reactive free hydroxyl radicals, which are powerful oxidants that have the capacity to react with most of the organic compounds that are present in water.[34]

Nanomaterials play an important role in the development of AOPs to address various emerging environmental issues. Photochemical and electrochemical AOPs assisted by nanomaterials based catalysts have stimulated an increasing interest due to their unique advantages, such as mild operation conditions and no requirement for auxiliary chemicals.[35] Catalysts may generally be divided into two categories: 1) photocatalysts and 2) electrocatalysts. In photocatalysis, incident light energy is absorbed by the catalyst, which is then used to initiate a series of reactions. In electrocatalysis, the drive of the reaction to occur is generally provided by the applied bias.

During photocatalysis, when a material is irradiated with the appropriate energy, electrons are excited from the valence band to the conduction band, which leaves electron holes behind.[36] The excited electrons subsequently react with the O_2 molecules that are present in the water to produce $O_2^{\bullet-}$ species; the holes in valence band then react with H_2O molecules, which results in the formation of $OH^{\bullet}$ free radicals. These $O_2^{\bullet-}$ and $OH^{\bullet}$ species are highly oxidizing and react with organic pollutants reside in the water.[37] The mechanism of the photocatalyst may be given as:

$$\text{Photocatalyst} + h\nu \rightarrow \text{h}^+ + \text{e}-$$

$$O_2 + \text{e}- \rightarrow O_2^{\bullet-}$$

$$H_2O + \text{h}^+ \rightarrow H^+ + OH^{\bullet}$$

$$\text{Contaminant} + O_2^{\bullet-} \rightarrow \text{products}$$

$$\text{Contaminant} + OH^{\bullet} \rightarrow \text{products}$$
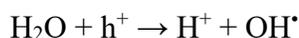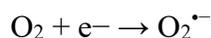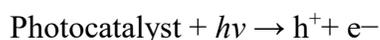
In recent years numerous semiconductor oxides have been explored for their utilization as photocatalysts. The prominent ones are TiO_2, WO_3, C_3N_4, CdS, SnO_2, SiO_2, ZrO_2, ZnO, Fe_2O_3, $SrTiO_3$, CeO_2, Sb_2O_4, and V_2O_5.[38-39] Among these materials, TiO_2 is the most optimal photocatalyst available due to its stability, low cost, and chemical inertness. The only limitation for the efficient use of TiO_2 lies in its relatively wide band gap (3.0 - 3.2 eV across all different crystal phase). This is because the optical absorption of TiO_2 resides only in the UV region of the solar spectrum. However, this region accounts for less than 5% of the overall solar energy. Hence, this problem necessitates resolution in order for TiO_2 to achieve efficient solar activity.[40]

The other primary concern in photocatalysis is electron-hole recombination, by which excited electrons fall back to the valence band to recombine with the holes, thereby significantly decreasing the activity of the catalyst. Thus, there is a need to improve the efficiency of the photocatalyst by increasing the absorption in the visible region of the spectra while decreasing the rate of electron-hole recombination.[41] Several methods, including doping, co-doping, and the decoration of TiO_2 nanomaterials with different metals and non-metals, have been explored by the research community. In my PhD study, a facile electrochemical reduction method was employed to electrochemically reduce tubular TiO_2 in order to achieve better catalytic activity in the dark, under UV light, and visible light.

Additionally, metal particles such as Pt, Au, Pd, etc., and metal oxides including IrO_2 and RuO_2, are considered to be efficient electrocatalysts in electrochemical AOPs.[42] However, the exorbitant cost and easy fouling of these metal catalysts are of significant concern insofar as their wide scale application at industrial scales, where very large electrodes are required. The activity of the electrocatalysts may be improved by various approaches, including the formation of bimetallic or trimetallic alloys, or deposited noble metal atoms on the surface. While depositing noble metal atoms on substrates with high surface areas, two benefits may arise. First, with

increased surface area, additional active sites are made available for reactions to occur, thus increasing the catalytic activity of the nanomaterials based electrocatalysts. Second, via the deposition of expensive noble metals on other nanomaterials, a lower volume of the noble metals are required; thus decreasing the overall cost of electrode fabrication.

Significant progress has been made in the development of new nanostructured materials toward the fabrication of ideal substrates to support the deposition of metal atoms. As mentioned previously, TiO_2 is a semiconductor oxide with very high resistance, thus it is not very conductive, which makes it an inefficient electrocatalyst. In my study, a very simple electrochemical method was used to increase the electrocatalytic properties of tubular nanostructured TiO_2. It was observed that with the electrochemical reduction, the electron donor density of the TiO_2 increased thousands times over than that of untreated TiO_2. In future these TiO_2 nanostructured materials might be employed as a substrate for the deposition of precious metal atoms for various green chemistry applications.

1.3 Noble metal atoms for fuel cell applications

Most of the energy presently used in the world is generated from the combustion of non-renewable sources such as coal, oil, natural gas, etc. Due to the rapidly increasing demand for energy worldwide, these non-renewable sources will inevitably be exhausted in the very near future. The extensive use of these resources is also significantly contributing to the rise of air pollution, and subsequently, global warming. Fuel cells operate in exactly the opposite manner from a typical coal based power plant, where the heat from burning fuel is used to mechanically generate electricity; however, in fuel cells energy is converted directly into electricity via an electrochemical reaction, which does not involve any mechanical conversion.[43]

It is not an exaggeration to propose that fuel cells may likely hold the key to resolving the future energy crisis. Much of the extensive research needed has been done over the last few of decades to develop highly efficient fuel cells. However, there still remain multiple limitations that prevent fuel cells from attaining widespread commercial application. Numerous metals, semiconductor oxides, and their combinations are under study by various research groups to find the optimal electrode material (e.g., Ni, Co, Pt, Pd, Ag, Fe, CuO, ZnO, ZrO_2, Al_2O_3, etc.).[44-45] Among these, Pt has proven itself as the best candidate; however, its high cost and propensity for getting poisoned are among the concerns that greatly hinder its extensive use.

The fouling of electrodes by fuels is also a very common phenomenon. Hydrogen, which typically does not lead to fouling, is a very impressive fuel option for fuel cell applications; however, it is expensive to produce and is even more difficult to store and transport safely. The most efficient types of fuel cells tend to operate at very high temperatures, which reduces their lifespan due to corrosion of the fuel cell components.[46] Optimal solutions for all of the above mentioned issues that fuel cells are facing may reside in the use of nanomaterials. Nanotechnologies can be used to solve these problems and numerous researchers have fabricated nanomaterials with different morphologies and compositions, which have assisted in making fuel cells less expensive, lighter, and more efficient.[47] Nanomaterials also provide extensive surface areas which hold a critical role in this process, as larger surface areas offer exponentially more active sites for chemical reactions to occur, thus more efficient fuel cells may be achieved. In this research work, nanoporous TiO_2 was employed as a substrate for the deposition of Pt and Pb nanoparticles. Nanoporous TiO_2 provided a very large surface area for the deposition of the metal nanoparticles. To reduce the quantity of expensive platinum and to minimize poisoning, lead was incorporated.

1.4 Dissertation, Rationale and Scope

The primary focus of this dissertation is to explore TiO_2 based nanomaterials for various environmental and energy applications, such as wastewater treatment and fuel cells. The primary research objectives are:

1.   To synthesize TiO_2 based nanomaterials via the anodization method using different electrolytes such as DMSO + HF and ethylene glycol + NH_4F.

2.   To design a novel electrochemical reduction approach to significantly enhance the photo and electrochemical properties of the TiO_2 nanostructured materials.

3.   To develop these highly active electrochemically reduced TiO_2 nanomaterials as novel electrocatalyst and photoelectrocatalyst for the oxidation of various organic pollutants such as Rh B (organic dye pollutant) and SA.

4.   To investigate the effect of the anodization time on the morphology and activity of TiO_2 nanomaterials.

5.   To explore TiO_2 nanomaterials as efficient substrates to form bifunctional electrode towards the development of solar-assisted fuel cells.

In the succeeding chapters, a detailed literature review that highlights recent advancements in the development of TiO_2 based nanomaterials is presented, followed by the details of the research conducted in this research work.

In Chapter 2, a thorough literature review is conducted in which various fabrication methods for the preparation of TiO_2 nanomaterials with different morphologies and dimensions are presented. Various 0, 1, 2, and 3 dimensional TiO_2 nanostructures are discussed along with their potential applications. In Chapter 3, different procedures that were employed in this research work to fabricate the nanomaterials are presented. Chapter 3 also discusses various characterization

techniques that were used to study the morphological, physical, and photoelectrochemical properties of the prepared TiO_2 nanomaterials. In Chapter 4, a novel electrochemical reduction method is presented that significantly enhanced the electrocatalytic activity of the TiO_2 nanotubes. The prepared materials were characterized by SEM, XRD, XPS, Cyclic voltammograms, Chronoamperometry and Mott-Schotty plots. The electrocatalytic degradation of SA was undertaken to evaluate the enhanced activity of the synthesized TiO_2 nanotubes.

Chapter 5 reports on the fabrication of TiO_2 nanotubes with various tube lengths and its effect on the electrochemical oxidation of lignin. The oxidation of lignin also exhibited a noticeable trend when TiO_2 nanotube electrodes with different tube lengths were used.

Chapter 6 elucidated the effects of electrochemical reduction toward increasing the photoelectrocatalytic activity of nanoporous TiO_2 electrodes. This increase in photocatalytic activity was studied under both UV and visible light irradiation. Mott-Schottky plots were employed to study the effects of electrochemical reduction on the electron donor density of the TiO_2 electrode. The photoelectrochemical degradation of Rh B was used to investigate the activity of the fabricated electrodes. Chapter 7 reports on the fabrication of nanoporous TiO_2 supported Pt and Pb electrodes for solar-assisted direct methanol fuel cells. A very facile photodeposition method is presented for the deposition of Pt and Pb onto the surface of nanoporous TiO_2 electrodes. The SEM images revealed that the Pt and Pb nanoparticles were very uniformly distributed on the surface of the TiO_2. A PtPb/EC-TiO_2 bifunctional electrode demonstrated much higher activity in contrast to Pt/TiO_2, which indicated that the addition of Pb to Pt had a synergistic electronic effect that resulted in an increase of activity.

References

(1)   Wu, P.; Hou, X.; Xu, J.-J.; Chen, H.-Y. *Chemical reviews* **2014**, *114,* 11027-11059.

(2)   Chen, X.; Liu, L.; Huang, F. *Chemical Society Reviews* **2015**, *44*, 1861-1885.

(3)   Feynman, R. P. *Engineering and science* **1960**, *23*, 22-36.

(4)   Daniel, M.-C.; Astruc, D. *Chemical reviews* **2004**, *104*, 293-346.

(5)   Ghosh, S. K.; Pal, T. *Chemical reviews* **2007**, *107*, 4797-4862.

(6)   Chen, X.; Mao, S. S. *Chem. Rev* **2007**, *107*, 2891-2959.

(7)   Hu, L.; Cui, Y. *Energy & Environmental Science* **2012**, *5*, 6423-6435.

(8)   Ong, C.; Goh, P.; Lau, W.; Misdan, N.; Ismail, A. *Desalination* **2016**, *393*, 2-15.

(9)   Pelgrift, R. Y.; Friedman, A. J. *Advanced drug delivery reviews* **2013**, *65*, 1803-1815.

(10)   Davis, M. E.; Zuckerman, J. E.; Choi, C. H. J.; Seligson, D.; Tolcher, A.; Alabi, C. A.; Yen, Y.; Heidel, J. D.; Ribas, A. *Nature* **2010**, *464*, 1067-1070.

(11)   Tabernero, J.; Shapiro, G. I.; LoRusso, P. M.; Cervantes, A.; Schwartz, G. K.; Weiss, G. J.; Paz-Ares, L.; Cho, D. C.; Infante, J. R.; Alsina, M. *Cancer discovery* **2013**, *3*, 406-417.

(12)   Selvan, S. T.; Tan, T. T. Y.; Yi, D. K.; Jana, N. R. *Langmuir* **2009**, *26*, 11631-11641.

(13)   Schladt, T. D.; Shukoor, M. I.; Schneider, K.; Tahir, M. N.; Natalio, F.; Ament, I.; Becker, J.; Jochum, F. D.; Weber, S.; Köhler, O. *Angewandte Chemie International Edition* **2010**, *49*, 3976-3980.

(14)   Liu, T.; Wang, C.; Gu, X.; Gong, H.; Cheng, L.; Shi, X.; Feng, L.; Sun, B.; Liu, Z. *Advanced Materials* **2014**, *26*, 3433-3440.

(15)   Goh, P.; Ng, B.; Lau, W.; Ismail, A. *Separation & Purification Reviews* **2015**, *44*, 216-249.

(16)   Barati, M.; Sadeghi, E. *Nanotechnology* **2001**, *12*, 277.

(17)   Zhang, L.; Cole, J. M. *ACS applied materials & interfaces* **2015**, *7*, 3427-3455.

(18)   Zhao, K.; Pan, Z.; Mora-Seró, I. n.; Cánovas, E.; Wang, H.; Song, Y.; Gong, X.; Wang, J.; Bonn, M.; Bisquert, J. *Journal of the American Chemical Society* **2015**, *137*, 5602-5609.

(19)   Alvarado, L.; Chen, A. *Electrochimica Acta* **2014**, *132*, 583-597.

(20)   Ramos, C.; García, A.; Diez, V. *Water research* **2014**, *67*, 203-215.

(21)   Wang, F.; Smith, D. W.; El-Din, M. G. *Journal of Environmental Engineering and Science* **2003**, *2*, 413-427.

(22)   Pignatello, J. J.; Oliveros, E.; MacKay, A. *Critical reviews in environmental science and technology* **2006**, *36*, 1-84.

(23)   Pera-Titus, M.; Garcıa-Molina, V.; Baños, M. A.; Giménez, J.; Esplugas, S. *Applied Catalysis B: Environmental* **2004**, *47*, 219-256.

(24)   Aplin, R.; Waite, T. *Water Science and Technology* **2000**, *42*, 345-354.

(25)   Ikehata, K.; Jodeiri Naghashkar, N.; Gamal El-Din, M. *Ozone: Science and Engineering* **2006**, *28*, 353-414.

(26)   Esplugas, S.; Bila, D. M.; Krause, L. G. T.; Dezotti, M. *Journal of Hazardous Materials* **2007**, *149*, 631-642.

(27)   Hung, H.-M.; Kang, J.-W.; Hoffmann, M. R. *Water environment research* **2002**, *74*, 545-556.

(28)   Destaillats, H.; Lesko, T. M.; Knowlton, M.; Wallace, H.; Hoffmann, M. R. *Industrial & engineering chemistry research* **2001**, *40*, 3855-3860.

(29)   Demeestere, K.; Dewulf, J.; Van Langenhove, H. *Critical Reviews in Environmental Science and Technology* **2007**, *37*, 489-538.

(30)   Hoffmann, M. R.; Martin, S. T.; Choi, W.; Bahnemann, D. W. *Chemical reviews* **1995**, *95*, 69-96.

(31)   Yang, S. Y.; Choo, Y. S.; Kim, S.; Lim, S. K.; Lee, J.; Park, H. *Applied Catalysis B: Environmental* **2012**, *111*, 317-325.

(32)   Park, H.; Bak, A.; Ahn, Y. Y.; Choi, J.; Hoffmannn, M. R. *Journal of hazardous materials* **2012**, *211*, 47-54.

(33)   Chang, X.; Thind, S. S.; Chen, A. *ACS Catalysis* **2014**, *4*, 2616-2622.

(34)   Liu, Z.-h.; Kanjo, Y.; Mizutani, S. *Science of the Total Environment* **2009**, *407*, 731-748.

(35)   Yang, Y.; Pignatello, J. J.; Ma, J.; Mitch, W. A. *Environmental science & technology* **2014**, *48*, 2344-2351.

(36)   Wang, D.; Li, R.; Zhu, J.; Shi, J.; Han, J.; Zong, X.; Li, C. *The Journal of Physical Chemistry C* **2012**, *116*, 5082-5089.

(37)   Tran, P. D.; Wong, L. H.; Barber, J.; Loo, J. S. *Energy & Environmental Science* **2012**, *5*, 5902-5918.

(38)   Zhang, J.; Wu, Y.; Xing, M.; Leghari, S. A. K.; Sajjad, S. *Energy & Environmental Science* **2010**, *3*, 715-726.

(39)   Xiang, Q.; Yu, J.; Jaroniec, M. *Chemical Society Reviews* **2012**, *41*, 782-796.

(40)   Chen, X.; Shen, S.; Guo, L.; Mao, S. S. *Chemical reviews* **2010**, *110*, 6503-6570.

(41)   Tian, J.; Zhao, Z.; Kumar, A.; Boughton, R. I.; Liu, H. *Chemical Society Reviews* **2014**, *43*, 6920-6937.

(42)   Ayati, A.; Ahmadpour, A.; Bamoharram, F. F.; Tanhaei, B.; Mänttäri, M.; Sillanpää, M. *Chemosphere* **2014**, *107*, 163-174.

(43)   Kraytsberg, A.; Ein-Eli, Y. *Energy & Fuels* **2014**, *28*, 7303-7330.

(44)   Chen, Z.; Higgins, D.; Yu, A.; Zhang, L.; Zhang, J. *Energy & Environmental Science* **2011**, *4*, 3167-3192.

(45)   Sun, C.; Hui, R.; Roller, J. *J Solid State Electrochem* **2009**, *14*, 1125-1144.

(46)   Fabbri, E.; Pergolesi, D.; Traversa, E. *Chemical Society Reviews* **2010**, *39*, 4355-4369.

(47)   Kamarudin, M.; Kamarudin, S. K.; Masdar, M.; Daud, W. R. W. *International Journal of Hydrogen Energy* **2013**, *38*, 9438-9453.

Chapter 2: Literature Review

2.1 Introduction

In 1972, Fujishima and Honda discovered the phenomenon of water splitting at a TiO_2 electrode under UV light irradiation.[1] Since then, tremendous effort have been devoted to the research of TiO_2 materials, which has led to a wide variety of prominent applications ranging from environmental remediation, to energy harvesting and storage.[2] During the last few decades, significant progress has been made in the area of synthesis and the exploration myriad types of nanostructured TiO_2 materials, due to the rapid development of nanoscience and nanotechnology.[3] TiO_2 based nanomaterials with precisely controlled dimensions and morphologies have no doubt become the most intensively studied semiconductor in materials science, owing to their superior properties, such as biological and chemical inertness, low cost, environmental compatibility, and high stability. However, TiO_2 is a wide-bandgap (3.0-3.2 eV) semiconductor in all its crystalline forms, with limited optical absorption in the UV region of the solar spectrum, which greatly hinders its widespread applications.[4] To address this issue, many approaches have been developed to fine tune the optical and electronic properties of TiO_2.[5] The following section will present a general review of the inherent properties of TiO_2, TiO_2 nanomaterials and synthesis approaches, the development of tubular TiO_2 nanomaterials, and a description of the efficient utilization of TiO_2 nanomaterials in potential environmental and energy applications.

2.2 Electronic and structural properties of TiO_2

2.2.1 Electronic properties

TiO_2 is a n-type semiconductor due to the presence of multiple Ti^{3+} centers and oxygen vacancies.[6] In TiO_2 materials, the valence band (VB) is formed by overlapping oxygen 2p orbitals,

while the conduction band (CB) is formed by 3d Ti orbitals. When TiO_2 absorbs sufficient energy, electrons are excited from the VB to the CB to provide excited electrons (e^-) in the VB and positive holes (h^+) in the CB. These e^- and h^+ may recombine or get trapped and react with O_2 or H_2O that are adsorbed on the surface. The overall efficiency of TiO_2 is primarily dependent on the competition between these processes.[7] As depicted in Figure 2.1, highly oxidizing species ($O_2^{\bullet-}$ and $OH^\bullet$) might be formed at CB and VB, respectively, and subsequently react with target compounds (typically organic pollutants).
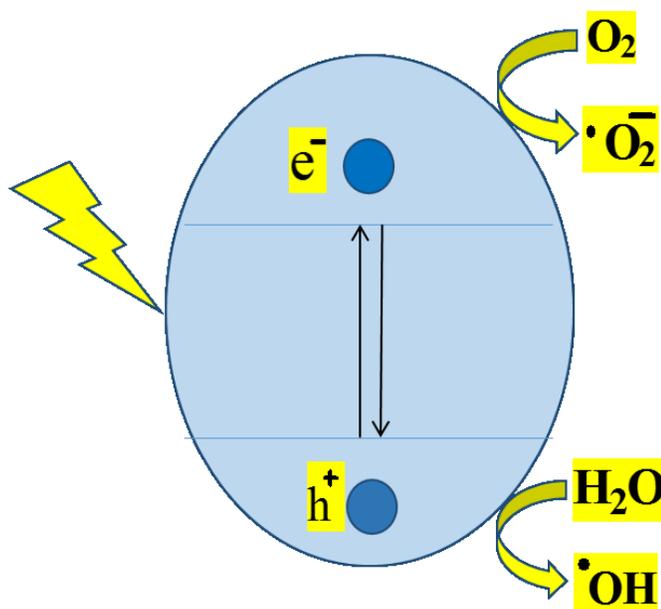
Figure 2.1. Schematic illustration for energetics and principal reaction mechanism of TiO_2 photocatalysis.

For most metal oxide semiconductors, VB is mainly composed of O 2p orbitals, such that they possess a similar VB energy (E_{VB}) potential edge.[8] However, in comparison with other metal oxide semiconductors, the proper CB position of TiO_2 makes it more suitable in achieving redox transformations for environmental applications.[9] The CB energy level (E_{CB}) of TiO_2 is -0.51 V at pH 7, which lies slightly above the reduction potential of oxygen ($E^o\, O_2/O_2^{\bullet-} = -0.33$ V); hence, it is beneficial for facile reactions. As relates to VB, the energy level (E_{VB}) of TiO_2 is 2.69 V, which

is more positive than the oxidation potentials of most organic and inorganic compounds. The highly oxidative h^+ not only reacts with water to form OH•, but also oxidizes a number of strongly adsorbed organic molecules directly at the surface.[10-11]

2.2.2 Structural properties

TiO_2 exists as three primary crystal phases: anatase, rutile, and brookite, as well as many other minor phases, such as monoclinic TiO_2 (B) and orthorhombic TiO_2 (R).[3,12-13] In comparison to anatase and brookite, rutile is considered as the most stable form of TiO_2 at high temperatures. However, anatase and brookite have the capacity to transform to the rutile phase through heating. In addition, it is possible to form pure anatase and rutile phases, while the pure brookite phase is more rare and difficult to synthesize without anatase or rutile. Therefore, brookite has not been well studied in terms of exploring its catalytic activity and other properties.[14-15]
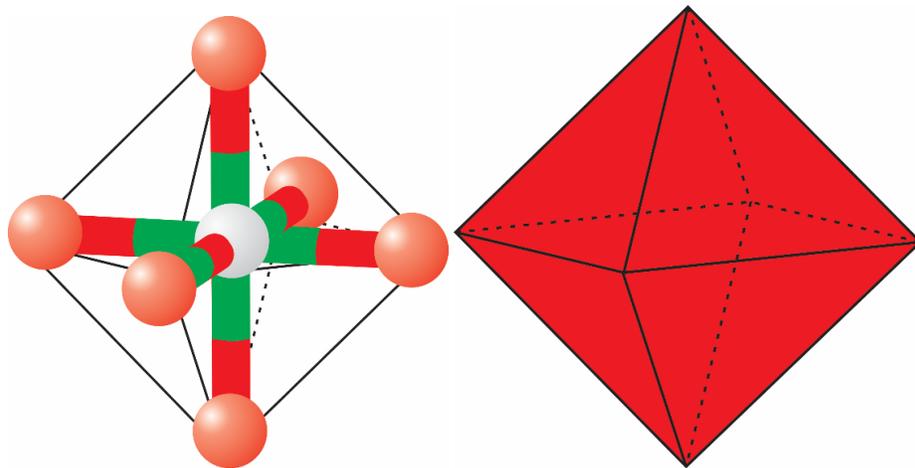
Figure 2.2. Schematic representation of the distorted TiO_6 octahedron of TiO_2 (anatase and rutile). Ti atom (white sphere) and oxygen atoms (orange spheres).

As shown in Figure 2.2, both anatase and rutile crystals may be visualized as chains of TiO_6 octahedra, where each Ti^{4+} ion is surrounded by an octahedron of 6 O^{2-} connecting through two apical and four equatorial bonds. While the distortion of each octahedron and the assembly pattern

of TiO_6 octahedra chains are different between anatase and rutile phases, which results in different mass densities and electronic band structures.[16] To be more specific, in the anatase phase, the conventional unit cell contains four TiO_2 units (12 atoms). Each O atom is coordinated to three Ti atoms, lying in the same plain through one long apical bond (1.979 Å) and two short equatorial bonds (1.932 Å). Each octahedron in the anatase bulk structure is in contact with eight neighbor octahedras; four through sharing an edge oxygen pair, and four by sharing a corner oxygen atom. In the rutile phase, the conventional unit cell contains two TiO_2 units (six atoms). Each O atom is coordinated to three Ti atoms, lying in the same plain through one apical bond (1.976 Å) and two equatorial bonds (1.946 Å). In the bulk structure of rutile, each octahedron is in contact with 10 neighbors; two through sharing an edge, and eight by sharing a corner.[17-18]

2.3 TiO_2 nanomaterials

At present, nanoscale level materials (nanomaterials) have been intensively explored with the rapid development of nanotechnology and nanoscience. TiO_2 nanomaterials have attained tremendous attention due to their broad applications, spanning environmental remediation to energy conversion. Even though, in its conventional powder or bulk form, TiO_2 may be utilized in our daily life as pigments, corrosion-protective coatings, and sunscreens, many of its more outstanding properties only become practicable when it is in nanometric form, which makes available large specific surface areas and additional unique size-dependent properties.[19-20] For many applications of TiO_2, particularly those related to catalytic reactions, optimal efficiency is contingent to a high degree on the specific surface area. Thus, enormous efforts worldwide have been invested in the design, synthesis, control, and further understanding of nanostructured TiO_2.[4]

2.3.1 Classification

In 2007, Pokropivny and Skorokhod proposed a classification scheme for nanostructured materials[21] that was based on the number of dimensions, which were not confined to the submicron or nanoscale range. In terms of this dimensionality perspective, nanostructured TiO_2 materials may be divided into zero-dimensional (0D), one-dimensional (1D), two-dimensional (2D) and three-dimensional (3D) nanostructured materials.

All of the dimensions of 0D nanostructures are within the submicron and nanoscale range and exhibit various shapes and forms individually, or as incorporated within a matrix, such as quantum dots, nanoparticles, or nanoclusters arrays, and nanolenses.[22-24] The most extensively investigated and utilized 0D TiO_2 nanostructured materials encompass solid, hollow, mesoporous and core-shell nanospheres. These entities have been investigated for a rich variety of applications including lithium-ion batteries, air purification, and photocatalysis due to their robust structural stability against repeated charge/discharge, high pore volume, excellent light-harvesting capabilities, good reversibility, and low polarization.[25-31] Nanospheres comprised of TiO_2 may be obtained by many approaches including hydrolysis,[32] hydrothermal method,[27] atomic layer deposition (ALD),[28] etc. A novel thin film fabrication technique referred to as ALD, has stimulated increasing interest in recent years, as uniform and conformal coatings at the atomic level may be deposited with this approach. The thickness of the coated layers may be precisely and easily controlled through varying the number of deposition cycles. Hollow TiO_2 nanospheres are typically synthesized with the assistance of cationic polystyrene (PS) nanospheres, which are employed as a template onto which the titanium species are coated. Subsequently, during the calcination step the titanium species are converted to TiO_2, with the simultaneous removal of the PS nanospheres, which results in the formation of hollow TiO_2 nanospheres.[33]

SU70 10.0kV 7.9mm x25.0k SE(U)   2.00um
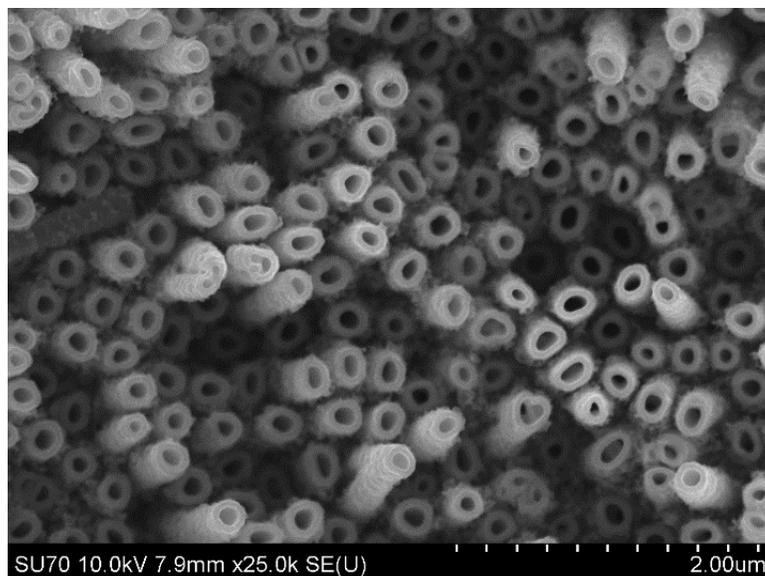
Figure 2.3. SEM image of TiO_2 nanotubes.

Nanostructures in the 1D category have only one dimension that is outside submicron and nanoscale range, and include nanotubes, nanowires, nanofibers, nanorods, etc. Over the last 15 years, 1D nanostructured TiO_2 materials have attracted considerable interest, given their wide range of potential applications and importance in research and development. Many methods have been employed to fabricate 1D TiO_2 nanomaterials: 1) TiO_2 nanotubes are generally fabricated by an anodization technique in a fluoride containing electrolyte; 2) TiO_2 nanofibers may be formed via an electrospinning strategy with precise size control; 3) TiO_2 nanorods and nanowires may be synthesized through hydrolysis or hydrothermal growth techniques.[34-35] Nanostructured 1D TiO_2 materials, particularly self-organizing TiO_2, such as tubular TiO_2 (Figure 2.3), possess multiple positive attributes, such as a 1D electron vertical path to the substrate, highly ordered surface area, and large surface-to-volume ratio. All of these merits are favorable for increasing the interfacial diffusion of organic pollutants and decreasing electron-hole recombination rates, which make 1D nanostructured TiO_2 an attractive candidate for environmental remediation applications.[36] It is in

this area, TiO$_2$ nanotubes have drawn the most attention, which will be addressed more extensively in the following section.

Nanostructured 2D entities such as nanofilms, nanolayers, and nanocoatings have two dimensions that are beyond the submicron and nanoscale range. These nanostructured materials exhibit unique shape-dependent characteristics and thereby have utility as building blocks for the key components of nanodevices. Nanosheets are likely the most studied 2D TiO$_2$ nanostructured materials, due to their high aspect ratio, excellent substrate adhesion, high light-collection efficiency, and surface smoothness. Nanosheets comprised of TiO$_2$ are typically synthesized via a hydrothermal method, and are either employed as a single layer, or as multilayered flake-shaped structures with flat surfaces. They may be integrated with surrounding matrix materials, and can serve as templates for additional 2D structured materials. Over the last decade, TiO$_2$ nanosheets incorporated with other materials have been studied for applications in Dye Sensitized Solar Cells (DSSCs), as they exhibit outstanding photoelectric conversion efficiency.[37-38] This is due to most conventional DSSCs employing 10-20 nanometer TiO$_2$ nanoparticles; however, the nanosheets could be transparent with minimal light scattering, as their dimensions are much smaller than the wavelength of visible light. Therefore, the introduction of 2D nanostructures as light-scattering centers might increase light harvesting capacities and electron transport rates.[39-40]

Bulk nanomaterials are those that are not confined to the nanoscale in any dimension, while possessing a nanocrystalline structure, or involving the presence of features at the nanoscale. In terms of nanocrystalline structure, bulk nanomaterials may be composed of a diverse arrangement of nanoscale crystals; most typically in different orientations. With respect to the presence of features at the nanoscale, 3D TiO$_2$ materials may contain dispersions of nanoparticles, bundles of nanowires, and nanotubes, as well as multiple nanolayers. Many 3D TiO$_2$ materials with large

surface areas have been reported, including 3D mesoporous structure networks, and hierarchical nanostructures.[41] Strategies that might be used to form complex 3D TiO$_2$ nanostructures encompass: 1) inclusion of proper templates as structure-directing agents;[42-44] 2) oriented attachment of primary nanoparticles;[45] 3) induced anisotropic growth with the assistance of specific capping agents.[46] In its 3D form, TiO$_2$ is a promising material for myriad applications, particularly sensors and batteries, owing to an extensive interface with electrolytes within the 3D structure. Moreover, in comparison with smaller dimensioned nanostructured materials, 3D TiO$_2$ provides improved electrolyte penetration.

2.3.2 Synthesis

A rich variety of physical and chemical synthesis techniques have been developed for the fabrication of nanostructured TiO$_2$ materials with well-controlled shapes, sizes, structures, dimensions, and geometries. In the following section, a number of the primary preparation approaches are briefly described.

2.3.2.1 Hydrothermal and solvothermal methods

Hydrothermal and solvothermal techniques are very convenient one-pot synthetic strategies. The hydrothermal method is a well-established technique for the synthesis of various highly homogeneous nanomaterials, and hybrid nanocomposite materials.[47] In this realm of TiO$_2$ nanomaterials formation, reactions take place in aqueous media within a tightly sealed system (e.g., Teflon-lined autoclave enclosed within a stainless steel vessel) under controlled temperatures and pressures. The internal pressure with the autoclave may be easily controlled via the applied temperature and the volume of the solution the autoclave contains. By heating the vessel, the temperature can be increased above the water boiling point, generating a vapor saturation pressure. Under such harsh reaction conditions, TiO$_2$ nanostructures may be formed. Typically, the anatase

form of TiO_2 will be obtained through this method, and dissolution-recrystallization is normally involved in this process.[48]

The solvothermal synthesis route is very similar to the hydrothermal route, and the sole difference between them is that the precursor solution used in former is non-aqueous. Many organic solvents with high boiling points, such as methanol, 1,4-butanol, and toluene have been employed in the solvothermal method in order to attain a higher temperature, which is not possible with aqueous solutions.[49-51] By altering certain experimental parameters, including the reaction temperature, time, solvent, and precursor, the dimensions, shape, and crystallinity of TiO_2 nanomaterials may be precisely controlled. In contrast to hydrothermal synthesis, size distribution and dispersion may also be improved through this approach.

Many types of TiO_2 nanostructured materials have been fabricated through hydrothermal and solvothermal methods, including TiO_2 nanowires, TiO_2 nanorods, TiO_2 nanotubes, and TiO_2 nanobelts.[48,52-54] This approach may also be easily employed to form composite nanomaterials. A TiO_2 nanospindle-reduced graphene oxide composite with enhanced photocatalytic activity was synthesized by Wu et al., who used a facile hydrothermal process.[55] TiO_2 nanospindles were prepared using a mixture of a titanium isopropoxide precursor, isopropylalcohol, and diethylenetriamine (DETA) by a hydrothermal approach. Subsequently, TiO_2 nanospindle-reduced graphene oxide hybrid nanostructures were obtained via a second hydrothermal step using a mixture of graphene oxide, ethanol, and TiO_2 nanospindles.

2.3.2.2 Sol-gel method

The sol-gel technique is a wet chemical process that is likely employed most often for the fabrication of all types of glass, ceramic, and metal oxide materials; particularly silicon and titanium oxides. Specifically, when the liquid is removed from the sol, it becomes a gel. A typical

sol-gel process includes four steps: hydrolysis, polymerization, drying, and thermal decomposition.[56-58] To fabricate TiO_2 nanomaterials, a titanium precursor (e.g., organic titanium complex or inorganic salt) is initially dispersed in water or a diluted acid. Subsequent to hydrolysis and polymerization reactions, a colloidal solution containing a dispersive TiO_2 (sol) is formed. Following the removal of the solvent, a gradual transition from the liquid sol into gelatinized solution (gel) ensues, which acts to control the dimensions and morphologies of the nanomaterials. Finally, solid TiO_2 nanomaterials may be obtained via the calcination of the wet gel.[59-61]

The control parameters of the sol-gel method related to size, shape, and structure have been systemically studied by Chemseddine and co-workers.[62] The sol-gel method may also be easily utilized to synthesize different TiO_2 polymorphs. Mesoporous TiO_2 nanoparticles comprised of anatase-brookite and anatase-brookite-rutile were fabricated by Mutuma et al. using a modified sol-gel method at low temperature.[63] Briefly, a mixture of titanium tetraisopropoxide and isopropyl alcohol was heated to 80 °C for 5 h to obtain a Ti precursor sol, after which the sol was allowed to gel at 25 °C for 24 h. Finally, the gel was filtered, rinsed, and calcined at various temperatures to obtain different crystalline forms. The mesoporous TiO_2 samples prepared through this approach exhibited well-dispersed small particulates, an extensive surface area, and high crystallinity.

2.3.2.3 Vapor deposition method

For the vapor deposition technique, as its name suggests, starting materials are vaporized and condensed on a substrate to form a solid thin film deposit. Vapor deposition methods may be roughly divided into two types, physical vapor deposition (PVD), and chemical vapor deposition (CVD). Both PVD and CVD have been widely employed to fabricate materials with a high degree of crystallinity, especially single crystal nanomaterials. When chemical reactions are involved in this process, it is referred to as CVD; otherwise, it is called PVD.[64-65]

In PVD, bulk starting materials are typically heated in high vacuum or inert gas environments under high temperatures, and sublimate into a vapor. Subsequently the vapor condenses into nanostructured materials on a substrate. Various types of PVD have been reported in the synthesis of TiO_2 nanomaterials, such as sputtering, molecular beam epitaxy, and laser ablation.[66]

Typically, chemical reactions, dissociation of reactive gases, and volatile precursors drive the CVD process. To date, a rich variety of CVD techniques have been developed toward the synthesis of nanomaterials, including aerosol assisted, plasma-enhanced, microwave plasma-assisted, hot filament, photo-initiated, etc.[67] Ponja et al. synthesized a hydrophobic TiO_2-SnO_2 composite film on a glass substrate, employing an aerosol assisted CVD technique, from the reaction of titanium isopropoxide (Ti source) and butyltin trichloride (Sn source) in ethyl acetate (O source).[68] In general, a mixture of titanium tetra-isopropoxide, tin butyl trichloride, and ethyl acetate was utilized as a precursor solution and added to a humidifier flask. The humidifier flask was then attached to the CVD whereupon an aerosol was generated, which was vaporised at room temperature under a flow of nitrogen gas.

2.3.2.4 Direct oxidation method

With the assistance of an appropriate oxidant or via anodization, the formation of TiO_2 nanomaterials may be achieved by the direct oxidation of Ti metal. Compared with pure oxygen, acetone has been reported to be a good oxygen source in the preparation of TiO_2 nanostructured materials.[69] In pure oxygen or mixed argon/oxygen environments, only crystal grains with random nanofibers were obtained. In contrast, highly dense and organized TiO_2 nanorods were formed using acetone as the oxygen source. This is due to the competition between oxygen and Ti diffusion, related to the oxidation of Ti. The fabrication of 1D TiO_2 nanotubes through the anodic oxidation of Ti plates has been intensively studied. Typically, in a two-electrode system, a Ti plate

is anodized in a fluoride containing electrolyte at a proper potential to form highly ordered tubular TiO$_2$ arrays. The development, mechanism, and morphology control of this approach will be discussed more extensively in the following section.

2.4 Tubular nanostructured TiO$_2$ materials

Tubular nanostructures have been intensely studied since carbon nanotubes were successfully synthesized by Iijima.[70] This attractive nanostructure comprises a unique combination of geometry and functionality, offering fascinating properties such as an extensive surface area, high electron mobility, excellent mechanical strength.[71-72]

2.4.1 Fabrication of tubular TiO$_2$ nanomaterials

2.4.1.1 Early stage approaches

To date, many approaches including electrochemical deposition, sol-gel, hydrothermal, solvothermal etc., have been utilized to synthesize TiO$_2$ nanotubes. In 1996, Hoyer was most likely the first researcher who successfully formed tubular TiO$_2$ via an electrochemical deposition method with the help of an alumina template.[73] In brief, anodic porous aluminum oxide was used as the starting material to fabricate a polymeric rod mold, followed by the generation of the tubular TiO$_2$ structure on the polymer mold by electrochemical deposition. Subsequently, the mold was dissolved in acetone to yield amorphous hydrous TiO$_2$ nanotubes. Many other techniques assisted by templates have since been studied to obtain tubular TiO$_2$, such as sol-gel and atomic layer deposition.[74-75] Many of the processes involve hydrolysis reactions of titanium alkoxide precursors and condensation. In this way, a developed gel-type polymeric Ti-O-Ti chain hydrolyzes and generates TiO$_2$ precipitates.

The hydro/solvothermal method is another well-demonstrated approach for the fabrication of tubular nanostructured TiO_2, which was first reported by Kasuga et al.[76-77] In this study, a TiO_2 powder was initially hydrothermally treated in an alkaline solution, followed by an acidic solution. The exfoliation of TiO_2 crystal planes then forms nanolayered sheets, which are rolled into tubes during the cooling process, or other treatments. Multishelled tubular structures with lengths of from tens to hundreds of nanometers may be generated through this approach.

All of the techniques discussed above have the capacity to yield single TiO_2 nanotubes, loose bundles, or clustered nanotubes, with a wide variety of lengths and tube diameters. In order to employ these structures for electrochemical applications or electrical characterizations, the nanotubes are generally required to be compacted into layers on an electrode substrate, which enables interfacial contact with electronic devices. Unfortunately, this process results in the random orientation of tubular TiO_2 on the substrate surface, which makes it impossible to preserve some of the advantageous merits of one-dimensional nanostructures, such as vertical 1D electron paths to the substrate.
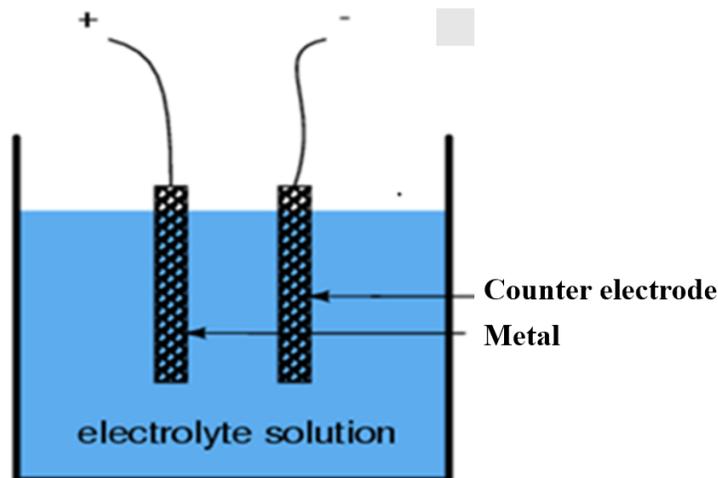
Figure 2.4. Set-up of the electrochemical anodization process.

2.4.1.2 Electrochemical anodization

Anodization is an electrochemical process that may produce metal oxides on suitable metals (e.g., valve metal) in a proper electrolyte under an electric field. More than half century ago, the formation of metal oxides via electrochemical anodization had been already studied.[78] Nevertheless, this approach has only been involved in the fabrication of TiO_2 nanostructures over the last two decades, and is considered to be one of the simplest, cheapest, and most straight-forward techniques. It is typically carried out using an inexpensive dual-electrode system (Figure 2.4) with an anodic voltage applied to an appropriate metal or alloy substrate. The nanostructured oxide layer can then be formed on the substrate surface through a simple electrochemical oxidation reaction under a suitable set of environmental conditions. In contrast to other approaches, electrochemical anodization can offer highly uniform self-organized oxide nanotube or nanoporous arrays that align perpendicularly to the substrate surface with controllable nanoscale geometries (tube lengths and diameters may be adjusted over large length scales).[79] Normally, the tubular arrays are inherently electrically attached to the metal substrate, as they are directly grown on the electrode substrate through electrochemical anodization. This makes the structure highly functional and easy to handle. It is also remarkable that the electrochemical anodization approach is not limited to titanium, but can be applied to a wide variety of other transition metals or alloys toward the synthesis of highly ordered oxide tubular nanostructures. Therefore, this technique has attracted extensive interest and has been well studied over the last 15 years.[80]

2.4.1.2.1 Development of electrochemical anodization approach

The first targeted work to form self-organized tubular nanoporous TiO_2 on a Ti plate was reported by Zwilling and co-workers in 1999.[81] The electrolyte studied in this work was chromic acid containing hydrofluoric acid, and the applied voltage between the two electrodes in the system

27

was varied from 0 to 10 V. The researchers found that in absence of hydrofluoric acid, only compact non-porous oxide films were obtained during titanium and titanium alloy anodization processes. Hence, it was recognized that small quantity of fluoride ions introduced into the electrolyte played a key role in the formation of self-organized oxide structures. The reason was that the added fluoride ions initiated competition between the Cr ions and F species toward the formation and dissolution of oxide films. This process led to the continuous growth of nanotubular structured oxide films. As the mechanism and operating conditions were not well studied in this initial work, the tubular nanoporous TiO_2 fabricated in this work was not highly organized and possessed inhomogeneous sidewalls.

Current techniques employed to fabricate highly ordered self-organizing tubular oxide nanostructures were primarily established and realized by Schmuki's group in Germany.[82-84] This team devoted enormous efforts toward the study of kinetics, operating conditions, and crucial parameters to improve the quality of the tubular structure ordering.
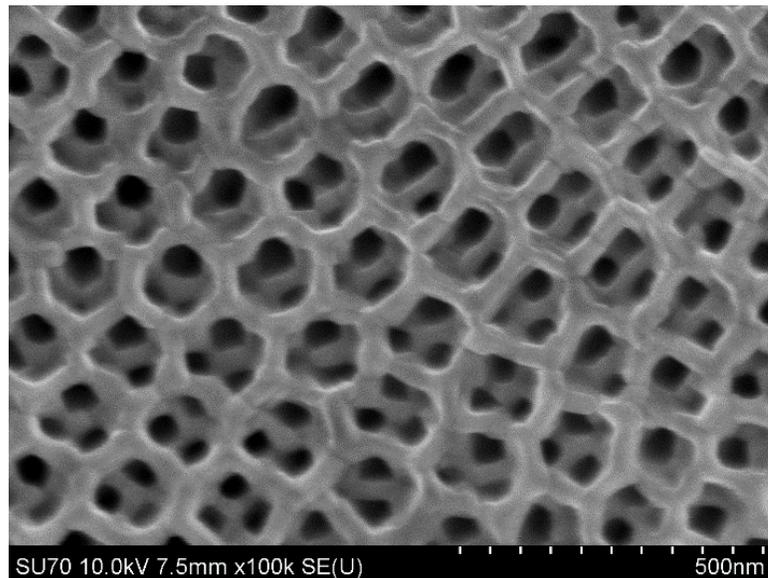
Figure 2.5. SEM image of nanoporous TiO_2 fabricated through multistep anodization approach.

In recent years, multistep anodization approaches have been discovered to further increase the ordering of tubular layers through pre-structured surfaces that offer geometric guidance. To achieve this, the first few tubular TiO_2 layers were removed from the metal surfaces, leaving behind a regular pattern of grooves. These grooves then served as initiation sites for the last anodization step of tube growth, and thus, resulted in a highly organized tubular structure with a large surface area (Figure 2.5).[85]

2.4.1.2.2 Growth mechanism

Self-organized tubular or porous oxide arrays may be achieved by an anodization process that involves a suitable metal with a sufficiently anodic voltage in an electrochemical set-up (as depicted in Figure 2.4). The basic mechanism for the formation of tubular TiO_2 nanostructures on Ti substrates is well established on the study of anodic growth of porous anodic alumina on Al.[86] Briefly, under an applied potential, the growth of an oxide layer is initiated on the anode surface, due to an anionic oxide flow. The following reactions may occur at electrolyte/oxide interface,

$$H_2O \rightarrow OH^- + H^+ \tag{1}$$

$$OH^- \rightarrow O^{2-} + H^+ \tag{2}$$

$$TiO_2 \rightarrow Ti^{4+} + 2O^{2-} \tag{3}$$
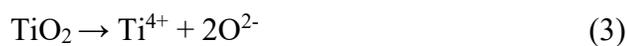
Then OH^- and O^{2-} anions traverse the oxide layer to form TiO_2 and titanium hydroxide at the oxide/Ti interface,

$$Ti + 2O^{2-} \rightarrow TiO_2 + 4e^- \tag{4}$$

$$Ti + x\ OH^- \rightarrow Ti(OH)_x + x\ e^- \tag{5}$$
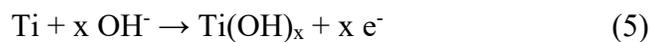
In the presence of fluorides in the electrolyte, the fluoride anions react with the newly formed TiO_2 and produce water-soluble $[TiF6]^{2-}$ species.

$$TiO_2 + 6F^- + 4H^+ \rightarrow [TiF6]^{2-} + 2H_2O \qquad (6)$$

With the proper concentration of fluoride, competition between the formation and dissolution of TiO_2 will be introduced, which facilitates the continuous growth of the tubular TiO_2 nanostructure.[86-87]

2.4.1.2.3 Morphological control

The morphologies of the formed tubular TiO_2 nanostructures may be tailored for specific applications by altering the anodization duration, applied anodic potential, and electrolyte composition. Generally speaking, the thickness of the nanotube layer might be linearly increased with the anodization time, and the etching rate may specifically define the tube length. To be more specific, in a fluoride-containing solution, a state of equilibrium between the formation of TiO_2 nanotubes at the bottom, and etching at the top of the nanotubes is established at some point.[88] In a long-duration anodization experiment, the effect of etching may be clearly observed, as the nanotube walls are thinned out at the top in accordance with the anodization time. The thinning nanotube walls typically lead to inhomogeneous grass-like or bundling top structures, due to a lack of mechanical support (the nanotubes are not able to support their own weight or resist capillary forces during the calcination process).[89] Normally, the tube length is restricted to 500-600 nm in acidic electrolytes, while 2-4 μm tube lengths might be achieved in neutral solutions, owing to more rapid etching rates under lower pH.[84] Extreme long tubes of over 20 μm may be achieved in an organic electrolyte such ethylene glycol, glycerol, and dimethyl sulfoxide, with some assisted pretreatment.[90] F. Mohammadpour and co-workers successfully synthesized highly ordered 23 μm long TiO_2 nanotubes without a nanograss top layer, at just 2 h of anodization. The key step of the fabrication process was the electropolishing pretreatment of the Ti foil in an ethanol-containing solution, which generates footprints on the Ti surface with small diameters that act as a nucleation

layer following anodization. The anodization was carried out in an ethylene glycol based electrolyte that contained 0.3 wt% NH_4F and 2 vol% H_2O at a constant potential of 60 V.

It is well accepted that the diameters of formed nanotubes are linearly controlled by, and depend on the applied anodic voltage, while other parameters are kept constant,[88,91-92] where higher applied voltages result in larger tube diameters. Additionally, the inner diameter at the TiO_2 nanotube opening is typically larger than the diameter at its base, due to the etching process.[93] In fact, anodization is a transition process, from the nanoporous to the nanotube structure, which means that the diameter of nanopores at the base gradually become larger, and the nanopores split into nanotubes with the anodization duration.[94] Also, with longer anodization periods, the conductivity of the electrolyte increases, which accelerates the etching rate, and thus nanotubes with larger diameters are observed. The diameter may be further affected by the anodizing temperature, since the etching rate is more rapid at higher temperatures.

The formation of tubular or porous structures are primarily due to the $[TiF6]^{2-}$ species that are produced by fluorine ions; therefore, the concentration of fluorine primarily determines the etching rate. Hydrofluoric acid, ammonium fluoride, or other fluorine salts have been employed in the synthesis of TiO_2 nanotubes via anodization.[81,85,95] A stable metal oxide layer may be formed if the electrolyte contains a very low concentration of fluoride ions ($\leqslant$0.05 wt%). Intermediate fluoride concentrations (0.2%-0.4%) that are optimized for nanotube synthesis, initiate a competition between oxide formation and Ti^{4+} solvatizaion. No oxide layer will be formed if higher concentrations of the fluoride ions are used, as they react with titanium ions to form $[TiF^{6+}]$.

Water content also plays a critical role in the growth of nanotubes, as on one hand, water is required to form TiO_2, and on the other hand, it might increase the etching rate. It has been reported

that very long nanotubes with smooth walls may be obtained in organic electrolytes with low water content.[96]

2.5 Modification of TiO₂ nanomaterials

In modern science and engineering, the efficient utilization of solar energy is a major goal. Although TiO_2 has proven itself as a promising photocatalyst, its relatively wide bandgap (3.0-3.2 eV in all its crystalline forms) greatly hinder its activity. Therefore, the modification of TiO_2 to alter its electronic, photonic, and structural properties to enable visible-light absorption has attracted tremendous interest.[97] Generally, to significantly enhance the activity of TiO_2, there are two challenges to overcome: 1) narrow its wide bandgap to promote electron-hole charge separation; 2) increase the quantity of working electrons and holes on the surface, which translates to restraining electron-hole recombination. Currently, it is well accepted that the introduction of additional elements into the TiO_2 lattice structure, or onto its surface (through doping and decoration), are the primary and efficient approaches for the modification of TiO_2.

2.5.1 Doping

Doping is a common approach in semiconductor materials science for the introduction of foreign impurities into the lattice structures of other materials for the purpose of modulating their properties.[97] To date, a number of efficient doping methods have been reported, including thermal treatment,[98] ion-implantation,[99] sputtering,[100] hydrogen treatment,[101] self-doping by reduction approaches[35], and the use of alloy substrates to grow nanostructures.[102] Generally, doping may be categorized into two types: substitutional doping and interstitial doping. When substitutional doping occurs, substitutional impurities replace host atoms. For example, N atoms might serve as dopants in TiO_2 to replace O atoms. To achieve successful substitutional doping, the selected dopants must possess dimensions that are relatively close to that of the host atoms. Interstitial

doping refers to the impurities that occupy interstitial vacant sites between the lattice atoms within the host lattice. Both types of doping may modify the electronic band structure by generating impurity levels in the band gap, which increases the quantity of functional electrons and holes; thus enhancing activity.

Doping with metals (Cr, V) or non-metals (N, P, S, C, B, F) have been studied intensively to narrow the optical bandgap of TiO_2; thus improving the visible-light photocurrent response.[103-107] Among these, nitrogen doping is no doubt considered to be the most studied and successful approach, as: 1) N2p states are close to O2p states (valence band of TiO_2), such that their states may effectively merge together to decrease the band gap; 2) the diameters of N and O atoms are quite close, which is beneficial for the introduction of N to the TiO_2 lattice. In 1986, nitrogen doped TiO_2 was initially discovered by Sato, when preparing TiO_2 powder from commercial titanium hydroxide that contained a NF_4OH impurity. However, it was not until 2001 that the first successful band structure modification via a N sputtering doping procedure was carried out, where the enhanced photocatalytic activity was interpreted as band gap narrowing.[108] Inspired by this work, a wide range of other dopant candidates were explored in the following years.

Over last five years, many novel doping approaches have been studied for the modification of TiO_2 nanomaterials, such as hydrogen doping, and self-doping. In 2011, Chen and co-workers first reported the preparation of black TiO_2 nanoparticles via a hydrogen treatment.[101] Pure white TiO_2 nanoparticles were introduced to a 20.0 bar pure H_2 atmosphere at 200°C for 5 days, whereupon the pure white TiO_2 changed completely to black. This strategy successfully shifted the bandgap of TiO_2 to ~1.54 eV (806.8 nm) with an optical onset ~1.0 eV (~1200 nm). It was confirmed by TEM that the hydrogen treated black TiO_2 nanoparticles featured a lattice-disordered

shell, which was believed to host the possible hydrogen dopant, and consequently introduced the midgap states.

Self-doping TiO$_2$ has also been studied in very recent years using chemical and electrochemical reduction strategies.[109] Through the reduction treatment, a very small quantity of Ti^{4+} was reduced to Ti^{3+}, whereafter the TiO$_2$ nanomaterials showed a navy or black color and intense absorption in the visible light range. The existence of Ti^{3+} may be confirmed by XPS. To date, Al, Zn, imidazole, CaH$_2$, and NaBH$_4$ have been reported as efficient reductants,[109-113] and a facile electrochemical reductive doping process has also been reported by various groups.[114-115]

2.5.2 Decoration

The decoration of TiO$_2$ surfaces with nanoparticles (metals, polymers, and semiconductors) is another well-studied and efficient method for the modification of TiO$_2$ through altering its surface properties and even bending its band gap. The loading of nanoscale metals, particularly noble metals, onto the surface of TiO$_2$ comprises one of the most frequently employed decoration approaches in recent years. A great number of metals (e.g., Pt, Au, Pd, Ru, Rh, and Ag) have been successfully decorated onto TiO$_2$ surfaces by photodeposition, chemical deposition, impregnation, etc.[116-118] Metal ions have a great impact on charge carrier recombination rates, interfacial electron transfer rates, and catalytic reactions that occur on the surface. Pt decorated TiO$_2$ nanotubes exhibited a significant enhancement in photocatalytic activity, as the Pt nanoparticles serve as electron trapping sites.[119] When Au and Ag nanoparticles possess the proper dimensions and morphologies, they may even impact charge transfer via their special property of localized surface plasmonic resonance (collective free electron charge oscillation).[120-121] Therefore, the efficient decoration with metals may significantly enhance conductivity and catalytic activities.

Narrow-bandgap semiconductor (CdS, PbS, CdSe) decorated TiO_2 are also under study to achieve a smaller band gap. These semiconductors with a bandgap of 2-2.4 eV can decrease the onset energy for light absorption; hence, enable TiO_2 to be utilized under solar light exposure. [122-123]

The coupling of dyes or other molecules for the provision of suitable energy levels to TiO_2 surfaces is another very promising strategy for the modification of TiO_2 to exploit the solar spectrum. This approach has been successfully investigated for dye-sensitized solar cells (to be discussed in more detail in the following section).

2.6 Applications of TiO_2 nanomaterials

2.6.1 Photocatalyst and electrocatalyst for wastewater treatment

It is widely considered that TiO_2 is the best photocatalyst available because of its various properties, such as high photostability, chemical inertness, low cost, and non-toxicity. Intense research has been focused on the development of the TiO_2 based nanomaterials for their utilization in the photooxidation of various organic, inorganic pollutants, as well as bacteria, and other bio-organism.[124] In general, a photocatalyst functions when photons are irradiated onto it, which results in the excitation of electrons from the VB to the CB. These excited electrons react with oxygen molecules to form $O_2^{\bullet-}$, and the holes in the conduction band react with water molecules to produce $OH^{\bullet}$.[7] These highly active radical species possess robust oxidation activities and thus play a key role in the oxidation of organic pollutants. Since TiO_2 is a semiconductor oxide, it possesses a very large band gap (3.0-3.2 eV in all crystalline forms).[4] High energy containing photons are required to excite electrons in TiO_2, from the VB to the CB; therefore, it may only be excited by UV irradiation. If visible or solar light activity is required for TiO_2, electronic modification must be performed to decrease its band gap.[97]

There are a number of reports that describe the use of TiO_2 nanoparticles for the photooxidation of various pollutants. This activity may be referred to as first generation TiO_2 where no modification is done.[125] Maness et al. studied the bactericidal activities of photocatalytic TiO_2 reactions, and on exploring its mechanisms concluded that both UV light and TiO_2 are necessary for the oxidation of *E. Coli* bacteria. The second generation of TiO_2 relates to improvements in the photocatalytic properties of the TiO_2 structure when metal doping is performed. Various metals such as W, Fe, Al, Co, Os, Re, V, etc. have been explored. Fe(II)-doped TiO_2 spherical shells were recently fabricated by Xu et al. for the photocatalytic removal of Cr(VI) from plating wastewater under exposure of sunlight. The researchers fabricated these Fe(II)-doped TiO_2 spherical shells via a hydrothermal method, where $FeSO_4 \cdot 7H_2O$ was used as the precursor for Fe, and $TiOSO_4 \cdot 2H_2O$ as the precursor for Ti.[124]

Third generation TiO_2 is anion doped, where the band gap of TiO_2 is reduced through the addition of various anions, such as F, N, C, S etc. Asahi et al. fabricated N doped TiO_2 to significantly augment its photocatalytic activity toward the oxidation of methylene blue. The N 2p orbital is very close to the O2p orbital, which constitutes the valence band of TiO_2; thus, they may easily overlap each other, which results in a decrease of the band gap.[108] Wu et al. reported on a novel approach for the synthesis of a N and F co-doped mesoporous TiO_2 photocatalyst via a single-step combustion method. In their study TiF_4 was used as the precursor to provide the sources of Ti and F, and urea was used as the fuel, as well as the source of the N dopant. Their results demonstrated that co-doping with N and F significantly narrowed the bandgap energy of TiO_2, and when this co-doped TiO_2 was employed under visible light for the oxidation of acetic acid, an excellent photocatalytic activity was observed.[126] Thind and coworkers fabricated N and W co-doped TiO_2 nanomaterials using the abovementioned solution combustion method.[127] Titanium tetra isopropoxide was employed as the titanium precursor, urea as the fuel and source of N, and

sodium tungstate as the W source. It was shown by the researchers that with this solution combustion method the N and W atoms were well incorporated into the lattice structure of the titania, thus leading to a significant red shift in the absorption edge of the co-doped TiO_2, which decreased the band gap of the material. With this narrowing of the band gap, very high visible light activity was subsequently observed for the photodegradation of Rh B (dye pollutant). The co-doped materials exhibited a 14 fold enhancement in the visible light activity, as compared to P25, which is the best commercially available TiO_2. The photocatalytic activity of TiO_2 may also be employed to reduce toxic metal atoms to their non-toxic forms.

Zheng and coworkers synthesized hierarchical TiO_2/SnO_2 photocatalysts with different morphologies for the photocatalytic reduction of Cr (VI).[128] There are several other strategies being employed for the removal of heavy metals ions from wastewater, such as chemical precipitation, reverse osmosis, ion exchange, membrane filtration, and adsorption. These methods either do not completely remove the chemical, or are very costly to operate (e.g., very expensive membranes are required for membrane filtration, which have the requirement of frequent replacement). During the fabrication of TiO_2/SnO_2, various structures such as nanoparticles, nanosheets and nanobelts may be obtained from the hierarchical TiO_2/SnO_2 microspheres by adjusting the concentration of NaOH. When compared to P25 (TiO_2), the hierarchical TiO_2/SnO_2 nanobelts showed very high photocatalytic activity for the reduction of Cr (VI) under UV irradiation. The much higher photocatalytic activity of the TiO_2/SnO_2 composite might be attributed to improved charge separation, rapid and long-distance electron transport, and the large surface-to-volume ratio of the TiO_2/SnO_2 nanobelts.

Since TiO_2 is a semiconductor oxide and thus possesses very low electrical conductivity, it must be modified to be used as an electrocatalyst. Chang et al. used an electrochemical reduction method to increase the electrical conductivity of TiO_2 nanotubes that were fabricated by an

electrochemical anodization method.[35] A current of -5 mA/cm^2 was applied for 10 min to reduce the electrode, whereupon a significant change in the color of the electrode was observed by the researchers. The reduced TiO$_2$ nanotubes possessed a much higher overpotential for oxygen evolution than a Pt electrode, and exhibited high electrocatalytic activity toward the oxidation of salicylic acid. The electron density of the electrochemically reduced TiO$_2$ was found to be 33,000 times larger than that of untreated TiO$_2$. This treated TiO$_2$ had good electrical conductivity, and thus could be employed in various applications such as wastewater treatment, rather than expensive materials such as Pt, Ir, Au, etc.

2.6.2 Hydrogen Production

Honda and Fujishima produced H$_2$ for the first time in 1972, from water splitting with the assistance of the photocatalytic activity of TiO$_2$.[1] A considerable amount of research has since been focused on the development of new TiO$_2$ based nanomaterials to increase the efficacy of hydrogen production from water splitting. To increase the efficiency of this process modifications have been performed to make this hydrogen production possible under solar irradiation.[129] Cao et al. fabricated a novel bifunctional RuO$_2$@TiO$_2$@Pt photocatalyst using TiO$_2$ hollow spheres with RuO$_2$ and Pt deposited onto the external and internal shell surfaces, respectively.[130] The researchers employed this RuO$_2$@TiO$_2$@Pt for simultaneous photocatalytic H$_2$ production and organic pollutant degradation. A synergistic effect between the photocatalytic oxidation and reduction was observed. In this photocatalyst the primary role of RuO$_2$ was to ease the transfer of the holes that were generated on the TiO$_2$ following photon irradiation, subsequent to the oxidization/degradation of organic pollutants. The primary role of the Pt was to facilitate the transfer of the photoelectrons, which then reduced the protons to H$_2$. Due to the presence of RuO$_2$

and Pt, the electron-hole charge separation was increased; hence, reducing the electron hole recombination and increasing the photocatalytic activity of the TiO_2 toward the production of H_2.

Pt/TiO_2 nanosheets with exposed (001) facets were fabricated by Yu et al. using a hydrothermal treatment involving a tetrabutyl titanate and hydrofluoric acid mixture.[131] Subsequently Pt was deposited by a photochemical reduction method onto the TiO_2 nanosheets. The authors observed that following the deposition of the Pt nanoparticles onto the TiO_2, a significant enhancement in the photocatalytic production of H_2 was observed. The effects of fluorination on photocatalytic activities were also studied, and it was concluded that all fluorinated TiO_2 nanosheets exhibited a much higher photocatalytic activity than Degussa P-25 TiO_2.

Wang et al. studied hydrogen production over fine Au-Pt alloyed TiO_2 photocatalysts.[132] Using a chemical reduction method, the researchers deposited very fine metal nanoparticles (2-3 nm; Au, Pt, and alloyed Au-Pt), with a narrow size distribution, onto the TiO_2. Their results showed that in contrast to the TiO_2, an almost 10 fold enhancement in photocatalytic hydrogen evolution was observed when these alloyed nanocomposites were employed. The authors concluded that more robust metal-supported interactions between the alloyed structures and TiO_2, and higher electron populations on the Au-Pt/TiO_2 photocatalysts, (in comparison to bare TiO_2), played the most important role in enhancing the H_2 production activity.

2.6.3 Dye-sensitized solar cells (DSSCs)

With increases in the human population, energy demands are skyrocketing and are exerting immense pressure on the production of non-renewable sources. These non-renewable sources are limited and their extensive use also causes pollution, which is clearly deteriorating the natural environment. To fulfill this rising energy demand, various new techniques are being developed, which include dye-sensitized solar cells (DSSCs).[2] DSSCs provide a very promising renewable

alternative to non-renewable energy sources. The high conversion efficiency, simple design, and low cost manufacturing are some of the desirable features of DSSCs. Nanomaterials comprised of TiO_2, which possess high chemical stability, low toxicity, and high surface areas are likely the best materials to use for the fabrication of anodes. The high surface area of TiO_2 nanomaterials provides greater dye adsorption. Toward the achievement of higher conversion efficiencies, intense research is being focused on improving the conversion efficiency of TiO_2 nanomaterials.[133]

Wang et al. employed a facile sol-gel method to fabricate yttrium and nitrogen co-doped TiO_2 nanoparticles for DSSC applications.[134] With the addition of yttrium with nitrogen, the surface of the TiO_2 increases significantly, which allows it to absorb additional dye. The optimal value of the doping concentration imparts a 5.41% light to electricity conversion efficiency, which was 18% higher in comparison to a pure TiO_2 electrode. The co-doping of nitrogen and yttrium within the TiO_2 lattice structure resulted in the suppression of the charge recombination as indicated by the EIS studies.

The hydrothermal preparation of TiO_2 loaded with Au nanoparticles was conducted by Muduli et al.[135] The Au loaded TiO_2 demonstrated a solar energy conversion efficiency of 6%, which was significantly higher than the unloaded TiO_2 nanoparticles. Electrochemical impedance studies on the materials revealed that the charge transfer resistance and the recombination of electrons with I^{3-} at the TiO_2/electrolyte interface was lower for TiO_2-Au in contrast to unloaded TiO_2 nanoparticles.

2.6.4 Fuel cells

Fuel cells convert the chemical energy of a reaction into electricity with water as a by-product. Electrodes composed of TiO_2 have undergone extensive studies for fuel cell applications. There are different types of TiO_2 integrated fuel cells, with two important ones listed below.[136]

2.6.4.1 Proton exchange membrane fuel cells (PEMFCs)

For these types of fuel cells, a solid polymer electrolyte is employed for the exchange of ions between the two electrodes.[137] The large surface areas of the TiO_2 nanoparticles may be employed in the fabrication of electrodes for PEMFCs. Since TiO_2 is a semiconductor oxide with poor electrical conductivity at low temperatures, the use of TiO_2 in electrochemical systems is very inefficient. To enable the utility of TiO_2 in PEMFCs, the conductivity TiO_2 must be improved. The most straightforward strategy for doing this is through the doping of TiO_2 with metals, which may significantly enhance its electrochemical conductivity.[138] Gojkovic and coworkers fabricated Nb doped TiO_2 using an acid-catalyzed sol-gel method.[139] By doping TiO_2 with Nb, two objectives were accomplished; firstly, the surface area of the material was increased, and secondly an enhancement in electrical conductivity was observed. The high surface area of the Nb-TiO_2 facilitated the deposition of Pt and Ru nanoparticles. It was subsequently observed that the oxidation of pre-adsorbed CO and methanol on the Pt–Ru/Nb–TiO_2 was more rapid than on Pt/Nb–TiO_2. This meant that Nb-TiO_2 is a promising replacement for high surface area carbon supports in PEMFC anodes.

The rate determining step in PEMFCs is the oxygen reduction reaction (ORR) at the cathode. Contingent on the electrode material, the ORR may take place by direct $2e^-$, $4e^-$, or two $2e^-$ pathways. The $4e^-$ ORR process is an ideal mechanism for the development of fuel cells with high efficiency, and Pt/C is the most widely used electrocatalyst for the ORR.[140] The high cost and low availability of precious metal catalysts hamper large scale applications. Therefore, TiO_2 has been investigated as an excellent candidate for the support of precious metal catalysts due to its synergistic effects and high stability.[141] It was concluded that metal nanoparticles supported on a TiO_2 catalyst exhibited higher activity toward the ORR than precious metal/C catalysts. To create

metal-free catalysts for the oxygen reduction reaction, Yu et al. fabricated a reduced graphene oxide (rGO) supported (N, F)-codoped TiO_2 hybrid (TiO_2/rGO). Their experimental results showed that the onset potential of the ORR under the catalysis of TiO_2/rGO was ~-0.20 V (vs. Hg/Hg_2Cl_2). The electron transfer number was calculated to be ~3.98, which meant that a very favourable four electron transfer was occurring. The TiO_2/rGO catalyst also exhibited a much higher catalytic activity for the ORR, and much better stability than the commercial Pt/C catalyst. These results confirmed that TiO_2/rGO catalysts may be efficiently employed as a highly active non-precious metal catalyst for the ORR.

2.6.4.2 Direct methanol fuel cells (DMFCs)

Direct methanol fuel cells (DMFCs) are capable alternative power sources for a variety of transportation and portable applications. The prominent rationale for their development encompsses their environmental sustainability, low toxicity, and very high energy density (6100 Wh kg^{-1}).[142] Hu et al. synthesized a double-shell PtRu/TiO_2 catalyst, where Pt and Ru nanoparticles were prepared by combining a facile microwave-assisted method with L-ascorbic acid as the soft reductant.[143] The electrochemical results showed that the peak current density of PtRu/TiO_2 for methanol oxidation reaction was twice as high as that of Pt/C in acidic media. The researchers showed that the double-shell PtRu/TiO_2 is a promising electrocatalyst with high performance for DMFCs. There are numerous scientific reports that describe the use of TiO_2 as an electrode material for the methanol oxidation reaction.[144-146]

2.7. Summary and perspectives

To date, significant progress has been made in the synthesis, modification, and implementation of TiO_2 nanomaterials. Numerous approaches have been developed to fabricate TiO_2 nanomaterials with various dimensions, phases, and morphologies, which have led to myriad

applications, ranging from photocatalysis to energy conversion. However, a number of challenges restrain the expansion of the utilization of TiO_2 nanomaterials. Hence, advances in the study of TiO_2 nanomaterials should encompass 1) increasing charge separation and solar light activity; 2) decreasing the electron-hole recombination rate; 3) the fabrication and modification of TiO_2 nanomaterials with facile, inexpensive, and accessible techniques and materials; 4) increasing the lifetime and stability of TiO_2 nanomaterials; 5) restricting the use of hazardous materials, and requiring that the research community and industry work to incorporate safe, biologically and environmentally compatible elements for TiO_2 nanomaterials research and toward product commercialization.

References

(1)   Fujishima, A. *nature* **1972**, *238*, 37-38.

(2)   Grätzel, M. *Nature* **2001**, *414*, 338-344.

(3)   Liu, L.; Chen, X. *Chemical reviews* **2014**, *114*, 9890-9918.

(4)   Ma, Y.; Wang, X.; Jia, Y.; Chen, X.; Han, H.; Li, C. *Chemical reviews* **2014**, *114*, 9987-10043.

(5)   Kubacka, A.; Fernandez-Garcia, M.; Colon, G. *Chemical Reviews* **2011**, *112*, 1555-1614.

(6)   Hernández-Alonso, M. D.; Fresno, F.; Suárez, S.; Coronado, J. M. *Energy & Environmental Science* **2009**, *2*, 1231-1257.

(7)   Szczepankiewicz, S. H.; Colussi, A.; Hoffmann, M. R. *The Journal of Physical Chemistry B* **2000**, *104*, 9842-9850.

(8)   Ohtani, B. *Chemistry letters* **2008**, *37*, 216-229.

(9)   Jeon, T. H.; Choi, W.; Park, H. *The Journal of Physical Chemistry C* **2011**, *115*, 7134-7142.

(10)   Kim, J.; Choi, W. *Environmental science & technology* **2011**, *45*, 3183-3184.

(11)   Park, H.; Bak, A.; Jeon, T. H.; Kim, S.; Choi, W. *Applied Catalysis B: Environmental* **2012**, *115*, 74-80.

(12)   Lin, C.-H.; Chao, J.-H.; Liu, C.-H.; Chang, J.-C.; Wang, F.-C. *Langmuir* **2008**, *24*, 9907-9915.

(13)   Akimoto, J.; Gotoh, Y.; Oosawa, Y.; Nonose, N.; Kumagai, T.; Aoki, K.; Takei, H. *Journal of Solid State Chemistry* **1994**, *113*, 27-36.

(14)   Ohno, T.; Higo, T.; Murakami, N.; Saito, H.; Zhang, Q.; Yang, Y.; Tsubota, T. *Applied Catalysis B: Environmental* **2014**, *152*, 309-316.

(15)   Kuo, H.-L.; Kuo, C.-Y.; Liu, C.-H.; Chao, J.-H.; Lin, C.-H. *Catalysis Letters* **2007**, *113*, 7-12.

(16)   Linsebigler, A. L.; Lu, G.; Yates Jr, J. T. *Chemical reviews* **1995**, *95*, 735-758.

(17)   Nie, X.; Zhuo, S.; Maeng, G.; Sohlberg, K. *International Journal of Photoenergy* **2009**, *2009*.

(18)   Chen, X.; Mao, S. S. *Chem. Rev* **2007**, *107*, 2891-2959.

(19)   Fierro, J. L. G. *Metal oxides: chemistry and applications*; CRC press, 2005.

(20)   Ozin, G. A.; Arsenault, A. C.; Cademartiri, L. *Nanochemistry: a chemical approach to nanomaterials*; Royal Society of Chemistry, 2009.

(21)   Pokropivny, V.; Skorokhod, V. *Materials Science and Engineering: C* **2007**, *27*, 990-993.

(22)   Zhu, X.; Cicek, A.; Yanik, A. A. CLEO: Science and Innovations, 2016; p STh3H. 2.

(23)   Lim, S. Y.; Shen, W.; Gao, Z. *Chemical Society Reviews* **2015**, *44*, 362-381.

(24)   Zheng, D.; Huang, C.; Wang, X. *Nanoscale* **2015**, *7*, 465-470.

(25)   Zhang, W.; Zhou, W.; Wright, J. H.; Kim, Y. N.; Liu, D.; Xiao, X. *ACS applied materials & interfaces* **2014**, *6*, 7292-7300.

(26)   Tang, H.; Zhang, D.; Tang, G.; Ji, X.; Li, C.; Yan, X.; Wu, Q. *Journal of Alloys and Compounds* **2014**, *591*, 52-57.

(27)   Yang, H. G.; Zeng, H. C. *The Journal of Physical Chemistry B* **2004**, *108*, 3492-3495.

(28)   Bai, Y.; Yan, D.; Yu, C.; Cao, L.; Wang, C.; Zhang, J.; Zhu, H.; Hu, Y.-S.; Dai, S.; Lu, J. *Journal of Power Sources* **2016**, *308*, 75-82.

(29)   Liu, M.; Piao, L.; Lu, W.; Ju, S.; Zhao, L.; Zhou, C.; Li, H.; Wang, W. *Nanoscale* **2010**, *2*, 1115-1117.

(30)   Xiang, Q.; Yu, J.; Jaroniec, M. *Chemical Communications* **2011**, *47*, 4532-4534.

(31)   Lü, X.; Huang, F.; Mou, X.; Wang, Y.; Xu, F. *Advanced Materials* **2010**, *22*, 3719-3722.

(32)   Kondo, Y.; Yoshikawa, H.; Awaga, K.; Murayama, M.; Mori, T.; Sunada, K.; Bandow, S.; Iijima, S. *Langmuir* **2008**, *24*, 547-550.

(33)   Wang, L.; Sasaki, T.; Ebina, Y.; Kurashima, K.; Watanabe, M. *chemistry of materials* **2002**, *14*, 4827-4832.

(34)   Hu, A.; Zhang, X.; Luong, D.; Oakes, K.; Servos, M.; Liang, R.; Kurdi, S.; Peng, P.; Zhou, Y. *Waste and Biomass Valorization* **2012**, *3*, 443-449.

(35)   Chang, X.; Thind, S. S.; Chen, A. *ACS Catalysis* **2014**, *4*, 2616-2622.

(36)   Li, D.; Xia, Y. *Nano Letters* **2003**, *3*, 555-560.

(37)   Tan, B.; Wu, Y. *The Journal of Physical Chemistry B* **2006**, *110*, 15932-15938.

(38)   Zhao, L.; Yu, J.; Fan, J.; Zhai, P.; Wang, S. *Electrochemistry Communications* **2009**, *11*, 2052-2055.

(39)   Law, M.; Greene, L. E.; Johnson, J. C.; Saykally, R.; Yang, P. *Nature materials* **2005**, *4*, 455-459.

(40)   Ohsaki, Y.; Masaki, N.; Kitamura, T.; Wada, Y.; Okamoto, T.; Sekino, T.; Niihara, K.; Yanagida, S. *Physical Chemistry Chemical Physics* **2005**, *7*, 4157-4163.

(41)   Wang, C.; Yin, L.; Zhang, L.; Qi, Y.; Lun, N.; Liu, N. *Langmuir* **2010**, *26*, 12841-12848.

(42)   Huang, J.-q.; Huang, Z.; Guo, W.; Wang, M.-l.; Cao, Y.-g.; Hong, M.-c. *Crystal Growth and Design* **2008**, *8*, 2444-2446.

(43)   Perlich, J.; Kaune, G.; Memesa, M.; Gutmann, J. S.; Müller-Buschbaum, P. *Philosophical Transactions of the Royal Society of London A: Mathematical, Physical and Engineering Sciences* **2009**, *367*, 1783-1798.

(44)   Lechmann, M. C.; Kessler, D.; Gutmann, J. S. *Langmuir* **2009**, *25*, 10202-10208.

(45)   Liu, B.; Zeng, H. C. *Journal of the American Chemical Society* **2004**, *126*, 8124-8125.

(46)   Goossens, A.; Maloney, E. L.; Schoonman, J. *Chemical Vapor Deposition* **1998**, *4*, 109-114.

(47)   Yang, J.; Mei, S.; Ferreira, J. M. F. Materials Science Forum, 2004; p 556-559.

(48)   Tian, J.; Zhao, Z.; Kumar, A.; Boughton, R. I.; Liu, H. *Chemical Society Reviews* **2014**, *43*, 6920-6937.

(49)   Yin, S.; Fujishiro, Y.; Wu, J.; Aki, M.; Sato, T. *Journal of Materials Processing Technology* **2003**, *137*, 45-48.

(50)   Kim, C.-S.; Moon, B. K.; Park, J.-H.; Chung, S. T.; Son, S.-M. *Journal of crystal growth* **2003**, *254*, 405-410.

(51)   Kang, M. *Journal of Molecular Catalysis A: Chemical* **2003**, *197*, 173-183.

(52)   Enache-Pommer, E.; Liu, B.; Aydil, E. S. *Physical Chemistry Chemical Physics* **2009**, *11*, 9648-9652.

(53)   Bavykin, D. V.; Parmon, V. N.; Lapkin, A. A.; Walsh, F. C. *Journal of Materials Chemistry* **2004**, *14*, 3370-3377.

(54)   Zhou, W.; Du, G.; Hu, P.; Li, G.; Wang, D.; Liu, H.; Wang, J.; Boughton, R. I.; Liu, D.; Jiang, H. *Journal of Materials Chemistry* **2011**, *21*, 7937-7945.

(55)   Wu, H.; Fan, J.; Liu, E.; Hu, X.; Ma, Y.; Fan, X.; Li, Y.; Tang, C. *Journal of Alloys and Compounds* **2015**, *623*, 298-303.

(56)   Wight, A.; Davis, M. *Chemical reviews* **2002**, *102*, 3589-3614.

(57)   Zhang, H.; Banfield, J. F. *Chemistry of materials* **2005**, *17*, 3421-3425.

(58)   Lee, J. H.; Yang, Y. S. *Materials chemistry and physics* **2005**, *93*, 237-242.

(59)   Mahendiran, R.; Pandiyaraj, K. N.; Kandavelu, K.; Saravanan, D. *Journal of NanoScience and NanoTechnology* **2014**, *2*, 79-82.

(60)   Rodríguez-Reyes, M.; Dorantes-Rosales, H. J. *Journal of sol-gel science and technology* **2011**, *59*, 658-661.

(61)   Tahir, M.; Amin, N. S. *Applied Catalysis B: Environmental* **2015**, *162*, 98-109.

(62)   Chemseddine, A.; Moritz, T. *European journal of inorganic chemistry* **1999**, *1999*, 235-245.

(63)   Mutuma, B. K.; Shao, G. N.; Kim, W. D.; Kim, H. T. *Journal of colloid and interface science* **2015**, *442*, 1-7.

(64)   Rao, C.; Vivekchand, S.; Biswas, K.; Govindaraj, A. *Dalton Transactions* **2007**, 3728-3749.

(65)   Alarcón-Lladó, E.; Estradé, S.; Prades, J. D.; Hernandez-Ramírez, F.; Arbiol, J.; Peiró, F.; Ibáñez, J.; Artús, L.; Morante, J. R. *CrystEngComm* **2011**, *13*, 656-662.

(66)   Wu, J.-M.; Shih, H. C.; Wu, W.-T. *Chemical physics letters* **2005**, *413*, 490-494.

(67)   Boyd, D. A.; Greengard, L.; Brongersma, M.; El-Naggar, M. Y.; Goodwin, D. G. *Nano letters* **2006**, *6*, 2592-2597.

(68)   Ponja, S.; Sathasivam, S.; Chadwick, N.; Kafizas, A.; Bawaked, S. M.; Obaid, A. Y.; Al-Thabaiti, S.; Basahel, S. N.; Parkin, I. P.; Carmalt, C. J. *Journal of Materials Chemistry A* **2013**, *1*, 6271-6278.

(69)   Peng, X.; Chen, A. *Journal of Materials Chemistry* **2004**, *14*, 2542-2548.

(70)   Iijima, S. *nature* **1991**, *354*, 56-58.

(71)   Rao, C. N. R.; Müller, A.; Cheetham, A. K. *The chemistry of nanomaterials: synthesis, properties and applications*; John Wiley & Sons, 2006.

(72)   Lieber, C. M. *Solid state communications* **1998**, *107*, 607-616.

(73)   Hoyer, P. *Langmuir* **1996**, *12*, 1411-1413.

(74)   Suzuki, Y.; Yoshikawa, S. *Journal of Materials Research* **2004**, *19*, 982-985.

(75)   Kisumi, T.; Tsujiko, A.; Murakoshi, K.; Nakato, Y. *Journal of Electroanalytical Chemistry* **2003**, *545*, 99-107.

(76)   Kasuga, T.; Hiramatsu, M.; Hoson, A.; Sekino, T.; Niihara, K. *Langmuir* **1998**, *14*, 3160-3163.

(77)   Kasuga, T.; Hiramatsu, M.; Hoson, A.; Sekino, T.; Niihara, K. *Advanced Materials* **1999**, *11*, 1307-1311.

(78)   Fleischmann, M.; Thirsk, H.; Delahay, P. *Vol. 3Interscience, New York* **1963**, 123.

(79)   Paramasivam, I.; Macak, J.; Selvam, T.; Schmuki, P. *Electrochimica Acta* **2008**, *54*, 643-648.

(80)   Albu, S. P.; Ghicov, A.; Macak, J. M.; Schmuki, P. *physica status solidi (RRL)-Rapid Research Letters* **2007**, *1*, R65-R67.

(81)   Zwilling, V.; Darque‑Ceretti, E.; Boutry‑Forveille, A.; David, D.; Perrin, M.-Y.; Aucouturier, M. *Surface and Interface Analysis* **1999**, *27*, 629-637.

(82)   Macak, J. M.; Sirotna, K.; Schmuki, P. *Electrochimica Acta* **2005**, *50*, 3679-3684.

(83)   Macak, J. M.; Tsuchiya, H.; Taveira, L.; Aldabergerova, S.; Schmuki, P. *Angewandte Chemie International Edition* **2005**, *44*, 7463-7465.

(84)   Macak, J. M.; Tsuchiya, H.; Schmuki, P. *Angewandte Chemie International Edition* **2005**, *44*, 2100-2102.

(85)   Chang, X.; Thind, S. S.; Tian, M.; Hossain, M. M.; Chen, A. *Electrochimica Acta* **2015**, *173*, 728-735.

(86)   Mor, G. K.; Varghese, O. K.; Paulose, M.; Shankar, K.; Grimes, C. A. *Solar Energy Materials and Solar Cells* **2006**, *90*, 2011-2075.

(87)   Su, Z.; Zhou, W. *Advanced materials* **2008**, *20*, 3663-3667.

(88)   Macak, J.; Hildebrand, H.; Marten-Jahns, U.; Schmuki, P. *Journal of Electroanalytical Chemistry* **2008**, *621*, 254-266.

(89)   Albu, S. P.; Schmuki, P. *physica status solidi (RRL)-Rapid Research Letters* **2010**, *4*, 151-153.

(90)   Mohammadpour, F.; Behzadi, F.; Moradi, M. *Materials Letters* **2015**, *150*, 81-83.

(91)   Bauer, S.; Kleber, S.; Schmuki, P. *Electrochemistry Communications* **2006**, *8*, 1321-1325.

(92)   Yasuda, K.; Macak, J. M.; Berger, S.; Ghicov, A.; Schmuki, P. *Journal of the electrochemical society* **2007**, *154*, C472-C478.

(93)   Su, Z.; Zhou, W. *Journal of Materials Chemistry* **2011**, *21*, 357-362.

(94)   Macak, J. M.; Albu, S. P.; Schmuki, P. *physica status solidi (RRL)-Rapid Research Letters* **2007**, *1*, 181-183.

(95)   Zwilling, V.; Aucouturier, M.; Darque-Ceretti, E. *Electrochimica Acta* **1999**, *45*, 921-929.

(96)   Macak, J. M.; Tsuchiya, H.; Taveira, L.; Aldabergerova, S.; Schmuki, P. *Angewandte Chemie* **2005**, *117*, 7629-7632.

(97)   Choi, W.; Termin, A.; Hoffmann, M. R. *Angewandte Chemie* **1994**, *106*, 1148-1149.

(98)   Vitiello, R.; Macak, J.; Ghicov, A.; Tsuchiya, H.; Dick, L.; Schmuki, P. *Electrochemistry Communications* **2006**, *8*, 544-548.

(99)   Ghicov, A.; Macak, J. M.; Tsuchiya, H.; Kunze, J.; Haeublein, V.; Frey, L.; Schmuki, P. *Nano Letters* **2006**, *6*, 1080-1082.

(100)   Morikawa, T.; Asahi, R.; Ohwaki, T.; Aoki, K.; Taga, Y. *Japanese Journal of Applied Physics* **2001**, *40*, L561.

(101)   Chen, X.; Liu, L.; Peter, Y. Y.; Mao, S. S. *Science* **2011**, *331*, 746-750.

(102)   Aruna, S.; Tirosh, S.; Zaban, A. *Journal of Materials Chemistry* **2000**, *10*, 2388-2391.

(103)   Mikulas, T.; Fang, Z.; Gole, J. L.; White, M. G.; Dixon, D. A. *Chemical Physics Letters* **2012**, *539*, 58-63.

(104)   Inturi, S. N. R.; Boningari, T.; Suidan, M.; Smirniotis, P. G. *The Journal of Physical Chemistry C* **2013**, *118*, 231-242.

(105)   Liu, B.; Chen, H. M.; Liu, C.; Andrews, S. C.; Hahn, C.; Yang, P. *Journal of the American Chemical Society* **2013**, *135*, 9995-9998.

(106)   Choi, W.; Termin, A.; Hoffmann, M. R. *The Journal of Physical Chemistry* **1994**, *98*, 13669-13679.

(107)   Wang, Y.; Hao, Y.; Cheng, H.; Ma, J.; Xu, B.; Li, W.; Cai, S. *Journal of Materials Science* **1999**, *34*, 2773-2779.

(108)   Asahi, R.; Morikawa, T.; Ohwaki, T.; Aoki, K.; Taga, Y. *science* **2001**, *293*, 269-271.

(109)   Wang, Z.; Yang, C.; Lin, T.; Yin, H.; Chen, P.; Wan, D.; Xu, F.; Huang, F.; Lin, J.; Xie, X. *Energy & Environmental Science* **2013**, *6*, 3007-3014.

(110)   Zhao, Z.; Tan, H.; Zhao, H.; Lv, Y.; Zhou, L.-J.; Song, Y.; Sun, Z. *Chemical Communications* **2014**, *50*, 2755-2757.

(111)   Zou, X.; Liu, J.; Su, J.; Zuo, F.; Chen, J.; Feng, P. *Chemistry–A European Journal* **2013**, *19*, 2866-2873.

(112)   Kang, Q.; Cao, J.; Zhang, Y.; Liu, L.; Xu, H.; Ye, J. *Journal of Materials Chemistry A* **2013**, *1*, 5766-5774.

(113)   Tominaka, S.; Tsujimoto, Y.; Matsushita, Y.; Yamaura, K. *Angewandte Chemie International Edition* **2011**, *50*, 7418-7421.

(114)   Xu, C.; Song, Y.; Lu, L.; Cheng, C.; Liu, D.; Fang, X.; Chen, X.; Zhu, X.; Li, D. *Nanoscale research letters* **2013**, *8*, 1.

(115)   Zhang, Z.; Hedhili, M. N.; Zhu, H.; Wang, P. *Physical Chemistry Chemical Physics* **2013**, *15*, 15637-15644.

(116)   Jang, J. S.; Choi, S. H.; Kim, H. G.; Lee, J. S. *The Journal of Physical Chemistry C* **2008**, *112*, 17200-17205.

(117)   Zhang, F.; Miao, S.; Yang, Y.; Zhang, X.; Chen, J.; Guan, N. *The Journal of Physical Chemistry C* **2008**, *112*, 7665-7671.

(118)   Yogi, C.; Kojima, K.; Takai, T.; Wada, N. *Journal of materials science* **2009**, *44*, 821-827.

(119)   Jakob, M.; Levanon, H.; Kamat, P. V. *Nano Letters* **2003**, *3*, 353-358.

(120)   Zhang, N.; Liu, S.; Fu, X.; Xu, Y.-J. *The Journal of Physical Chemistry C* **2011**, *115*, 9136-9145.

(121)   Hou, W.; Liu, Z.; Pavaskar, P.; Hung, W. H.; Cronin, S. B. *Journal of catalysis* **2011**, *277*, 149-153.

(122)   Kongkanand, A.; Tvrdy, K.; Takechi, K.; Kuno, M.; Kamat, P. V. *Journal of the American Chemical Society* **2008**, *130*, 4007-4015.

(123)   Sun, W.-T.; Yu, Y.; Pan, H.-Y.; Gao, X.-F.; Chen, Q.; Peng, L.-M. *Journal of the American Chemical Society* **2008**, *130*, 1124-1125.

(124)   Xu, S.; Pan, S.; Xu, Y.; Luo, Y.; Zhang, Y.; Li, G. *Journal of hazardous materials* **2015**, *283*, 7-13.

(125)   Maness, P.-C.; Smolinski, S.; Blake, D. M.; Huang, Z.; Wolfrum, E. J.; Jacoby, W. A. *Applied and environmental microbiology* **1999**, *65*, 4094-4098.

(126)   Wu, G.; Wen, J.; Nigro, S.; Chen, A. *Nanotechnology* **2010**, *21*, 085701.

(127)   Thind, S. S.; Wu, G.; Tian, M.; Chen, A. *Nanotechnology* **2012**, *23*, 475706.

(128)   Zheng, Y.; Luo, C.; Liu, L.; Yang, Z.; Ren, S.; Cai, Y.; Xiong, J. *Materials Letters* **2016**.

(129)   Amano, F.; Prieto-Mahaney, O.-O.; Terada, Y.; Yasumoto, T.; Shibayama, T.; Ohtani, B. *Chemistry of Materials* **2009**, *21*, 2601-2603.

(130)   Cao, B.; Li, G.; Li, H. *Applied Catalysis B: Environmental* **2016**, *194*, 42-49.

(131)   Yu, J.; Qi, L.; Jaroniec, M. *The Journal of Physical Chemistry C* **2010**, *114*, 13118-13125.

(132)   Wang, F.; Jiang, Y.; Lawes, D. J.; Ball, G. E.; Zhou, C.; Liu, Z.; Amal, R. *ACS Catalysis* **2015**, *5*, 3924-3931.

(133)   Yang, S.; Zheng, Y. C.; Hou, Y.; Yang, X. H.; Yang, H. G. *Physical Chemistry Chemical Physics* **2014**, *16*, 23038-23043.

(134)   Saeki, M.; Akagi, H.; Fujii, M. *Journal of chemical theory and computation* **2006**, *2*, 1176-1183.

(135) Muduli, S.; Game, O.; Dhas, V.; Vijayamohanan, K.; Bogle, K.; Valanoor, N.; Ogale, S. B. *Solar Energy* **2012**, *86*, 1428-1434.

(136) Matos, J.; Borodzinski, A.; Zychora, A. M.; Kedzierzawski, P.; Mierzwa, B.; Juchniewicz, K.; Mazurkiewicz, M.; Hernández-Garrido, J. C. *Applied Catalysis B: Environmental* **2015**, *163*, 167-178.

(137) Antolini, E. *Applied Catalysis B: Environmental* **2009**, *88*, 1-24.

(138) Park, K.-W.; Seol, K.-S. *Electrochemistry Communications* **2007**, *9*, 2256-2260.

(139) Gojković, S. L.; Babić, B.; Radmilović, V.; Krstajić, N. *Journal of Electroanalytical Chemistry* **2010**, *639*, 161-166.

(140) Vračar, L. M.; Gojković, S. L.; Elezović, N.; Radmilović, V.; Jakšić, M.; Krstajić, N. *J New Mater Electrochem Syst* **2006**, *9*, 99-106.

(141) Yu, J.; Liu, Z.; Zhai, L.; Huang, T.; Han, J. *International Journal of Hydrogen Energy* **2016**, *41*, 3436-3445.

(142) Li, Y.; Liu, C.; Liu, Y.; Feng, B.; Li, L.; Pan, H.; Kellogg, W.; Higgins, D.; Wu, G. *Journal of Power Sources* **2015**, *286*, 354-361.

(143) Hu, Y.; Zhu, A.; Zhang, C.; Zhang, Q.; Liu, Q. *International Journal of Hydrogen Energy* **2015**, *40*, 15652-15662.

(144) Zhuang, W.; He, L.; Zhu, J.; An, R.; Wu, X.; Mu, L.; Lu, X.; Lu, L.; Liu, X.; Ying, H. *International Journal of Hydrogen Energy* **2015**, *40*, 3679-3688.

(145) Qin, Y. H.; Li, Y.; Lv, R. L.; Wang, T. L.; Wang, W. G.; Wang, C. W. *Journal of Power Sources* **2015**, *278*, 639-644.

(146) Chen, H.; Wang, S. X.; Zhao, W. L.; Zhang, N. N.; Zheng, Y. P.; Sun, Y. M. *Acta Physico-Chimica Sinica* **2015**, *31*, 302-308.

Chapter 3: Materials and methods

3.1 Introduction

This chapter briefly discusses the methods employed to synthesize the TiO_2 nanomaterials in this study. The different instrumentation and techniques utilized to characterize the fabricated TiO_2 nanomaterials are also presented in this chapter.

3.2 Experimental

3.2.1 Materials

Titanium plates (99.2%) were purchased from Alfa Aesar, and Rh B was purchased from BDH, UK. Ethylene glycol (99.5%) and methanol were purchased from Caledon Laboratories Ltd Canada. All other utilized chemicals were of reagent grade and purchased from Sigma-Aldrich.

The water (18.2 MΩ cm) that was utilized for all experimental solutions was purified by a Nanopure Diamond water system. All solutions were deaerated with ultrapure Ar (99.999%) prior to the experiments.

3.2.2 Instruments and electrochemical experiments

The surface morphology, composition and crystalline phase of the synthesized TiO_2 nanomaterials were characterized by field-emission scanning electron microscopy (FE-SEM, Hitachi SU 70), XRD (Philips PW 1050-3710 Diffractometer with Cu Ka radiation) and XPS (Omicron EA-125 energy analyzer and a multichannel detector). All binding energies reported in this work were corrected using the C 1s peak at 284.5 eV as an internal standard. The broad Ti 2p region of the sample was fitted using XPSPEAK41 software. The UV/vis spectra of organic

solution were recorded to monitor the oxidation process in situ, using a Cary 50 UV/vis spectrophotometer. The total organic carbon (TOC) of the organic solution prior to and after the degradation was measured using a TOC analyser (TOC-L CPH, Shimadzu). EPR spectra were recorded on a Bruker A200- 9.5/12 at 100 K.

The electrochemical measurements were carried out at room temperature (20 ± 2 °C) using a Voltalab 40 Potentiostep (PGZ301). A three-electrode cell system was employed for the electrochemical studies. A Pt coil with a 10 cm^2 surface area was utilized as the auxiliary electrode, and a Ag/AgCl electrode was used as the reference electrode.

An ADAC SystemsTM Cure SpotTM 50 with an intensity of 7.4 mW cm^{-2} was employed as UV-visible light source. A Small Collimated Beam Solar Simulator (SF150C, Sciencetech Inc) with an intensity of one Sun was employed to introduce solar light into the reactor. The visible light source employed in this study consisted of an Oriel system including a 300 W xenon arc lamp. Meanwhile, infrared light and all light wavelengths below 400 nm were blocked by a water filter and an optical filter (Edmund Optical Co. GG420), respectively. The intensity of resulting light between 400 and 700 nm was measured to be ~2.50 mW cm^{-2} using a Cole-Palmer Instrument (Radiometer Series 9811).

3.2.3 Synthesis of TiO$_2$ nanomaterials

3.2.3.1 Synthesis of TiO$_2$ nanotubes

The TiO$_2$ nanotubes were directly grown on titanium plates through a one-step anodization process in a two-electrode cell with a Ti plate (1.25 cm × 0.8 cm × 0.5 mm) as the anode, and a Pt coil as the cathode, respectively. To begin with, the Ti plates were sonicated in acetone for 15 min, and then etched in 18% HCl at 85 °C for 10 min. The prepared Ti plates were then anodized in

DMSO + 2% HF at 40 V for a different period of time varied from 4 H to 20 H. Then, to obtain an anatase crystal structure, the fabricated TiO_2 nanotubes were annealed at 450 ℃ for 3 hours.[1]

3.2.3.2 Synthesis of nanoporous TiO₂

Received Ti was cut into Ti pieces (1.25 cm × 0.8 cm × 0.5 mm) and initially sonicated in acetone followed by rinsing with ultrapure water. The clean titanium plates were then etched in 18% HCl at 85 °C for 10 min. After etching, the titanium plates were thoroughly rinsed with ultrapure water and immerged into an electrochemical cell as an anode for anodization. The electrolyte was ethylene glycol + 0.3 wt% NH_4F + 2 wt% H_2O and the counter electrode was platinum mesh. After the initial 5 hours anodization at 50 V, the irregular as-fabricated nanoporous TiO_2 layer was peeled off with masking tape. Then the same Ti plate was anodized for another 2 hours at 50 V, afterwards the TiO_2 layer was removed again by applying masking tape. Lastly, a 15 minutes anodization at 50 V was carried out on this Ti plate to generate the final highly ordered nanoporous TiO_2. Next the electrode was annealed at 450°C for 3 h to ensure the formation of anatase crystal structure of TiO_2.[2]

3.3 Modification of TiO₂ nanomaterials

The TiO_2 nanomaterials were treated in 0.1 M H_2SO_4 at different cathodic current densities varied from -2.5 mA cm^{-2} to -10 mA cm^{-2} for a different period of time varied from 2.5 min to 40 min.

For photochemical deposition of Pt and Pb, 20 microliters from an equimolar solution of 0.1 M $Pb(NO_3)_2$ and 0.1 M $H_2PtCl_6 • 6H_2O$ were taken and added into 5 mL of 50% methanol solution (v/v) with nanoporous TiO_2 electrode suspended in it. This solution was degassed with continuous flow of Ar and then caped and was irradiated under UV light for 1 h. For comparison a Pt deposited

TiO$_2$ electrode was fabricated with 40 microliters of 0.1 M H$_2$PtCl$_6$ • 6H$_2$O under the same conditions.

3.4 Catalytic activities measurements

The catalytic activity of the fabricated TiO$_2$ nanotubes was evaluated by measuring electrochemical oxidation of SA or lignin solution at different applied current densities, in which the TiO$_2$ nanotubes electrode was used as electrocatylyst. The photoelectrocatalytic oxidation of RhB was investigated to examine the photoelectrocatalytic activity of the synthesized nanoporous TiO$_2$ under UV-visible light, solar light and visible light with the applied electrode potential of 1.0 V versus Ag/AgCl. In all the oxidation experiments, the solutions were stirred by a magnetic stirrer, and the samples were collected at regular time intervals to monitor the oxidation process by UV-visible spectrometer. The Pt and Pd nanocomposite modified nanoporous TiO$_2$ was tested as bifunctional electrode for methanol oxidation under solar irradiation. In all the photochemical experiments, the distance between the surface of the TiO$_2$ electrode and light source was kept constant.

References

(1)   Chang, X.; Thind, S. S.; Chen, A. *ACS Catalysis* **2014**, *4*, 2616-2622.

(2)   Chang, X.; Thind, S. S.; Tian, M.; Hossain, M. M.; Chen, A. *Electrochimica Acta* **2015**, *173*, 728-735.

Chapter 4: Electrocatalytic Enhancement of Salicylic Acid Oxidation at Electrochemically Reduced TiO₂ Nanotubes[*]

4.1 Introduction

TiO₂ is undeniably one of the most intensely studied semiconductors in materials science due to its unique combination outstanding properties, such as biological and chemical inertness, high efficiency, low cost, environmental tolerance and high stability.[1-4] Despite significant efforts that have been expended toward the application of TiO₂ as a photocatalyst,[5] its photochemical utility has been impeded by the fact that it may only be activated by UV light, owing to its large bandgap (~3.0 eV for rutile and ~3.2 eV for anatase).[6-8] As a consequence, there has arisen a great interest in the performance of bandgap engineering (e.g., narrowing of the bandgap) and myriad techniques have been applied to toward enabling TiO₂, to efficiently utilize solar energy. These approaches encompass doping with non-metal elements, reduction via the application of vacuum or reducing conditions (e.g., H₂), chemical vapor deposition and high energy particle bombardment.[9-16]

Salicylic acid (SA) is a common organic water pollutant that is generated by cosmetic industries, pharmaceutical wastewater, paper mill wastewater and landfill leachate.[17-20] It is known, for example, that salicylic acid has an ototoxic effect and can also bring about salicylism, fetal abnormalities and central nervous system depression damage.[21-22] Therefore, a heightened interest in the investigation of advanced technologies to treat SA has evolved, driven by the inefficiencies of conventional treatment processes. Recent studies have indicated that advanced

---

* Most of the results presented in this chapter have been published in *ACS Catalysis* **2014**, 4, 2616-2622.

oxidation processes (AOPs), especially electrochemical methods, are very attractive for the treatment of water that has been contaminated with organic substances.[23-30] In contrast with other technologies (e.g., wet air oxidation processes (WAO)) that require severe operational conditions,[31-32] the removal of pollutants utilizing electrochemical methods may be achieved at room temperature under ambient atmospheric pressure. A wide variety of anode materials have been reported to facilitate the electrochemical remediation of organic compounds, including carbon, Pt, PbO_2, IrO_2, SnO_2, Pt-Ir, and boron-doped diamond (BDD) electrodes.[33-38] Although these catalysts are widely employed due to their high electric conductivity, they also harbor a number of weak points such as toxicity, high energy consumption and expense. Since the discovery of the photocatalytic oxidation of water over TiO_2, minimal research has been conducted in the study of TiO_2 as an electrocatalyst because its low electrical conductivity prevents its use as such. There exist a few reports in the literature that describe the modification of TiO_2 with carbon or noble metals with the aim of increasing its conductivity and subsequent use for the electrochemical reduction of organic pollutants. To the best of our knowledge, no work has been reported that utilizes electrochemically reduced TiO_2 as an electrocatalyst for the electrochemical oxidation of SA in wastewater treatment.

In the present work, it is reported on the discovery of the significantly enhanced electrochemical activity of TiO_2 nanotubes that were treated by electrochemical reduction and tested as a novel electrocatalyst for the electrochemical oxidation of SA. SEM, XRD, XPS, CV, chronamperometry and chronopotentiometry were employed to characterize the structure, morphology, composition, and electrochemical activity of the TiO_2 nanotubes. The effects of time and current on the electrochemical reduction process were investigated to elucidate optimal treatment conditions. Moreover, the electrocatalytic behavior of the reduced TiO_2 was studied

using the electrochemical oxidation of 30 ppm SA in 0.1 M H_2SO_4 under a 3 mA cm^{-2} applied current at room temperature. The oxidation of SA at treated TiO_2 nanotubes was found to be 6.3 times greater than that at a Pt electrode. In addition, the stability and donor density of the TiO_2 nanotubes were also studied.

4.2 Experimental

4.2.1 Materials

Reagent grade salicylic acid (99+%) and titanium plates (99.2%) were purchased from Sigma-Aldrich and Alfa Aesar, respectively, and used as received. All other utilized chemicals were of reagent grade and used as supplied. The water (18.2 MΩ cm) that was utilized for all experimental solutions was purified by a Nanopure Diamond® water system.

4.2.2 Fabrication and treatment of TiO_2 nanotubes

The fabrication of TiO_2 nanotubes is already discussed in section 3.2.3.1 of chapter 3. The TiO_2 nanotubes were then treated in 0.1 M H_2SO_4 at different cathodic current densities which varied from -2.5 to -10 mA cm^{-2} for a different period of time varied from 2.5 to 40 min.

4.2.3 Characterization of the synthesized TiO_2 nanotubes

The synthesized TiO_2 nanotubes were characterized by SEM (JEOL5900LV) and XRD (Philips PW 1050-3710 Diffractometer with Cu Kα radiation). The surface composition was examined by XPS (Omicron EA-125 energy analyzer and a multi-channel detector). All binding energies reported in this work were corrected using the C1s peak at 284.5 eV as an internal standard. The broad Ti2p region of the sample was fitted using XPSPEAK41 software. A three-electrode cell system was employed for the electrochemical studies. A Pt coil with a 10 cm^2 surface area was utilized as the auxiliary electrode, and a Ag/AgCl electrode was used as the reference

electrode. To enable a comparison to the TiO_2 working electrodes, a 1 cm^2 polycrystalline Pt wire was also employed as the working electrode. The current density was calculated based on the geomentric surface area. The electrochemical measurements were carried out at room temperature (20 ± 2 °C) using a Voltalab 40 Potentiostep (PGZ301). CV, chronoamperometry and chronopotentiometry were used to characterize the electrochemical activity of TiO_2 nanotubes. Cyclic voltammograms (CVs) were recorded in a 0.1 M H_2SO_4 solution at a sweep rate of 20 mV/s, whereas chronoamperometric curves were measured where the electrode potential was held at 0 V for 30 s and then increased to 2.4 V for 5 min. Mott–Schottky plots were measured at a fixed frequency of 500 Hz in a 0.1 M H_2SO_4 solution.

4.2.4 Electrochemical Oxidation of Salicylic Acid in 0.1 M H_2SO_4

The synthesized TiO_2 nanotubes were utilized as the working electrode, a Pt coil served as the counter electrode, whereas the reference electrode was comprised of Ag/AgCl. The UV/vis spectra of SA were recorded over the range of 200–450 nm in order to monitor the oxidation process in situ, using a Cary 50 UV/vis spectrophotometer, displaying two peaks at ca. 236 and 302 nm, respectively. The peak at 236 nm was employed as the calibration curve due to the relatively high sensitivity.

A seven-point calibration was conducted with SA concentrations that varied from 0 to 30 ppm. A linear relationship was achieved with the regression equations C(ppm) = 16.40A – 0.1102 (Figure not shown). Good correlation coefficients (R^2 = 0.999) indicated that the 236 nm peak could be used to adequately convert absorbance readings to concentrations.

4.3 Results and discussion

4.3.1 Characterization of TiO$_2$ nanotubes

The structure and morphology of the TiO$_2$ nanotubes were characterized by SEM. As shown in Figure 4.1A, the synthesized self-organized nanotubes consisted of pored arrays with uniform diameters of ca. 100 nm where the pore lumens were open at the top of the layer. The EDX of the nanotubes (Figure 4.1B) illustrated strong oxygen and titanium peaks, which confirmed the composition of the formed nanotube arrays. Figure 4.1C revealed the corresponding XRD patterns of the prepared TiO$_2$ nanotubes prior to and following the electrochemical reduction. Except for the peaks (marked with stars), derived from the Ti substrate, all of the diffraction peaks were attributed to the tetragonal anatase TiO$_2$, showing that the formed TiO$_2$ nanotubes exist in the anatase phase. Moreover, the XRD spectra prior to and following the electrochemical reduction were almost identical, indicating that there was no alteration in the crystalline structure subsequent to the electrochemical reduction.

4.3.2 Electrochemical reduction of TiO$_2$ nanotubes

In order to elucidate the optimal electrochemical reduction conditions, the effects of applied current and time on the electrochemical activity of the TiO$_2$ nanotubes were examined with different applied current densities, spanning -2.5, -5, -7.5 and -10 mA cm^{-2} over different timelines, respectively. The second cycles of the CVs of the TiO$_2$ nanotubes prior to and following electrochemical reductions, which employed different current densities, are depicted in Figure 4.2A and 4.2B, respectively. The shape of the CVs and the corresponding currents
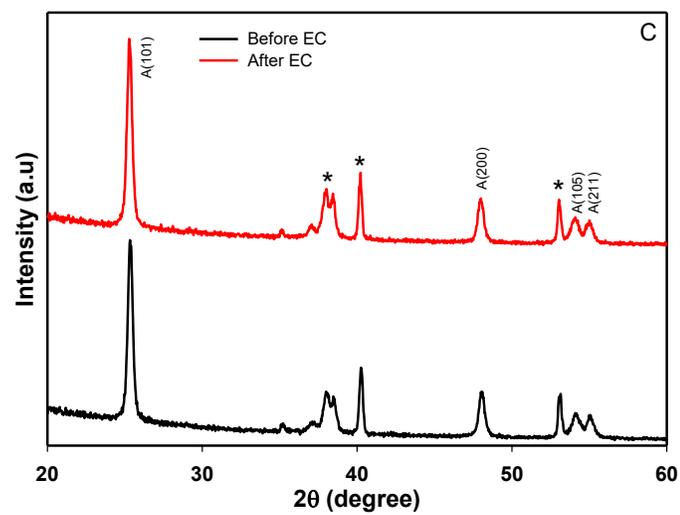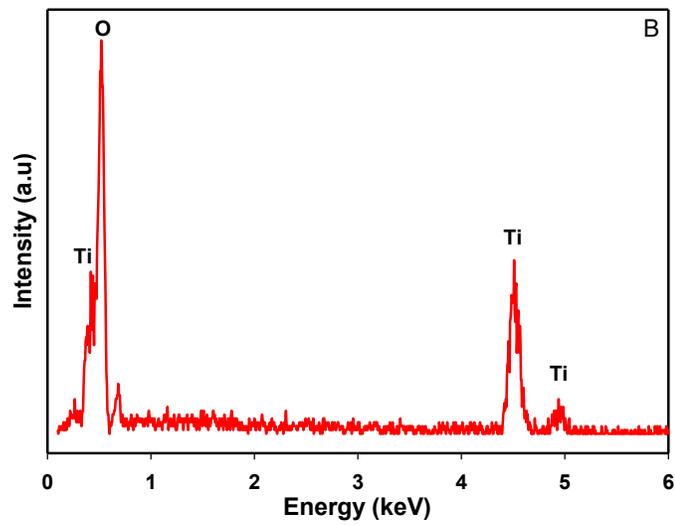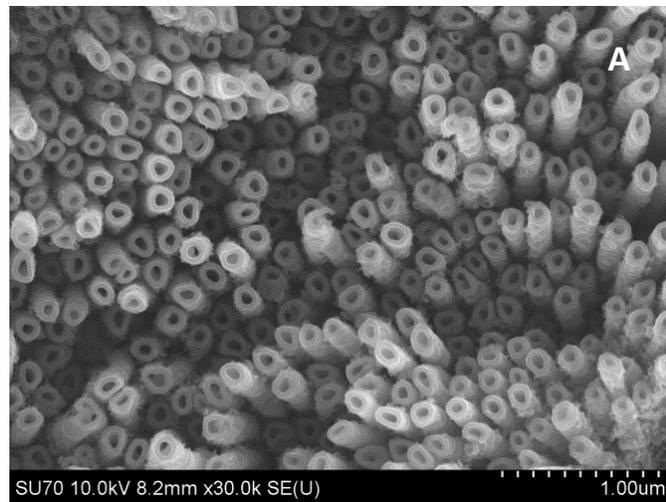
Figure 4.1 SEM image (A), EDX (B) and XRD (C) of the fabricated TiO$_2$ nanotubes.
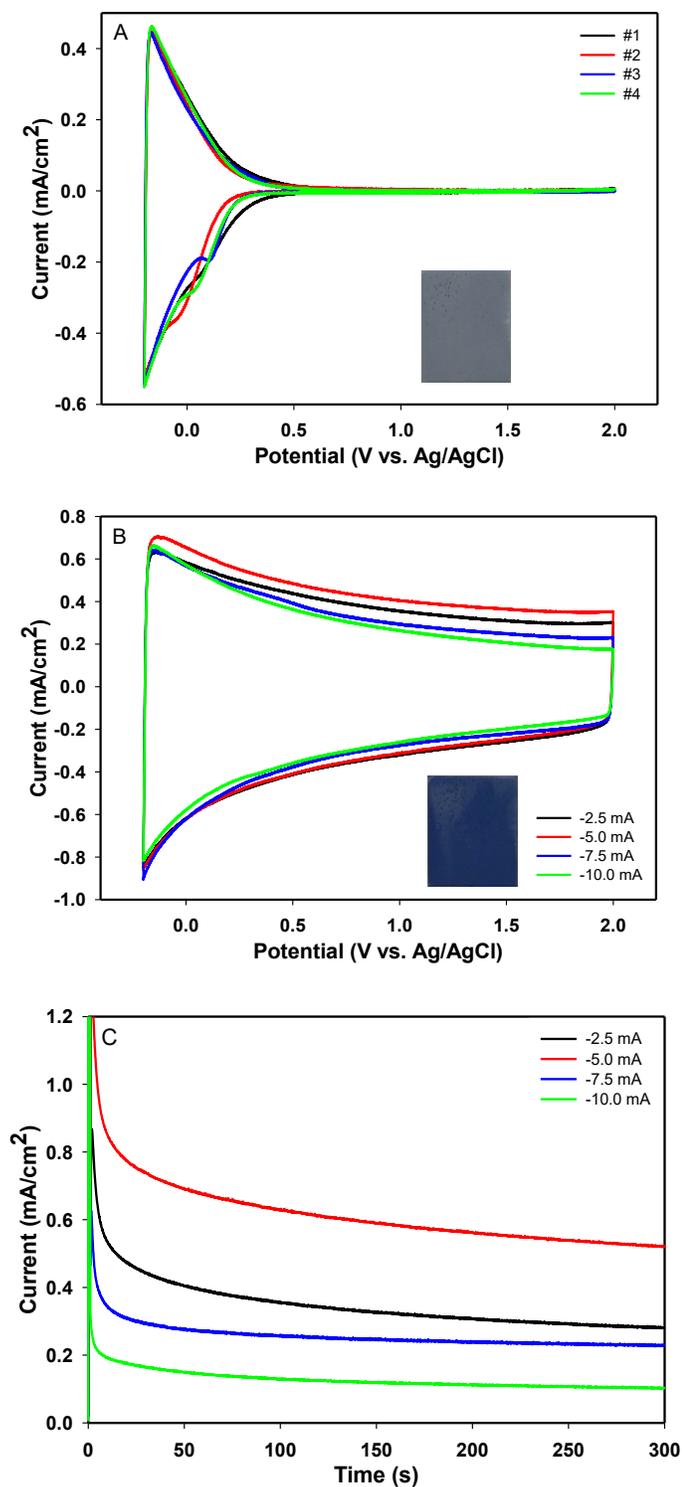
Figure 4.2 CVs of the TiO_2 nanotubes electrodes (A) prior to and (B) following the treatment at different currents for 10 min in 0.1 M H_2SO_4 at a sweep rate of 20 mV/s. (C) Chronoamperometric curves of the TiO_2 nanotubes electrodes treated at different currents for 10 min in 0.1 M H_2SO_4. Insets in (A) and (B) are the digital images of the TiO_2 nanotubes prior to and following electrochemical reduction.

remained constant with the subsequent cycling. The CVs of four electrodes (#1 - #4) of the TiO_2

nanotube prior to electrochemical reduction are very similar and they may be divided into two

distinct regions: (I) the region at an initial stage where hydrogen adsorption/desorption proceeds

between -0.2 and 0.35 V; and (II) the double-layer charging region, between 0.35 and 2.0 V. As

shown in Figure 4.2B, the current was significantly increased following the electrochemical

reduction with various applied current densities varied from -2.5 to -10 mA cm^{-2}, especially in

Region II. An almost rectangular CV curve was observed, showing that the electrochemically

treated TiO_2 nanotubes behaved as a pure capacitor. Meanwhile, the color of the TiO_2 nanotube

electrode was dramatically affected by the electrochemical reduction process. As can be seen in

the insets of Figure 4.2A and B, the original gray color of the electrode was transitioned to dark

blue, indicative of structural changes in the TiO_2 that were initiated by the treatment. Figure 4.2C

presents the chronoamperometric curves of the TiO_2 nanotubes that were treated under different

current densities for 10 min, showing that the achieved steady-state current densities of the treated

TiO_2 nanotubes strongly depend on the applied cathodic current densities. The cathodic tratement

under -5.0 mA cm^{-2} resulted in the highest steady-state current.

To optimize the cathodic treatment conditions, we further investigated the effect of time on

the electrochemical reduction of the TiO_2 nanotubes at -5.0 mA cm^{-2}. Figure 4.3 presents the CVs

and chronoamperometric curves of the TiO_2 nanotubes before and after the cathodic treatment over

different time intervals. As shown in Figure 4.3A, even being reduced for only 2.5 min, the CV

was dramatically changed in comparison with the initial CV. However, no obvious changes were

observed when the reduction time was increased from 2.5 to 40 min. In contrast, significant

differences were seen in the chronoamperometric curves presented in Figure 4.3B. Figure 4.3C

displays the steady-state current densities which were measured from the chronoamperometric
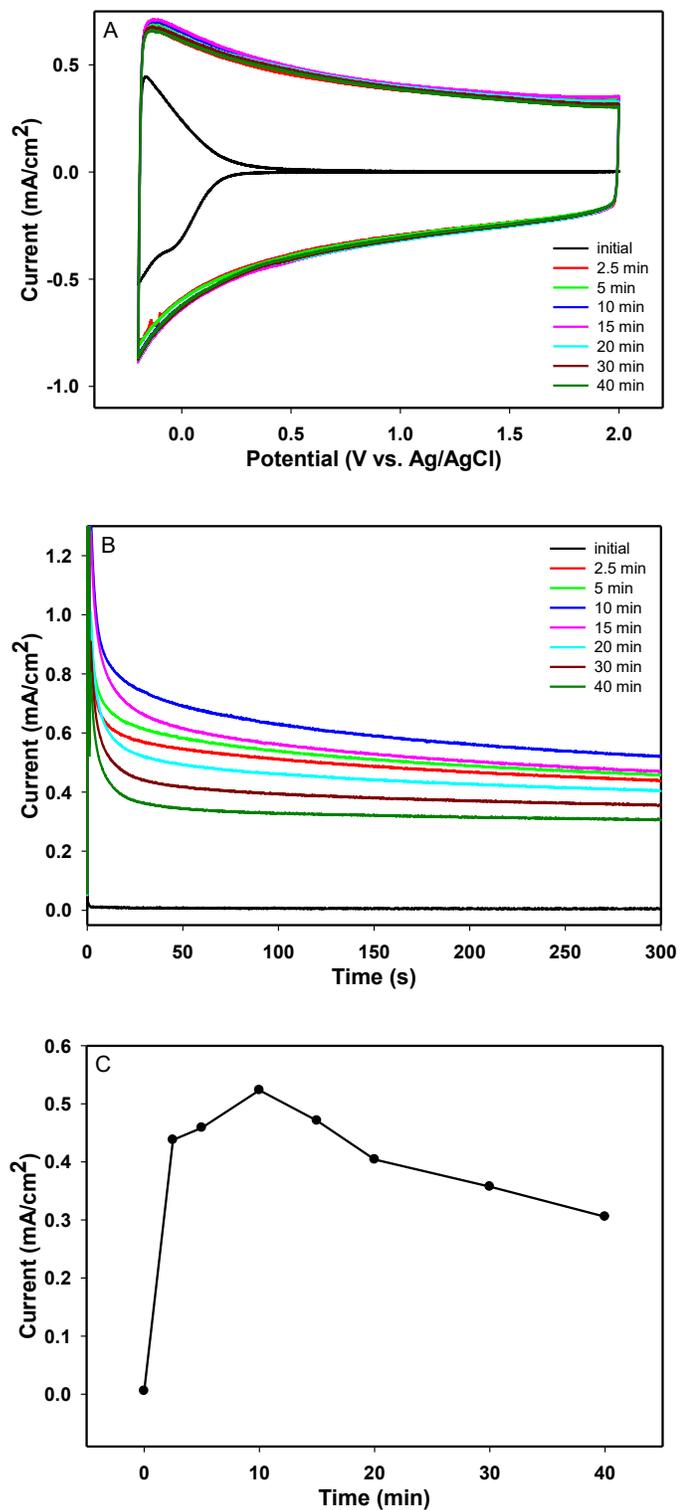
Figure 4.3 (A) CVs and (B) Chronoamperometric curves of the TiO_2 nanotube electrode before and after being cathodically treated at -5 mA cm^{-2} for different time periods in 0.1 M H_2SO_4 at 2.4 V. (C) Plot of the stead-state currents measured at 300 s from the curves presented in panel B *versus* the time of the electrochemical treatment.

curves at 300 s, showing that 10 min was optimal in maintaining the highest current density, which is approximately 30 times higher than that of the untreated TiO_2 nanotube electrode. Higher current or longer time may decrease the stability of the TiO_2 nanotubes or even results in detaching the TiO_2 nanotubes from the Ti substrate.
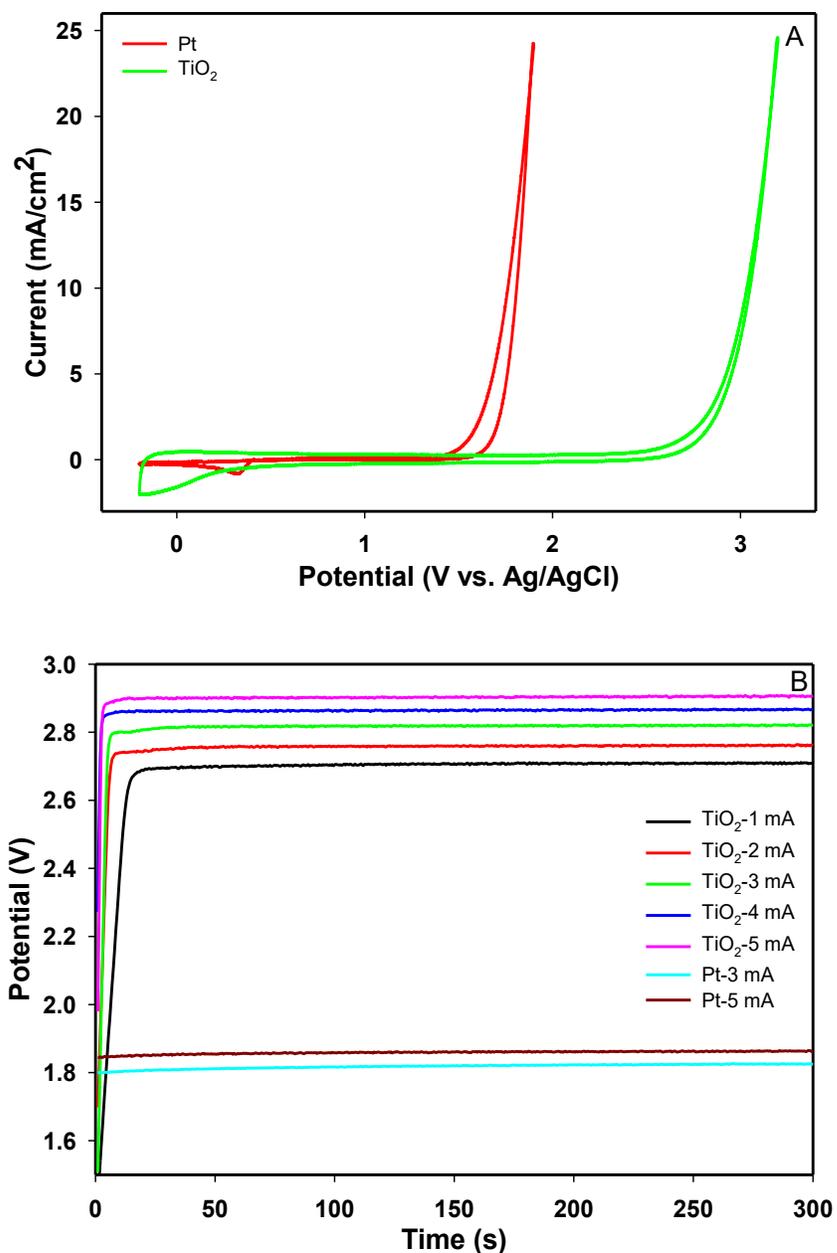
Figure 4.4 Comparison of the CVs (A) and chronopotentiometric curves (B) of the treated TiO_2 nanotubes and a Pt electrode recorded in 0.1 M H_2SO_4 + 30 ppm SA.
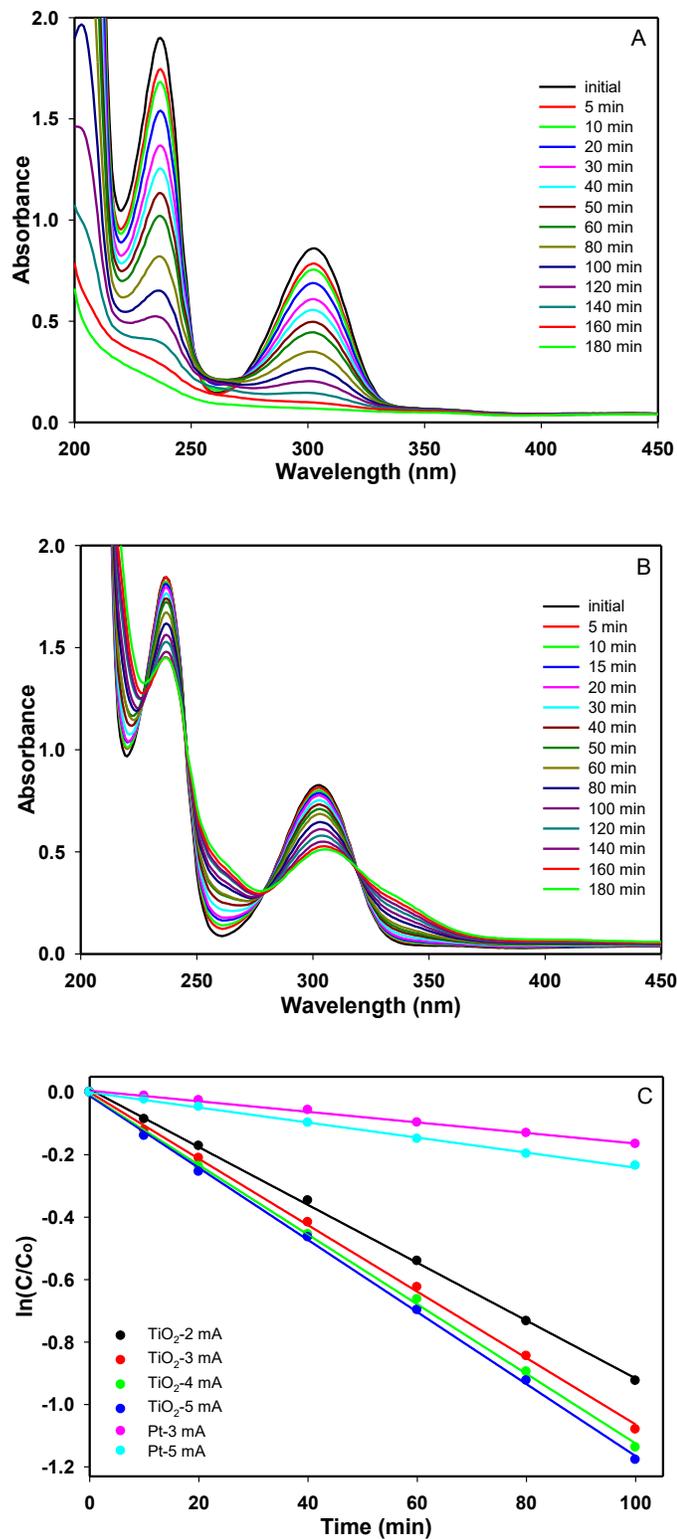
Figure 4.5 The absorbance spectra for the electrochemical oxidation of 30 ppm SA in 0.1 M H_2SO_4 at (A) the treated TiO_2 nanotubes and (B) the Pt electrode with a current density of 3 mA cm^{-2}. (C) Plot of $ln(C/C_o)$ *versus* time of the electrochemical oxidation of SA at the treated TiO_2 nanotubes and the Pt electrode with different current densities.

Table 4.1 The first-order kinetic constants and relative coefficients for the electrochemical oxidation of SA at the TiO_2 nanotubes treated at -5 mA cm^{-2} for 10min and a Pt electrode.

Electrode	Current density (mA cm^{-2})	Rate Constant (min^{-1})	R^2
TiO_2 nanotubes	2.0	9.22×10^{-3}	0.999
TiO_2 nanotubes	3.0	1.06×10^{-2}	0.999
TiO_2 nanotubes	4.0	1.11×10^{-2}	0.999
TiO_2 nanotubes	5.0	1.15×10^{-2}	0.999
Pt	3.0	1.69×10^{-3}	0.997
Pt	5.0	2.40×10^{-3}	0.998

4.3.3 Electrochemical oxidation of SA at the treated TiO_2 nanotube electrode

For Comparison, a polycrystalline Pt electrode with a geometric surface area of 1 cm^2 was also tested in this study. The CVs of the treated TiO_2 nanotubes cathodically treated under the optimal conditions (-5.0 mA cm^{-2} and 10 min) and the Pt electrode, recorded in 30 ppm SA in a 0.1 M H_2SO_4 solution, are presented in Figure 4.4A, showing that the overpotential for oxygen evolution was dramatically increased from ~1.3 V for the Pt electrode to ~2.6 V for the treated TiO_2 nanotubes. It is interesting to notice that the CV curve of the treated TiO_2 nanotubes recorded in the absence of SA was almost identical to the CV curve measured in the presence of SA as shown in Figure 4.4A, indicating that direct electrochemical oxidation of SA occured due to the generation of ·OH at the TiO_2 nanotubes. The significant potential increase was further evidenced by the chronopotentiometric (CP) measurements presented in Figure 4.4B. It is well known that the high overpotentail for oxygen evolution is highly beneficial to the electrochemical oxidation of organic pollutants. Lead dioxide and BDD electrodes have been widely studied as anode materials for electrochemical treatment of wastewater because of their inherent high overpotential for oxygen evolution.[39] All the aforementioned results suggest that the treated TiO_2 nanotubes can be classified as an 'inactive' electrode, like BDD, and would be more optimal for applications in the electrochemical oxidation of organic pollutants than the Pt electrode.

In order to determine the enhanced activity of electrochemically treated TiO_2 nanotube electrode, we investigated the electrochemical oxidation of SA at different applied current densities. Figure 4.5A presents the time dependence of the spectra absorbance of 30 ppm SA in 0.1 M H_2SO_4 with an applied current of 3 mA cm^{-2} during the electrochemical oxidation at the treated TiO_2 nanotubes. The UV-Vis spectra were taken every 5 min for the initial 10 min, then every 10 min for the remaining 50 min and every 20 min for the final 2 h. The absorbance peaks of SA at 236 (Peak *a*) and 303 nm (Peak *b*) decreased with the increase of the electrochemical oxidation time. Peak *a* approached 0.197 after 3 h of degradation, corresponding to ca. 90% removal of SA from the solution. For comparison, the electrochemical oxidation of SA was also performed at a Pt polycrystalline electrode under the same experimental condition (Figure 4.5B), where a ca. 21% removal of SA from solution was observed.

On the basis of the linear regression equation developed in Section 2.4 and the absorbance peak at 236 nm, we calculated the concentrations of SA during electrochemical oxidation. As shown in Figure 4.5C, the electrochemical oxidation of SA at treated TiO_2 nanotubes and Pt wires was fitted well based on the first-order kinetics. The derived rate constants are listed in Table 4.1 The rate was increased from 9.22×10^{-3} to 1.06×10^{-2} min^{-1} with an increase of the applied current density from 2.0 to 3.0 mA cm^{-2}, showing that higher applied currents had a positive effect on the oxidation of SA at the treated TiO_2 nanotubes. However, the rate constant was only slightly increased with the further increase of the current density from 3.0 to 4.0 and 5.0 mA cm^{-2}. In cognizance of power consumption, 3.0 mA cm^{-2} was selected as the optimized current for the electrochemical oxidation of SA at the treated TiO_2 nanotubes. It is interesting to note that the rate constant for the oxidation of SA at the treated TiO_2 nanotubes is over six times higher than that at the Pt electrode at the applied current density of 3.0 mA cm^{-2}. Comparison of the UV-Visible

spectra displayed in Figure 4.5A and Figure 4.5B indicates that the mechanisms of the SA oxidation are different. Complete oxidation of SA occurred on the treated TiO_2 nanotubes due to the generation of $\cdot OH$, whereas partial oxidation was observed on the Pt electrode. All these results further show that the high overpotential of oxygen evolution is benefical towards the electrochemical oxidation of organic pollutants.
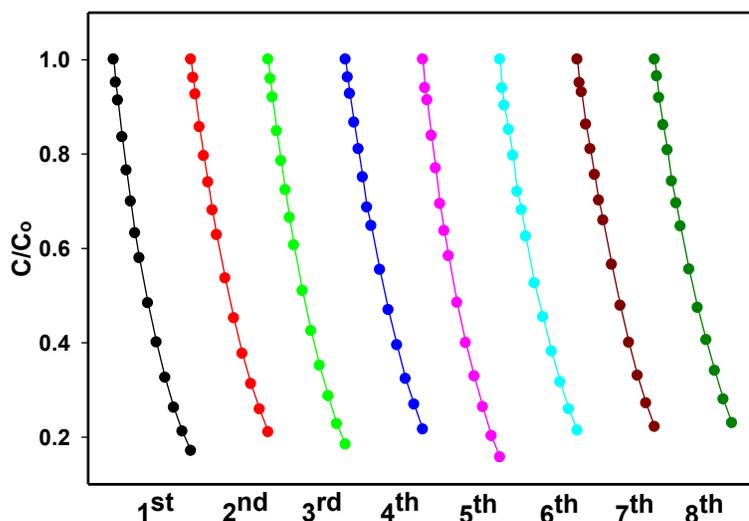
Figure 4.6 Stability tests of the treated TiO_2 nanotubes. Plots of C/C_o *versus* time of electrochemical oxidation of 30 ppm SA at the applied current density of 3 mA cm^{-2}.

4.3.4 Electrochemical stability of the treated TiO_2 nanotubes

To further examine the electrocatalytic stability of the electrochemically reduced TiO_2 nanotubes, eight cycles of the electrochemical oxidation of 30 ppm SA in a 0.1 M H_2SO_4 solution were carried out. The applied current density was 3.0 mA cm^{-2} and the oxidation duration was 3 h. As seen in Figure 4.6, the SA concentration changes for each run, which were further fitted using first order kinetics. The relative standard deviation obtained from the quantitative analysis of kinetic curves was only ca. 1%, which was indicative of the remarkable stability of the electrochemically treated TiO_2 nanotubes.
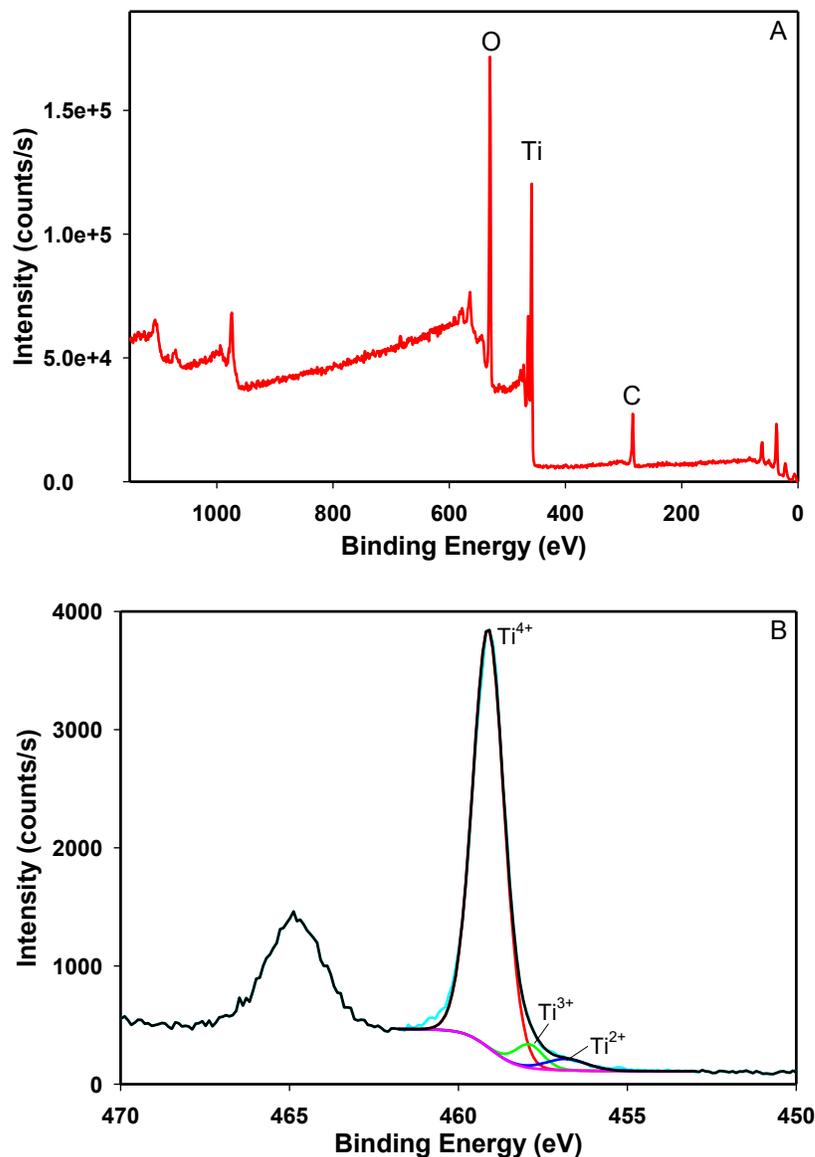
Figure 4.7. (A) XPS survey scan spectrum of as-prepared TiO_2 nanotubes and a high-resolution XPS spectrum of Ti of the TiO_2 nanotubes after being treated at -5 mA cm^{-2} for 10 min.

4.3.5 XPS analysis and Mott-Schottky study

To elucidate the high catalytic activity and stability of the TiO_2 nanotubes enabled by the cathodic treatment, XPS was employed to characterize the change of chemical compositions and electronic states of the TiO_2 nanotube electrodes before and after the electrochemical reduction. The XPS survey scan of the TiO_2 nanotubes is presented in Figure 4.7A, showing that the Ti2p

core level was at 458.78 eV, the O1s core level was at 530.06 eV, while the C1s core level was at 284.58 eV, which further confirmed the composition of the formed nanotube arrays. The high-resolution XPS spectrum of TiO_2 nanotubes after being treated in 0.1 M H_2SO_4 with -5 mA cm^{-2} for 10 min is shown in Figure 4.7B. It reveals that the peaks for Ti^{4+}, Ti^{3+} and Ti^{2+} were centered at 459.11, 457.90 and 456.81 eV, respectively. This clearly illustrated the presence of different Ti oxidation states within the sample. The atomic percentages of different oxidation states of Ti and O were calculated from XPS prior to and following electrochemical reduction. The level of Ti(IV) decreased from 93.86% to 92.13% subsequent to reduction, while Ti(III) and Ti(II) increased, following the reduction, from 3.81% to 4.61% and 2.33% to 3.25%, respectively. This revealed that a portion of the Ti(IV) was transformed to Ti(III) and Ti(II) during the electrochemical reduction process. In addition, the level of O (II) decreased from 86.39% to 78.97% after the 10-minute reduction, indicating an increase of oxygen vacancies which may further enhance the electrochemical activity of the treated TiO_2 nanotubes.

To further characterize the change of the electronic properties of the TiO_2 nanotubes prior to and following the electrochemical reduction, Mott-Schottky measurements were carried out in a 0.1 M H_2SO_4 solution.[40-41] Figure 4.8 presents the Mott-Schottky plots of the as-synthesized TiO_2 nanotubes and electrochemically treated TiO_2 nanotubes. A sigmoidal plot was observed in the investigated potential range, which was typical for n-type semiconductors. There was a good linear relationship between C^{-2} and the potential in the range of 0.3 and 0.6 V for the non-treated TiO_2 nanotubes, as well as the electrochemically treated TiO_2 nanotubes. It is intriguing to note that the donor density of the electrochemically treated TiO_2 nanotubes was estimated from the Mott-Schottky relationship to be 3.1×10^{22} cm^{-3}, which is over 33,000 times larger than that of the

untreated TiO$_2$ nanotubes (9.3×10^{17} cm^{-3}), showing that the electrochemical treatment significantly increased the conductivity of the TiO$_2$ nanotubes.
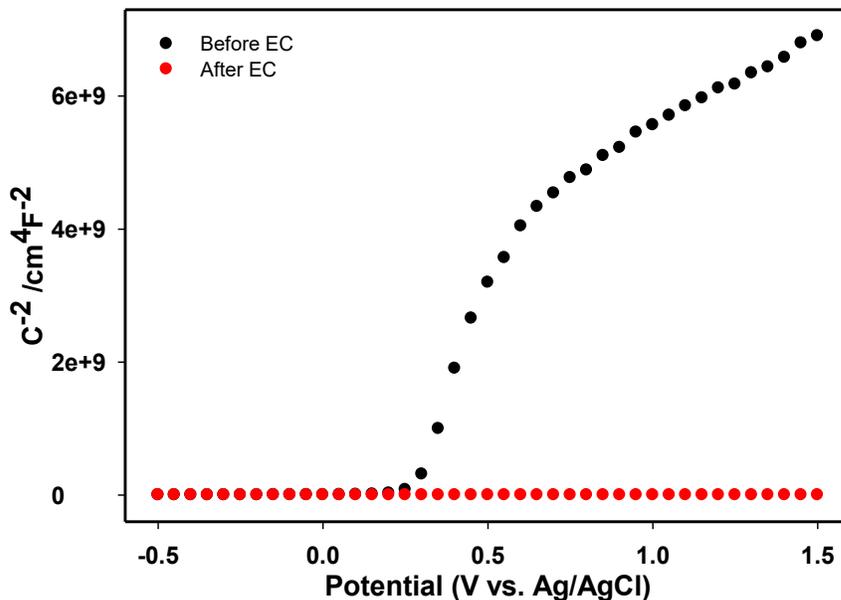
Figure 4.8 Mott-Schotty plots of the TiO$_2$ nanotubes obtained in 0.1 M H$_2$SO$_4$ at 500 Hz prior to and following the electrochemical reduction.

4.4. Conclusions

In summary, it has been demonstrated a facile and effective approach for the significant enhancement of the electrocatalytic activity of the TiO$_2$ nanotubes. For the first time, TiO$_2$ nanotubes were treated via electrochemical reduction and tested as a novel catalyst for the electrochemical oxidation of SA. Optimal reduction conditions were investigated, which revealed that a -5 mA cm^{-2} applied current under 10 min of electrochemical reduction gave the best results. The reduced TiO$_2$ nanotubes possessed a much higher overpotential for oxygen evolution than a Pt electrode and exhibited a high electrocatalytic activity toward the oxidation of SA. Using a 30 ppm SA solution, ca. 90% of SA was electrochemically oxidized over 3 h at 3.0 mA cm^{-2}; and under the identical operational conditions, an only ca. 21% removal of SA was observed at a Pt

polycrystalline electrode. The rate constant for the electrochemical oxidation of SA at the reduced TiO$_2$ nanotubes was determined to be 1.06×10^{-2} min^{-1}, which is over six times higher than that at the Pt electrode. The high electrocatalytic activity and stability of the TiO$_2$ nanotubes enabled by the facile electrochemical reduction can be attributed to: (i) the decrease of Ti(IV); (ii) the increase of Ti(II) and Ti(III); (iii) the increase of the oxygen vacancies; and (iv) the significant improvement of the the donor density. The cathodically treated TiO$_2$ nanotubes possesses a similar overpotential for oxygen evolution as the boron-doped diamond electrode, one of the highest performance electrode materials for the electrochemical oxidation of organic pollutants, but with a significantly lower cost. Thus, the facile approach described in this study opens a door for the development of high-performance electrode materials for electrochemical treatment of wastewater and green chemistry applications.

References

(1) Tian, M.; Wu, G.; Chen, A. *ACS Catal*. **2012**, *2*, 425-432.

(2) Wu, G.; Nishikawa, T.; Ohtani, B.; Chen, A. *Chem. Mater*. **2007**, *19*, 4530-4537.

(3) Yu, Y.; Ren, J.; Liu, D.; Meng, M. *ACS Catal.* **2014**, *4*, 934-941.

(4) Luan, Y.; Jing, L.; Xie, Y.; Sun, X.; Feng, Y.; Fu, H. *ACS Catal*. **2013**, *3*, 1378-1385.

(5) Muñoz-Batista, M.; Gómez-Cerezo, M.; Kubacka A.; Tudela, D.; Fernández-García M. *ACS Catal.* **2014**, *4*, 63-72.

(6) Lee, W. J.; Lee, J. M.; Kochuveedu, S. T.; Han, T. H.; Jeong, H. Y.; Park, M.; Yun, J. M.; Kwon, J.; No, K.; Kim, D. H.; Kim, S. O. *ACS Nano*, **2012**, 6, 935-943.

(7) Chen, X. B.; Mao, S. S. *Chem. Rev*. **2007**, *107*, 2891-2959.

(8) Hwang, Y. J.; Hahn, C.; Liu, B.; Yang, P. *ACS Nano*. **2012**, *6*, 5060-5069.

(9) Shiraishi, Y.; Fujiwara, K.; Sugano, Y.; Ichikawa, S.; Hirai, T. *ACS Catal*. **2013**, *3*, 312-320.

(10) Hashimoto, K.; Masuda, Y.; Kominami, H. *ACS Catal*. **2013**, *3*, 1349-1355.

(11) Li, K.; Chai, B.; Peng, T.; Mao, J.; Zan, L. *ACS Catal*. **2013**, *3*, 170-177.

(12) Thind, S. S.; Wu, G.; Chen, A. *Appl. Catal. B: Environ*. **2012**, *111*, 38-45.

(13) Shi, J.; Wang, X. D. *Energy Environ. Sci*. **2012**, *5*, 7918-7922.

(14) Thind, S. S.; Wu, G.; Tian, M.; Chen, A. *Nanotechnology* **2012**, *23*, 475706.

(15) Thompson, T. L.; Yates, J. T. *Chem. Rev*. **2006**, *106*, 4428-4453.

(16) Zuo, F.; Wang, L.; Wu, T.; Zhang, Z. Y.; Borchardt, D.; Feng, P. Y. *J. Am. Chem. Soc*. **2010**, *132*, 11856-11857.

(17) Ada´n, C.; Coronado, J. M.; Bellod, R.; Soria, J.; Yamaoka, H. *Appl. Catal., A.* **2006**, *303*, 199-206.

(18) Vilambi, N. R. K.; Chin, D. T. *J. Electrochem. Soc.* **1987**, *134*, 3074-3077.

(19) Mills, A.; Holland, C. E.; Davies, R. H.; Worsley, D. *J. Photochem. Photobiol. A.* **1994**, *83*, 257-263.

(20) Carlotti, M. E.; Sapino, S.; Trotta, M.; Vione, D.; Minero, C.; Peira, E. *J. Disper. Sci. Technol*. **2007**, *28*, 805-818.

(21) Matyasovszky, N.; Tian, M.; A. Chen. *J. Phys. Chem. A.* **2009**, 113, 9348-9353.

(22) Goi, A.; Veressinina, Y.; Trapido, M. *Chem. Eng. J*. **2008**, *143*, 1-9.

(23) Quiroz, M. A.; Reyna, S.; Martinez-Huitle, C. A.; Ferro, S.; DeBattisti, A. *Appl. Catal., B.* **2005**, *59*, 259-266.

(24) Tian, M.; Bakovic, L.; Chen, A. *Electrochim. Acta*. **2007**, *52*, 6517-6524.

(25) Borras, C.; Laredo, T.; Scharifker, B. R. *Electrochim. Acta*. **2003**, *48*, 2775-2780.

(26) Vinodgopal, K.; Hotchandani, S.; Kamat, P. V. *J. Phys. Chem*. **1993**, *97*, 9040-9044.

(27) Leng, W. H.; Zhu, W. C.; Ni, J.; Zhang, Z.; Zhang, J. Q.; Cao, C. N. *Appl. Catal. A.* **2006**, *300*, 24-35.

(28) Li, J.; Zhang, X.; Ai, Z.; Jia, F.; Zhang, L.; Lin, J. *J. Phys. Chem. C.* **2007**, *111*, 6832-6836.

(29) Tian, M.; Wu, G. S.; Adams, B.; Wen, J. L.; Chen, A. *J. Phys. Chem. C.* **2008**, *112*, 825-831.

(30) Yun, H. J.; Lee, H.; Joo, J. B.; Kim, W.; Yi, J. *J. Phys. Chem. C.* **2009**, *113*, 3050-3055.

(31) Yadav, B. R.; Garg, A. *Ind. Eng. Chem. Res.* **2012**, *51*, 15778-15785.

(32) Lefevre, S.; Ferrasse, J.; Faucherand, R.; Viand, A.; Boutin, O. *Energy*. **2012**, 41, 175-183.

(33) Tian, M.; Adams, B.; Wen, J.; Asmussen, R. M.; Chen, A. *Electrochim. Acta*. **2009**, *54*, 3799-3805.

(34) Martinez-Huitle, C. A.; Ferro, S. *Chem. Soc. Rev.* **2006**, *35*, 1324-1340.

(35) Comninellis, C. *Electrochim. Acta.* **1994**, *39*, 1857-1862.

(36) Canizares, P.; Lobato , J.; Paz, R.; Rodrigo, M. A.; Sa´ez, C. *Water Res*. **2005**, *39*, 2687-2703.

(37) Zhao, X.; Liu, H.; Qu, J. *Catal. Commun.* **2010**, *12*, 76-79.

(38) Rodgers, J. D.; Bunce, N. J. *Environ. Sci. Technol.* **2001**, *35*, 406-410.

(39) Pan, K.; Tian, M.; Jiang, Z.-H.; Kjartanson, B.; Chen, A. *Electrochim. Acta* **2012**, *60*, 147-153.

(40) Munoz, A.G. *Electrochim. Acta*. **2007**, *52*, 4167-4176.

(41) Gimenez, S.; Dunn, H. K.; Rodenas, P.; Fabregat-Santiago, F.; Miralles, S. G.; Barea, E. M.;

Trevisan, R.; Guerrero, A.; Bisquert, J. Gimenez, S. *J. Electroana. Chem*. **2012**, *668*, 119-125.

Chapter 5: Electrochemical Oxidation of Lignin at Electrochemically Reduced TiO₂ Nanotubes

5.1 Introduction

Lignin is an amorphous, aromatic polyphenolic macromolecule composed of phenyl propane units that are linked together by C-C and C-O bonds.[1] It is the second most abundant biopolymer on Earth, and constitutes ~20% of hardwoods and ~30% of softwoods.[2] Lignin is mostly obtained from sulphite, kraft, and soda process during the conversion of wood to wood pulp.[3] Lignin and lignin derivatives are a major component of pulp and paper mill wastewater, thus it is of environmental interest to discover novel and efficient ways to degrade lignin. Lignin is known for its relatively high resistance to biological and chemical degradation; however, it is a potential raw material for the generation of compounds such as activated carbon, vanillin, and vanillic acid, as well as a potential renewable source of aromatic and cyclohexyl compounds.[4-5] Several degradation methods have been studied previously, including the use of enzymes, high temperatures, photolysis, hydrogenolysis, hydrolysis, supercritical alcohol depolymerisation, microwave assisted depolymerisation, and powerful oxidants.[6-14]

In general, the above mentioned procedures are often difficult to control, do not show commercial viability, and are constrained by multiple limitations related to selective oxidation and the generation of solid residue-like chars.[15] Electrochemical oxidation has been described as an effective method for the oxidation of lignin.[16-17] There are a number of advantages for the use of electrochemical oxidation over other methods, including that it can provide improved control over the oxidation of complex organic compounds, and be employed to completely oxidize lignin to desired low molecular weight compounds.[18] The best advantage for the use of the electrochemical

technique is that it is a very environmentally compatible technique, a very low temperature and pressure is employed, and the primary driving force for the oxidation reaction is the electrons, which do not initiate any type of secondary pollution.[19] Although electrochemical oxidation has demonstrated many advantages, its extensive use has been prevented by the high cost of electrode materials. Many different types of electrode materials have been studied by different research groups.[20] Parpot et. al. investigated the electrochemical oxidative degradation of Kraft lignin on Pt, Au, Ni, Cu, DSA-O_2, and PbO_2 anodes. The researchers evaluated the production of vanillin, which is a value added product generated by means of formal kinetic analyses. They also discovered that the conversion and chemical yields were highly dependent on the applied current density, whereas the rate of the oxidation reaction was dependant on the composition of the electrode material.[21-25]

It is very important to develop novel, energy efficient and economical electrodes for the oxidation of lignin. Titania (TiO_2) is a metal oxide semiconductor that is far cheaper than other electrode materials (e.g., platinum, gold, nickel, or boron doped diamond). Further, it is a chemically inert, stable, efficient, and non-toxic electrode,[26] and its electrochemical, photochemical, and photoelectrochemical properties have been studied extensively. Another considerable advantage for the use of titania is that it may be synthesized in various nanoscale morphologies such as tubes, porous structures, rods, flowers, platelets etc. with extensive surface areas.[27]

TiO_2 nanotubes are the most studied morphology of this material as they possess very high surface areas and may be easily grown on a titanium substrate, which provides greater stability and conductivity. TiO_2 nanotubes can be prepared on titanium substrates via anodization in a fluoride ion containing electrolyte.[28] TiO_2 nanotubes are not considered as good electrocatalysts due to low

conductivity and a large band gap. There are several reports in the literature where different methods have been employed to enhance the electrocatalytic activity of TiO_2 nanotubes. One straightforward method is to deposit novel metal nanoparticles or metal oxides onto the surface of the TiO_2 which significantly increases its activity.[29] Recently, another very intriguing and facile reduction approach is being considered as an optimal strategy to enhance the electrocatalytic activity of TiO_2. The prepared TiO_2 may be chemically reduced by treating it with hydrogen under controlled conditions, which can also be achieved electrochemically or photochemically.[30-33]

In this research work, a very facile electrochemically treated TiO_2 nanotube electrode was employed for the electrochemical oxidation of lignin. TiO_2 nanotubes were grown by anodizing the titanium plate and were treated electrochemically to reduce the TiO_2. A significant enhancement in activity toward the oxidation of lignin may be seen following the electrochemical reduction. The effect of the TiO_2 nanotubes on the oxidation of lignin was also evaluated by growing nanotubes of various lengths. The prepared electrodes were characterized by various analytical techniques.

5.2 Experimental

5.2.1 Chemicals and materials

The lignin used in this study was extracted from black liquor that was supplied by a local pulp and paper mill located in Northwestern Ontario, Canada. The black liquor was diluted to 30% (w/w), then heated and bubbled with CO_2 at 80 °C for 16 h. Since the solubility of lignin is relatively low in aqueous acidic solutions, the precipitated lignin was further rinsed and purified by a dilute H_2SO_4 solution. Titanium plates (99.2%) were purchased from Alfa Aesar, whereas all other chemicals used were of analytical grade, and purchased from Sigma-Aldrich. Pure water

(18.2 MΩ cm) was used for all experimental solutions and was obtained from a Nanopure Diamond™ UV ultrapure water purification system.

5.2.2 Preparation and treatment of TiO$_2$ nanotubes

The fabrication of TiO$_2$ nanotubes is already discussed in section 3.2.3.1 of chapter 3. The electrochemical (EC) treatment of the TiO$_2$ nanotubes was performed in a 0.1 M H$_2$SO$_4$ solution at a cathodic current density of -5 mA cm^{-2} for 10 min., where the current density was calculated based on the geometric surface area.

5.2.3 Characterization of the synthesized TiO$_2$ nanotubes

The surface morphology and composition of the synthesized TiO$_2$ nanotubes were characterized by field-emission scanning electron microscopy (FE-SEM, Hitachi SU 70) and a XPS (Omicron EA-125 energy analyzer and a multichannel detector). All binding energies reported in this work were corrected using the C 1s peak at 284.5 eV as an internal standard. The broad Ti 2p region of the sample was fitted using XPSPEAK41 software. The electrochemical performance of the TiO$_2$ nanotube electrode was characterized by cyclic voltammetry (CV), chronopotentiometry (CP) and electrochemical impedance spectroscopy (EIS) using a Voltalab 40 Potentiostep (PGZ301) at room temperature (20 ± 2 °C). All the electrochemical measurements were conducted in a three-electrode cell system, wherein an Ag/AgCl electrode was used as the reference electrode, and a Pt coil with a surface area of 10 cm^2 served as the auxiliary electrode. The 0.0 V of Ag/AgCl electrode was equivalent to 0.197 V versus a reversible hydrogen electrode (RHE). EPR spectra were recorded on a Bruker A200- 9.5/12 at 100 K.

5.2.4 Electrochemical oxidation of lignin

The electrocatalytic activities were further studied by utilizing the synthesized TiO_2 nanotubes as the working electrode during the electrochemical oxidation of lignin. A 100 ppm lignin + 0.1 M NaOH solution was stirred for the duration of the experiment with a magnetic stirrer. A Cary 50 UV-Vis spectrometer was employed to monitor the degradation of lignin in situ over the range of 250-500 nm, which displayed a strong peak at ca. 292 nm. The total organic carbon (TOC) of the lignin solution prior to and following the electrochemical degradation was measured using a TOC analyser (TOC-L CPH, Shimadzu). The products that resulted from the electrochemical oxidation of lignin were identified by HPLC (Varian Prostar 230) and confirmed via a comparison with standards.

5.3 Results and discussion

5.3.1 Characterization of TiO_2 nanotubes

SEM was employed to characterize the structures and morphologies of the TiO_2 nanotubes. As shown in Figure 5.1A, the synthesized highly ordered nanotubes consisted of pored arrays where the pore lumens were exposed at the top of the layer. The uniform outer diameters of the nanotubes and the thicknesses of the tube wall were ca. 200 nm and 50 nm, respectively. To obtain a view of the length of the nanotube array, a cross-sectional SEM observation was carried out. Figure 5.1B reveals that the vertical height of the TiO_2 nanotubes fabricated by 16 H was ~13.5 μm, and Figure 5.1C confirmed that the nanotubes grew longer with the synthesis duration.
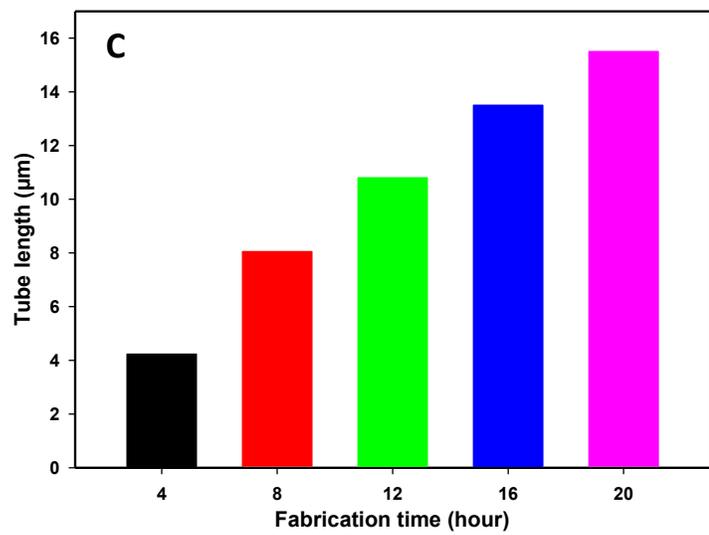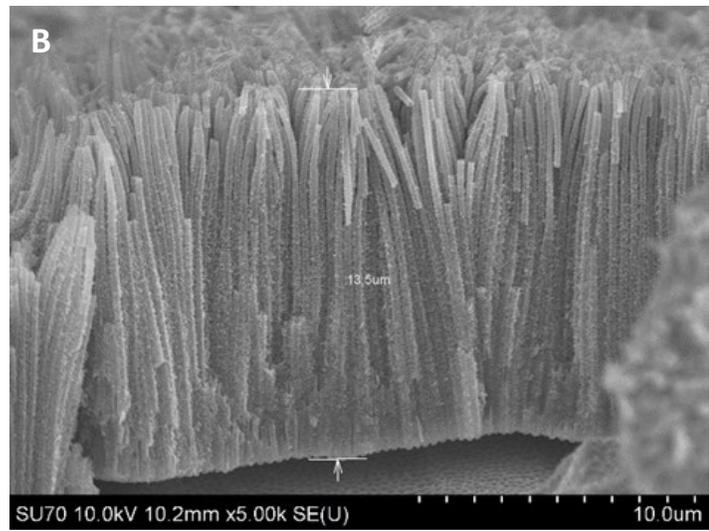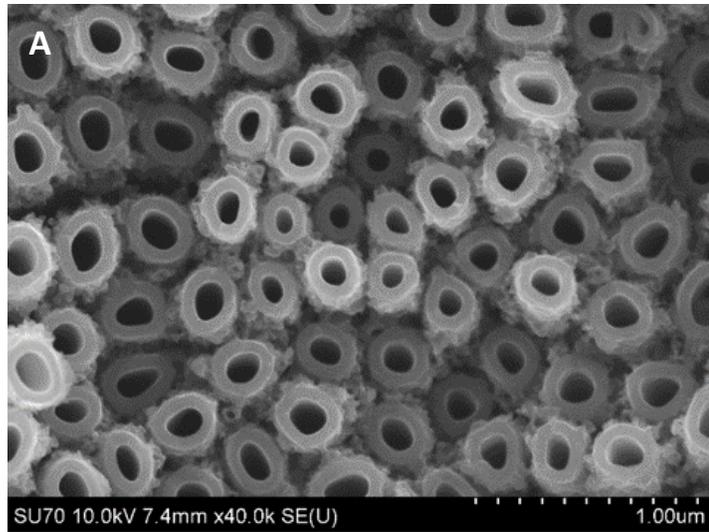
Figure 5.1 (A) SEM top view (B) cross-sectional view images of the synthesized TiO$_2$ nanotube electrode fabricated over 16 H and (C) tube length of TiO$_2$ nanotubes fabricated over various time periods.
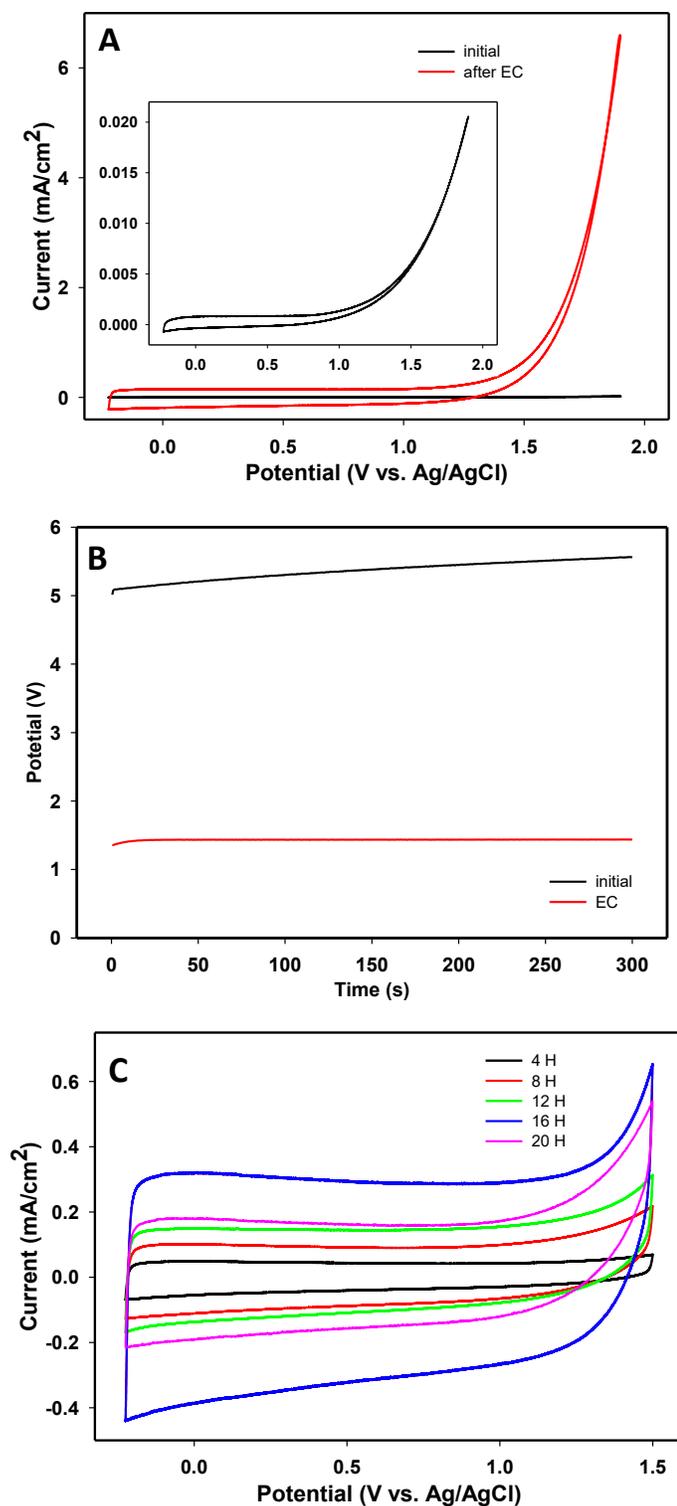
Figure 5.2 (A) CVs and (B) chronopotentiometric curves of TiO_2 nanotube electrode fabricated over 16 H, prior to and following the EC treatment, and (C) CVs of electrochemically treated TiO_2 nanotube electrodes fabricated over various time periods in 100 ppm lignin + 0.1 M NaOH. The inset of (A) is CV of the TiO_2 nanotube electrode fabricated over 16 H, prior to the EC treatment (Scan rate: 20 mV s^{-1}, applied current: 0.2 mA)

Figure 5.2A presents the CVs of the synthesized TiO_2 nanotubes fabricated over 16 H, prior to (black curve), and following (red curve) the EC treatment. All the CVs were recorded in a 100 ppm lignin + 0.1 M NaOH solution at a scan rate of 20 mV s^{-1}. The inset of Figure 5.2A depicts the CV of the synthesized TiO_2 nanotubes that were fabricated over 16 H, prior to the EC treatment. In comparison to the untreated TiO_2 nanotubes, the EC treated TiO_2 nanotube electrode delivered a clear pseudocapacitive characteristic between -0.225 V and 1.0 V, which may be attributed to the oxidation/reduction of surface hydroxyl groups and double-layer charging/discharging.[34-36] Meanwhile, the current density was significantly increased by ca. 197 times (at 0.0 V), 168 times (at 0.5 V), and 114 times (at 1.0 V), respectively.

Due to oxygen evolution, the current densities of both curves increased when scanning the electrode potential, from 1.0 to 1.9 V. Meanwhile, the TiO_2 nanotubes that underwent the EC treatment attained 6.58 mA cm^{-2} at 1.9 V, which was ~330 times than that of TiO_2 nanotubes prior to the EC treatment (0.02 mA). It also shows that the conductivity of the TiO_2 nanotubes was improved through the EC treatment process. Moreover, the overpotential for oxygen evolution was increased from ~1.0 V to ~1.5 V as a result of the EC treatment as well. As is well-known, the high overpotential for oxygen evolution is highly beneficial to the electrochemical oxidation of organic pollutants. The aforementioned results suggested that the EC treatment enabled the TiO_2 nanotubes to be more optimal electrocatalysts for environmental applications. Figure 5.2B shows the chronopotentiometric curves of the TiO_2 nanotube electrode fabricated over 16 H, prior to and following the EC treatment, with an applied current of 0.2 mA.

It was clear that the potential response was greatly decreased by the EC treatment, which also proved that the conductivity of the TiO_2 nanotubes was improved through the EC treatment. This was consistent with CV measurements. Figure 5.2C depicts the CVs of the electrochemically

treated TiO$_2$ nanotube electrodes that were fabricated over various time periods and collected in 100 ppm lignin + 0.1 M NaOH at a scan rate of 20 mV s^{-1}. As can be seen, all of the electrodes revealed an almost rectangular shape (as a pure capacitor) following the EC treatment. The current densities of the treated TiO$_2$ nanotubes strongly depended on the fabrication time, where a 16 H synthesis time resulted in the highest current density. While longer durations were observed to decrease the activity of the TiO$_2$ nanotubes, or even result in the formation of an inhomogeneous top structure and the detachment of the TiO$_2$ nanotubes from the Ti substrate.

To study changes in the electrochemical behaviors of the TiO$_2$ nanotubes prepared under different times and the effects of the EC treatment, all of the electrodes were investigated by electrochemical impedance measurements, which were done in a 100 ppm lignin solution in 0.1 M NaOH. The Nyquist plots obtained from the impedance studies are shown in Figure 5.3. These plots were recorded at an electrode potential of 1800 mV vs Ag/AgCl. Z' and Z" represent the real and imaginary components of the impedance, respectively. The obtained raw data was fitted by the equivalent circuit, which is shown as the inset of Figure 5.3B. In this circuit, Rs represents the solution resistance, Rp is the charge transfer resistance, and CPE (defined as CPE_T and CPE_P), represents the constant phase elements.

It may be observed from the figure that the raw data fitted very well with the proposed model. Figure 5.3A shows the Nyquist plot, where the impedance of the TiO$_2$ nanotube electrode fabricated over 16 H, prior to and following the electrochemical reduction, is presented. As it is evident that TiO$_2$ is a semiconductor, and thus provides a significant amount of resistance to the charge flow, the Nyquist plot of the untreated TiO$_2$ nanotube electrode showed very high impedance. When the same electrode was electrochemically treated by applying a -5mA cm^{-2} current density, the impedance of the electrode was significantly decreased. This indicates that the

EC treated TiO$_2$ nanotube electrode had improved conductivity in contrast to the untreated TiO$_2$ nanotube electrode. To compare the effects of the synthesis duration on the impedance of the electrodes, Nyquist plots were also run for different growth intervals of the treated TiO$_2$ nanotubes, with the resulting plots presented in Figure 5.3B. The corresponding data obtained after fitting for each electrode is listed in Table 5.1.
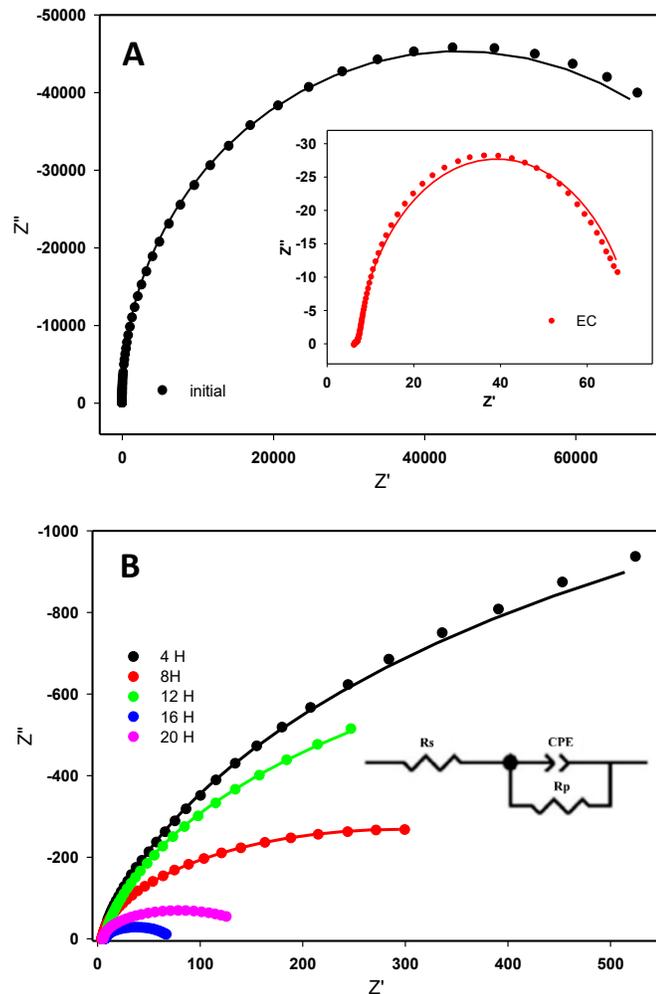
Figure 5.3. Nyquist plots of (A) a bare TiO$_2$ nanotube electrode and (B) electrochemically treated TiO$_2$ nanotube electrodes fabricated over various time periods in 100 ppm lignin + 0.1 M NaOH at an electrode potential of 1800 mV. The frequency was altered, from 40 kHz to 100 mHz. The amplitude of the modulation potential was 10 mV. The inset of (A) is the plot of electrochemically treated TiO$_2$ nanotube electrode fabricated over 16 H. The inset of (B) is the equivalent circuit that was used to fit the raw data.
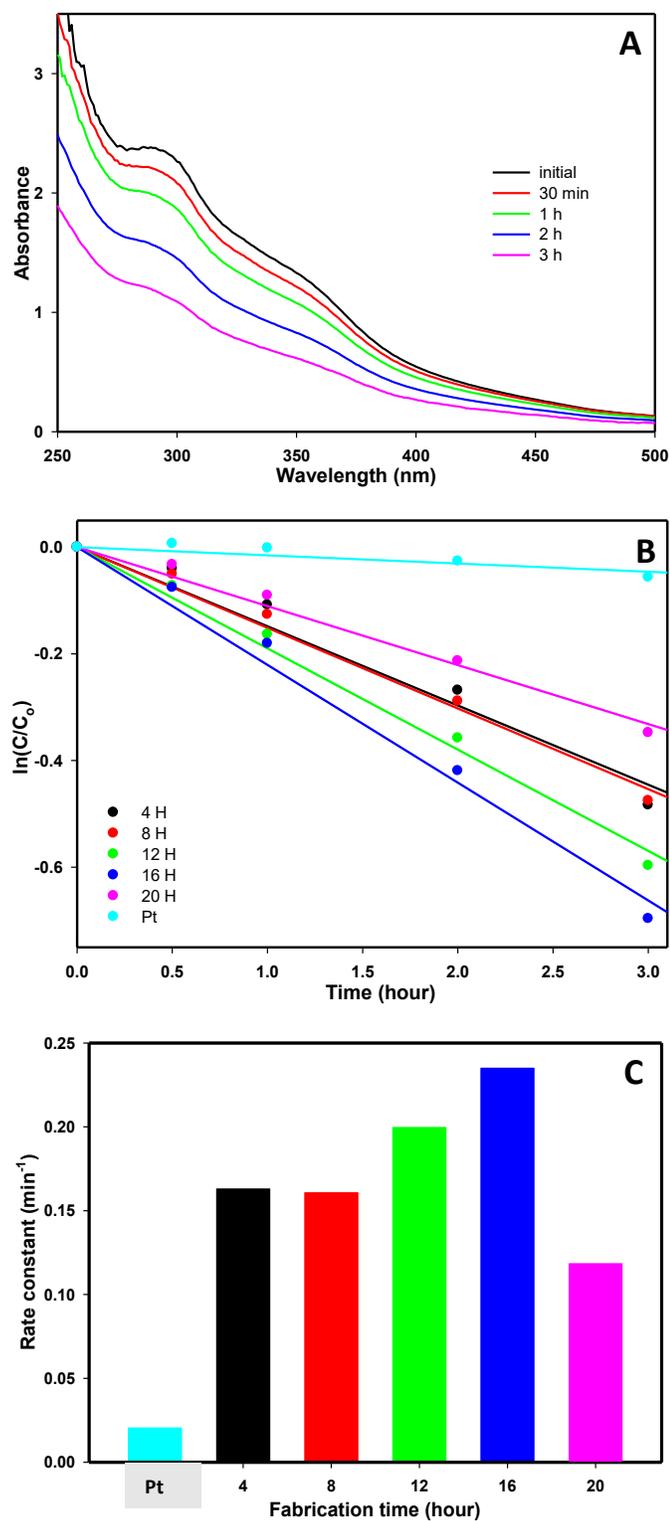
Figure 5.4. (A) Absorbance spectra for the electrochemical oxidation of 100 ppm of lignin in 0.1 M NaOH at the EC treated TiO_2 nanotube electrode with a current density of 4 mA cm^{-2} at 20 ℃. (B) plot of $ln(C/C_o)$ vs. time and (C) rate constants for the electrochemical oxidation of 100 ppm lignin in 0.1 M NaOH at electrochemically treated TiO_2 nanotube electrodes fabricated over various time periods under an applied current density of 4 mA cm^{-2} at 20 ℃.

It may be concluded that the lengths of the nanotubes played a critical role in the determination of their electrochemical properties. Longer nanotubes were further reduced and larger loads of active material were present on the electrode; hence, a decrease in the impedance was observed. It may be seen from the data values that the charge transfer resistance continued to decrease with increases in nanotube lengths until a threshold length was achieved, after which the *Rct* began to increase once again. This trend was observed until an optimal tube length was achieved for a 16 H growth duration electrode. Once the nanotubes were grown longer than that under the 16 H time period, a loss in the uniformity of the structure was observed, as can be seen in the SEM images. Longer nanotubes had a tendency to fall off easily and created very irregular structures across the electrode surface. The lack of morphological uniformity resulted in an increase in impedance.

5.3.2 Electrochemical oxidation of lignin at the treated TiO₂ nanotube electrode

To further analyze the catalytic activity, all of the electrodes were tested for the oxidation of 100 ppm of lignin dissolved in 0.1 M NaOH. Figure 5.4A shows the time dependence of the absorbance curve during the electrochemical oxidation of lignin at the 16 H treated electrode with an applied current of 4 mA cm^{-2}. The UV-vis spectra were recorded every 30 min. for the initial 1 H, then every 1 H for the final 2 H. It can be seen that a very significant decrease in the absorbance was achieved after just three hours of electrochemical oxidation. Figure 5.4B shows the kinetic curve for the electrochemical oxidation of lignin with TiO₂ nanotube electrodes that were synthesized under different durations. The results verified that the TiO₂ fabricated under the 16 H anodizing process demonstrated optimal electrochemical activity, which was consistent with the results obtained with the impedance studies. The logarithmic plots of lignin concentrations suggested a first order kinetic model for the degradation, which may be expressed as ln C/C_o = -

kt, where C_o is the initial concentration, C is the concentration of the lignin at time t, and k is the rate constant of the lignin degradation. The results in Figure 5.4C also indicate that the treated TiO$_2$ nanotube electrode activity toward the oxidation of lignin was even better than the Pt electrode.
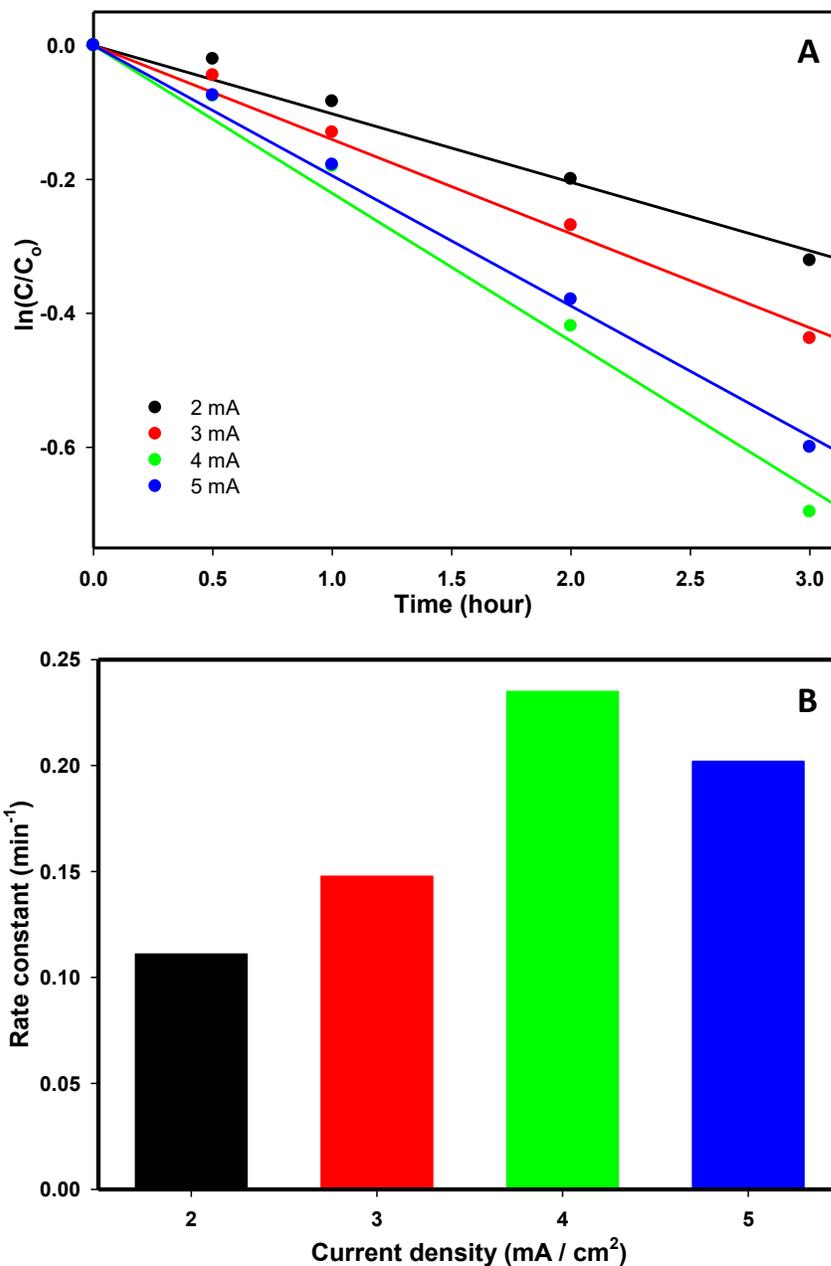
Figure 5.5. (A) Plot of ln(C/C$_o$) vs. time and (B) rate constants for the electrochemical oxidation of 100 ppm of lignin in 0.1 M NaOH at an electrochemically treated TiO$_2$ nanotube electrode fabricated over 16 H under different current densities at 20 °C.

93

Figure 5.5A illustrates the activity of the EC treated TiO_2-16 H toward the electrochemical oxidation of lignin under various applied currents. At all applied current densities the reactions followed first order kinetics, where higher applied current densities resulted in an increase of the rate constant of the lignin oxidation. It was concluded that the fastest reaction was achieved when a 4 mA cm^{-2} current density was applied. However, when the current was increased further, an increase in the gas evolution was observed, which tended to decrease the lignin oxidation rate. Figure 5.5B shows the comparison of the rate constant calculated the oxidation of lignin under different applied current densities. The value of the rate constant for 4 mA was 0.2349 min^{-1}, which was more than double that obtained at 2 mA cm^{-2}. At an applied current density of 5 mA cm^{-2}, the value of the rate constant was slightly less than that obtained with 4 mA cm^{-2}.

We have further studied the influence of temperature on the oxidation of lignin on the EC treated TiO_2 nanotube electrode, as the temperature was varied from 0 to 30 °C. The higher temperature led to more rapid lignin oxidation. The plot of ln (C/C_o) vs. time is shown in Figure 5.6A, and the kinetic rate constants were determined from the magnitude of the slope of the linear relationship. As the temperature increased from 0 to 30 ℃, the kinetic rate constant was elevated from 0.1165 to 0.2865 min^{-1}. The Arrhenius plot based on the kinetics data determined at 0, 10, 20, and 30 °C yields a straight line as shown in Figure 5.6B, from which the overall apparent activation energy (21 kJ mol^{-1}) was obtained for the oxidation of lignin. This value is close to that of hydroxyl radical reactions, which indicated that the oxidation of lignin was governed by the hydroxyl radical reaction.

To measure the efficiency of the electrochemical oxidation of lignin at the treated TiO_2 nanotube electrodes, the TOC content was further analyzed. As shown in Figure 5.7, the TOC removal with the EC treated TiO_2 nanotube electrode was very rapid, and in three hours an almost

70% TOC removal was achieved. The TOC values of lignin solutions under different treatment time are displayed in Table 5.2. The HPLC results indicated that the primary intermediates of lignin oxidation were vanillin and vanillic acid.
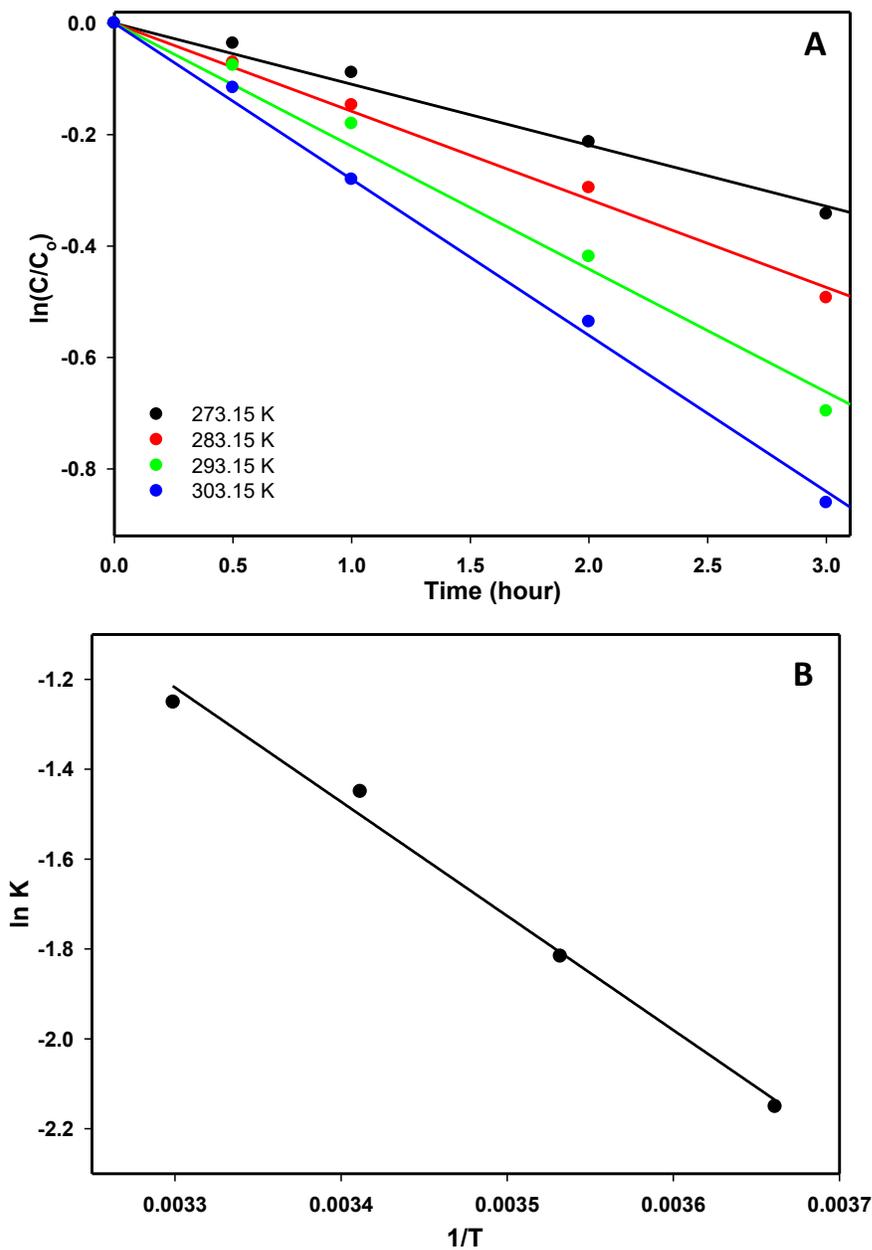

Figure 5.6. (A) Plot of $\ln(C/C_o)$ vs. time for the electrochemical oxidation of 100 ppm of lignin in 0.1 M NaOH at an electrochemically treated TiO_2 nanotube electrode fabricated over 16 H at 4 mA cm^{-2} under different temperatures and (B) plot of $\ln K$ vs. $1/T$.
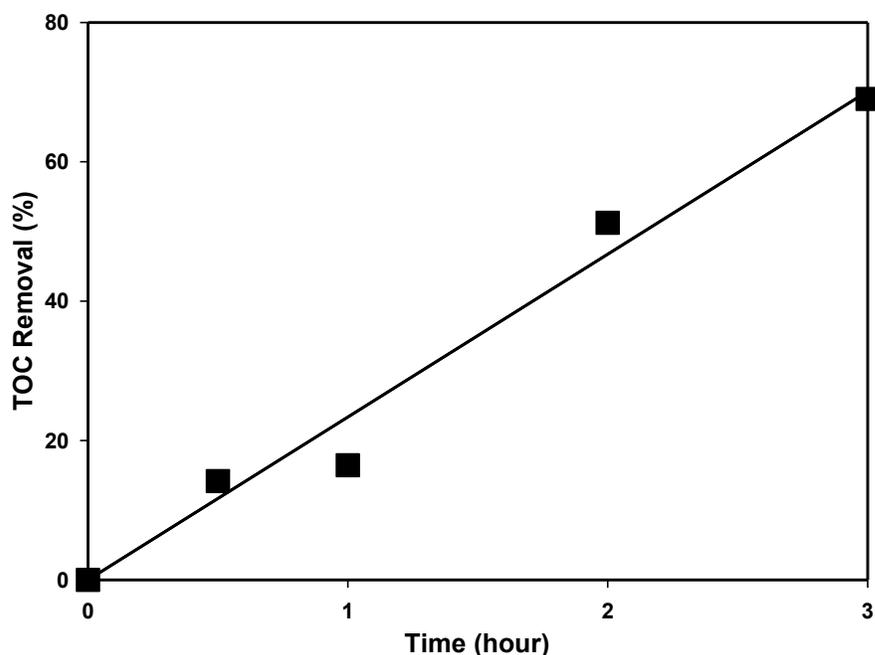
Figure 5.7. Plot of TOC removal of 100 ppm of lignin in 0.1 M NaOH vs. the electrochemical oxidation time.

Table 5.1. EIS data obtained from Nyquist plots of Figure 5.3.

Electrodes	Rs (Ω cm^2)		Rp (kΩ cm2)		CPE-T (μF cm^{-2})		CPE-P	
	Value	Error (%)	Value	Error (%)	Value	Error (%)	Value	Error (%)
16 H before EC	4.34	0.50	89023	0.92	9.24	0.47	1.012	0.08
4 H after EC	4.28	1.83	2706	16.70	1301.10	3.11	0.92	0.98
8 H after EC	4.19	0.24	582.90	1.21	2678.80	0.47	0.95	0.16
12 H after EC	6.88	0.18	1692	2.21	2475.80	0.36	0.93	0.14
16 H after EC	6.85	0.41	64.55	1.25	5179.70	1.60	0.90	0.59
20 H after EC	5.12	0.29	152.30	1.08	5157.10	0.74	0.94	0.28

Table 5.2. TOC of the lignin solution at different treatment time.

	TOC (mg/L)
100 ppm lignin + 0.1 M NaOH	50.22
After 30 min treatment	43.10
After 1 h treatment	41.96
After 2 h treatment	24.48
After 3 h treatment	15.56
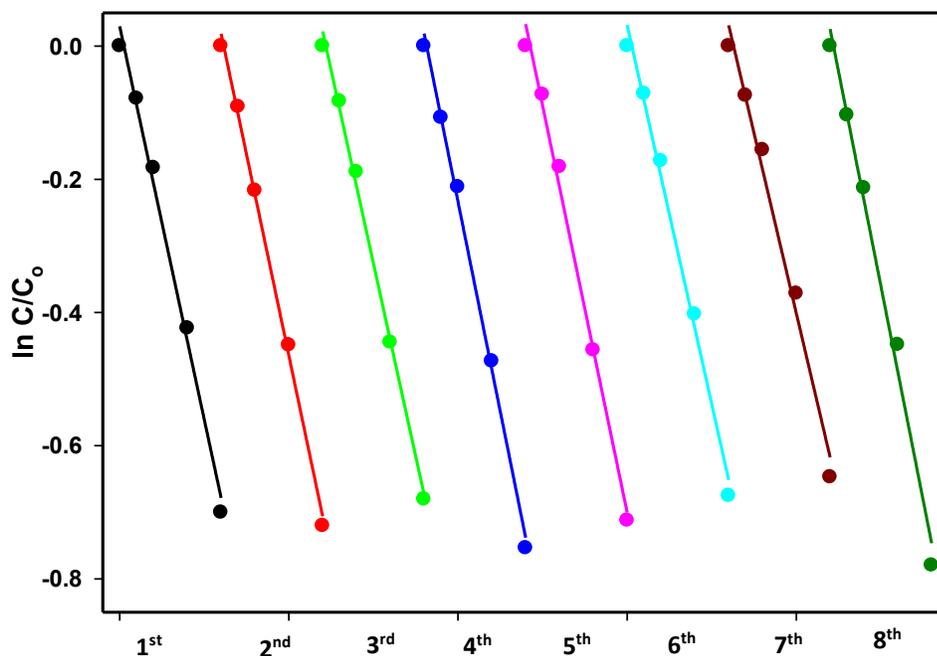
Figure 5.8. Stability tests of the treated TiO$_2$ nanotubes. (A) Plots of C/C$_o$ vs. time and (B) rate constants of electrochemical oxidation of 100 ppm of lignin in 0.1 M NaOH at an applied current density of 4 mA cm^{-2}.

Table 5.3. First-order kinetic constants and the relative coefficients for the stability tests.

Run	Rate Constant(min^{-1})	R^2
1	0.2361	0.993
2	0.2415	0.997
3	0.2320	0.996
4	0.2523	0.997
5	0.2445	0.993
6	0.2278	0.991
7	0.2163	0.987
8	0.2574	0.990

5.3.3 Electrochemical stability of the treated TiO$_2$ nanotube electrodes

To investigate the electrocatalytic stability of the EC treated TiO$_2$ nanotube electrocatalyst, eight lignin oxidation cycles were run using one TiO$_2$-16H electrode with a 4 mA cm^{-2} applied current density. Following each oxidation cycle the electrode was rinsed and reused for the next oxidation in a fresh lignin solution. During each oxidation cycle the lignin samples were taken out

at regular time intervals with the results presented in Figure 5.8, and the kinetic values shown in

Table 5.3. The rate constant values presented in this table revealed that the EC treated TiO_2

electrode retained high activity even after eight cycles of lignin oxidation.
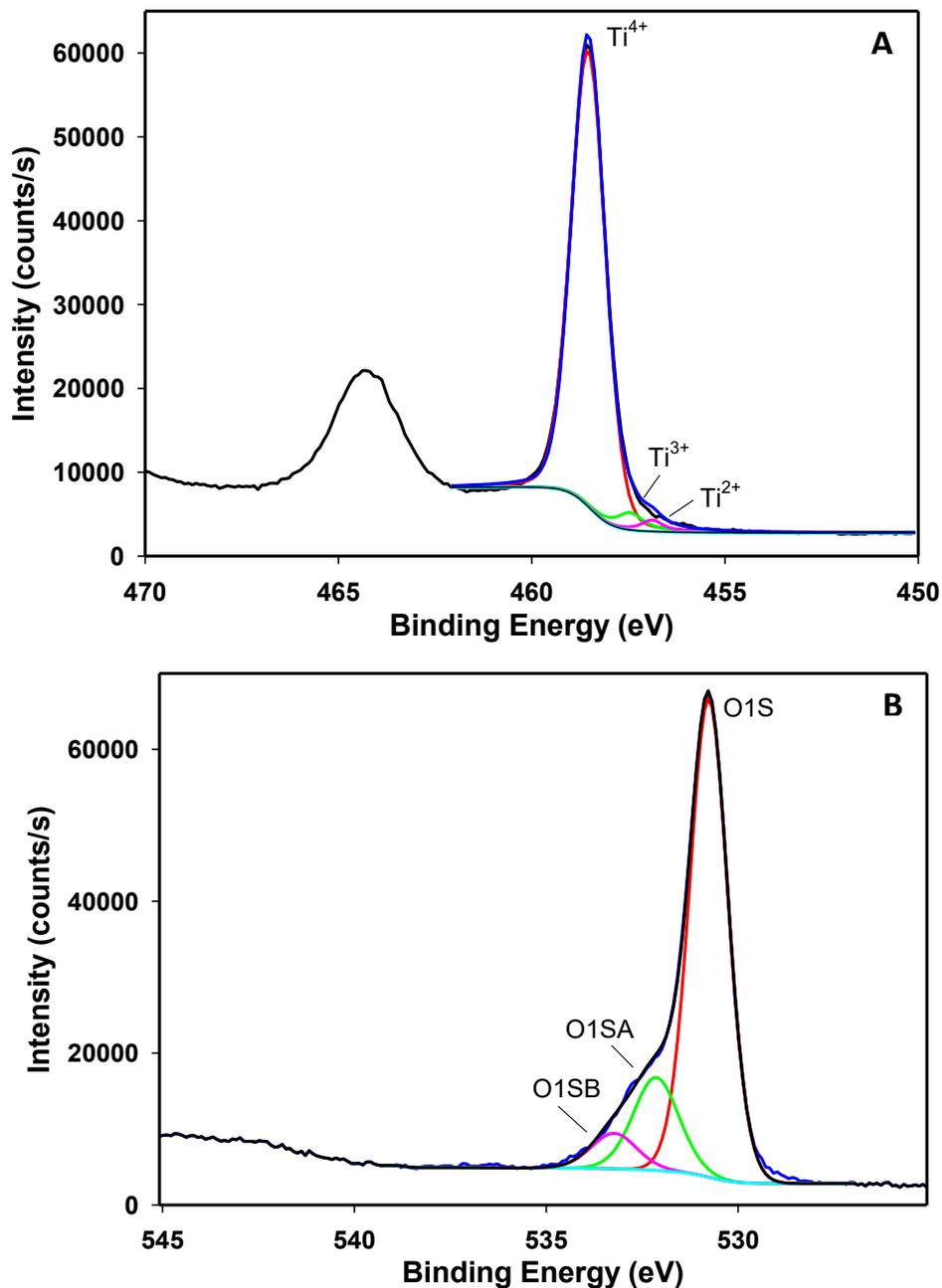
Figure 5.9. The high-resolution XPS spectrum of (A) Ti and (B) O of the TiO_2 nanotube electrode fabricated over 16 H following EC treatment.

Table 5.4. Binding Energies and XPS Atomic Ratios for Ti and O of TiO_2 before and after treatment.

Name	Binding Energy (eV)	Before EC (%)	After EC (%)
Ti^{4+}	458.57	95.11	93.46
Ti^{3+}	457.45	3.25	4.35
Ti^{2+}	456.88	1.64	2.10

Name	Binding Energy (eV)	Before EC (%)	After EC (%)
Ti-O	530.79	80.95	75.79
C=O	531.84	12.24	17.54
C-OH	532.83	6.81	6.68
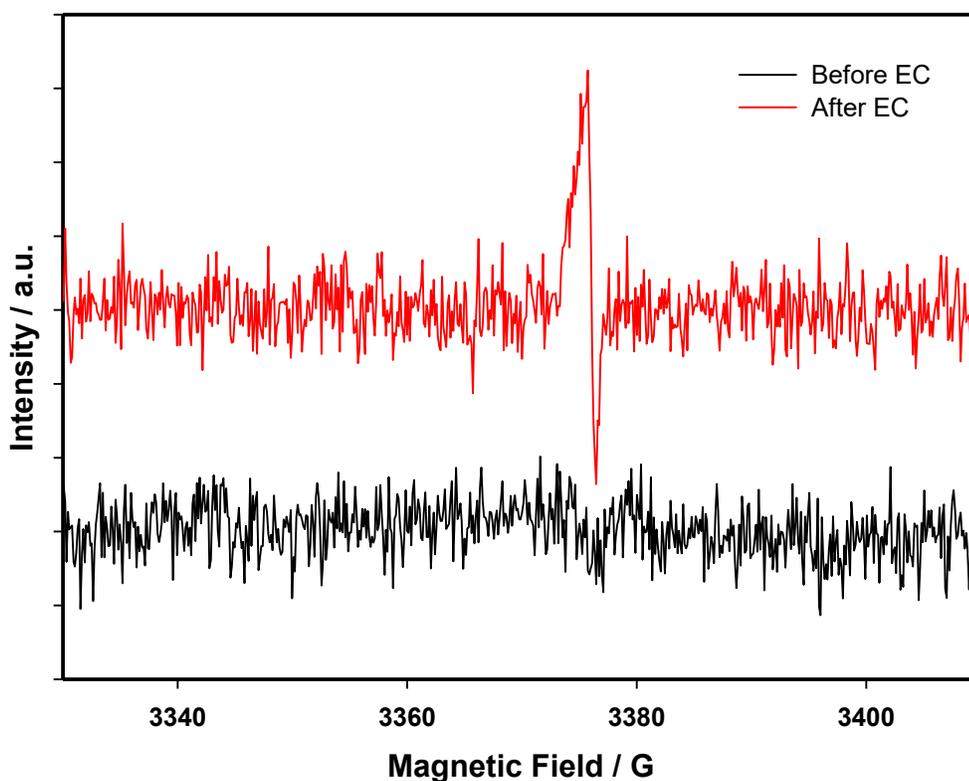
Figure 5.10. EPR spectra of the TiO_2 nanotubes prior to and following EC treatment. Microwave frequency: 9.4488 GHz.

5.3.4 XPS and EPR analysis

To understand the changes of electronic states and chemical compositions due to the EC treatment, XPS was carried out. Figure 5.9 depicts the high-resolution XPS spectrum of the Ti and O of the TiO_2 nanotube electrode synthesized over 16 H following the EC treatment, and Table

5.4 shows the atomic percentages of the various oxidation states of Ti and O that were calculated from XPS, prior to and following the EC treatment. It can be seen in Figure 5.9A, the peak located at 458.57 eV was attributed to Ti^{4+}, and the binding energies at 457.45 and 456.88 eV corresponded to Ti^{3+} and Ti^{2+}, respectively. This obviously verified the presence of various Ti oxidation states within the TiO_2 nanotubes. Moreover, the level of Ti(IV) declined from 95.11% to 93.46% following the EC treatment, while Ti(III) and Ti(II) increased from 3.25% to 4.35%, and 1.64% to 2.10%, respectively.

In other words, the reduction of Ti^{4+} was undoubtedly identified by XPS. As shown in Figure 5.9B, the O 1s peak can be deconvoluted into three peaks, where the most intense peak at 530.79 eV might be assigned to the lattice oxygen, whereas the other two peaks centered at 531.84 and 532.83 eV may be attributed to surface species such as hydroxyl groups, chemisorbed water, and/or oxygen. Furthermore, the level of the lattice oxygen decreased from 80.95% to 75.79% following the EC treatment, while the surface species increased. This may have been due to the increase of adsorption centers derived from oxygen vacancies that were generated by the EC treatment. This is very beneficial for the application of TiO_2 in wastewater treatment, as hydroxyl groups might produce highly oxidizing OH radicals, which can degrade myriad organic compounds. In addition, the recombination of electron-hole pairs might be repressed by the reaction of surface hydroxyl groups and photogenerated holes; therefore, charge transfer would be highly improved.

EPR spectroscopy was employed at 100 K on the TiO_2 nanotubes prior to and following the EC treatment to further detect paramagnetic species. As shown in Figure 5.10, the EPR spectra of the TiO_2 nanotubes before the EC treatment did not exhibit any clear signals to indicate the absence of paramagnetic species. However, a sharp peak at g = 1.9999 may be observed owing to the

formation of paramagnetic Ti^{3+} centers. These results are in agreement with the XPS studies presented above.

5.4. Conclusions

In summary, it has been demonstrated that various lengths of the fabricated TiO_2 nanotubes had a very significant effect on their electrocatalytic activity toward the oxidation of lignin. Electrodes with different lengths of TiO_2 nanotubes grown onto them were fabricated by anodizing titanium substrates over different time periods. These electrodes were then electrochemically reduced by applying -5 mA cm^{-2} for 10 min. SEM results showed nanotubes with lengths of ca. 4.23, 8.05, 10.80, 13.50, and 15.50 μm corresponding to 4, 8, 12, 16, and 20 H of anodization, respectively. Generally, with increases in the lengths of the nanotubes a broader double layer charging and discharging figure was obtained through cyclic voltammetry. However, the 16 H anodized electrode maintained the highest current response. Also, the TiO_2 nanotube electrode fabricated under 16 H of anodization gave the least charge transfer resistance, as compared to the electrodes prepared over 4, 8, 12, and 20 H. The 16 H anodized electrode also showed the fastest kinetics toward the electrochemical oxidation of lignin. The rate constant observed for the electrochemical oxidation of lignin with the 16 h treated TiO_2 was 11 times higher than a pure Pt electrode. The fabricated electrode exhibited very high rate of stability, as various cycles of lignin oxidation were run with the same electrode without any decrease in activity. Thus, this approach to fabricate TiO_2 nanotubes with optimal lengths followed by EC reduction might assist with the development of new and robust techniques for the oxidation of the lignin to various value-added products.

References

(1)   Deepa, A. K.; Dhepe, P. L. *ACS Catalysis* **2014**, *5*, 365-379.

(2)   Lanzalunga, O.; Bietti, M. *Journal of Photochemistry and Photobiology B: Biology* **2000**, *56*, 85-108.

(3)   Chatel, G.; Rogers, R. D. *ACS Sustainable Chemistry & Engineering* **2013**, *2*, 322-339.

(4)   Tian, M.; Wen, J.; MacDonald, D.; Asmussen, R. M.; Chen, A. *Electrochemistry Communications* **2010**, *12*, 527-530.

(5)   Pan, K.; Tian, M.; Jiang, Z.-H.; Kjartanson, B.; Chen, A. *Electrochimica Acta* **2012**, *60*, 147-153.

(6)   Nguyen, J. D.; Matsuura, B. S.; Stephenson, C. R. *Journal of the American Chemical Society* **2014**, *136*, 1218-1221.

(7)   Brown, M. E.; Chang, M. C. *Current opinion in chemical biology* **2014**, *19*, 1-7.

(8)   Kleine, T.; Buendia, J.; Bolm, C. *Green Chemistry* **2013**, *15*, 160-166.

(9)   Zhao, J.; Xiuwen, W.; Hu, J.; Liu, Q.; Shen, D.; Xiao, R. *Polymer Degradation and Stability* **2014**, *108*, 133-138.

(10)   Ma, R.; Hao, W.; Ma, X.; Tian, Y.; Li, Y. *Angewandte Chemie International Edition* **2014**, *53*, 7310-7315.

(11)   Pandey, M. P.; Kim, C. S. *Chemical Engineering & Technology* **2011**, *34*, 29-41.

(12)   Roberts, V.; Stein, V.; Reiner, T.; Lemonidou, A.; Li, X.; Lercher, J. A. *Chemistry–A European Journal* **2011**, *17*, 5939-5948.

(13)   Xu, C.; Arancon, R. A. D.; Labidi, J.; Luque, R. *Chemical Society Reviews* **2014**, *43*, 7485-7500.

(14)   Toledano, A.; Serrano, L.; Pineda, A.; Romero, A. A.; Luque, R.; Labidi, J. *Applied Catalysis B: Environmental* **2014**, *145*, 43-55.

(15)   Hu, J.; Shen, D.; Wu, S.; Zhang, H.; Xiao, R. *Journal of Analytical and Applied Pyrolysis* **2014**, *106*, 118-124.

(16)   Chen, A.; Rogers, E. I.; Compton, R. G. *Electroanalysis* **2010**, *22*, 1037-1044.

(17)   Tolba, R.; Tian, M.; Wen, J.; Jiang, Z.-H.; Chen, A. *Journal of Electroanalytical Chemistry* **2010**, *649*, 9-15.

(18)   Stärk, K.; Taccardi, N.; Bösmann, A.; Wasserscheid, P. *ChemSusChem* **2010**, *3*, 719-723.

(19)   Zhao, X.; Zhu, J. *ChemSusChem* **2016**, *9*, 197-207.

(20)   Shao, D.; Liang, J.; Cui, X.; Xu, H.; Yan, W. *Chemical Engineering Journal* **2014**, *244*, 288-295.

(21)   Parpot, P.; Bettencourt, A.; Carvalho, A.; Belgsir, E. *Journal of applied electrochemistry* **2000**, *30*, 727-731.

(22)   Belgsir, E.; Bettencourt, A.; Carvalho, A.; Parpot, P. *PORTUGALIAE ELECTROCHIMICA ACTA* **1997**, *15*, 413-416.

(23)   Zakzeski, J.; Bruijnincx, P. C.; Jongerius, A. L.; Weckhuysen, B. M. *Chemical reviews* **2010**, *110*, 3552-3599.

(24)   Ma, Y.-S.; Chang, C.-N.; Chiang, Y.-P.; Sung, H.-F.; Chao, A. C. *Chemosphere* **2008**, *71*, 998-1004.

(25)   Zhang, X.; Wang, T.; Ma, L.; Zhang, Q.; Huang, X.; Yu, Y. *Applied energy* **2013**, *112*, 533-538.

(26)   Fujishima, A.; Zhang, X.; Tryk, D. A. *Surface Science Reports* **2008**, *63*, 515-582.

(27)   Chen, X.; Mao, S. S. *Chem. Rev* **2007**, *107*, 2891-2959.

(28)   Tian, J.; Zhao, Z.; Kumar, A.; Boughton, R. I.; Liu, H. *Chemical Society Reviews* **2014**, *43*, 6920-6937.

(29)   Formo, E.; Lee, E.; Campbell, D.; Xia, Y. *Nano Letters* **2008**, *8*, 668-672.

(30)   Chen, X.; Liu, L.; Huang, F. *Chemical Society Reviews* **2015**, *44*, 1861-1885.

(31)   Chen, X.; Liu, L.; Peter, Y. Y.; Mao, S. S. *Science* **2011**, *331*, 746-750.

(32)   Sun, C.; Jia, Y.; Yang, X.-H.; Yang, H.-G.; Yao, X.; Lu, G. Q.; Selloni, A.; Smith, S. C. *The Journal of Physical Chemistry C* **2011**, *115*, 25590-25594.

(33)   Yu, X.; Kim, B.; Kim, Y. K. *ACS Catalysis* **2013**, *3*, 2479-2486.

(34)   Choi, D.; Blomgren, G. E.; Kumta, P. N. *Advanced Materials* **2006**, *18*, 1178-1182.

(35)   Fan, X.; Lu, Y.; Xu, H.; Kong, X.; Wang, J. *Journal of Materials Chemistry* **2011**, *21*, 18753-18760.

(36)   Oda, H.; Yamashita, A.; Minoura, S.; Okamoto, M.; Morimoto, T. *Journal of Power sources* **2006**, *158*, 1510-1516.

Chapter 6: Significant Enhancement of the Photoelectrochemical Activity of Nanoporous TiO₂ for Environmental Applications[*]

6.1 Introduction

The progressive degradation of water quality has become a critical issue globally, due to the rapid pace of industrial development and the cumulative discharge of myriad contaminants into ecosystems via wastewater.[1-3] Among the numerous contaminants that are released into the environment, a considerable quantity of dye pollutants from the textile, dyestuff, printing, cosmetics, plastics, and other industries, are rapidly emerging as one of the primary sources of environmental contamination.[4] As is known, dye pollutants may easily cause eutrophication and aesthetic pollution, while also having very toxic, mutagenic and carcinogenic effects in aquatic life and in humans.[5-6] Nevertheless, their complex and stable aromatic molecular structures enable them to successfully resist most conventional physical, chemical, and biological treatments. As a result, enormous efforts have been invested toward the development of feasible and efficacious dye wastewater treatment technologies.[7-8] Over the past two decades, advanced oxidation processes (AOPs) have emerged as an effective technology to address organic compounds, and comprise a major focus of research and development. AOPs belong to the category of chemical treatments and are based on the generation of highly reactive hydroxyl free radicals, which have the capacity to react with most organic and inorganic substances that reside in wastewater. According to various hydroxyl radical generation mechanisms, AOPs include wet oxidation, Fenton's process, ozone oxidation, ultrasonic processes, photocatalytic oxidation, and

---

electrocatalytic oxidation.[9-14] In comparison with other strategies, photocatalytically induced AOPs, which offer a clean, versatile and powerful tool for the removal of refractory organic pollutants, have attracted considerable interest. Their outstanding advantages include that no additional chemicals are required, they operate under mild conditions, using easily acquired equipment, and are economical and efficient. A wide variety of photocatalyst materials (e.g., TiO_2, WO_3, PbO_2, ZnO, ZnS, and CdS) have been reported to facilitate the oxidation of organic compounds.[15-18]

The properties of TiO_2 have been investigated extensively since the discovery of the photoelectrochemical oxidation of water over TiO_2 by Fujishima and Honda.[19-22] However, due to its large band gap (~3.0 eV for rutile and ~3.2 eV for anatase),[23-26] TiO_2 remains an inefficient candidate for utilization of solar energy. Therefore, it is desirable to perform band gap engineering to potentially enable this material for practical use. Various techniques have been employed to narrow the band gap of TiO_2, including doping with non-metal elements, which is the most common procedure for augmenting visible light photocatalytic activity. The doping of TiO_2 with C, N, F and S has demonstrated improvements in its UV-visible light response.[27-32] However, recent theoretical and experimental studies have raised questions in regard to this strategy and its suitability as the most efficient approach.

Reduced TiO_2 has attracted considerable interest, and various methods have been employed for the reduction of TiO_2, such as heating in the presence of reduction agents (e.g., H_2) and bombardment with high energy particles (electrons or Ar^+).[33-37] There are several factors, however, that have limited these methods for practical applications, including multiple steps, harsh conditions, and/or expensive facilities. Therefore, it remains a challenge to develop a facile and economical method for the synthesis of reduced TiO_2. In our recent work, it has been reported on

a new approach for the significant enhancement of the electrocatalytic activity of TiO_2 nanotubes, which were fabricated by the electrochemical oxidation of titanium in dimethyl sulfoxide (DMSO) with 2% HF. They were treated via electrochemical reduction and tested as an electrocatalyst for the electrochemical oxidation of salicylic acid[38] or treated using strong UV-visible light irradiation.[39] In the present work, a three-step electrochemical anodization process in ethylene glycol + 0.3 wt% NH_4F + 2 wt% H_2O was employed to synthesize highly ordered nanoporous TiO_2, which was then electrochemically reduced by applying a current density of -5 mA cm^{-2} for 10 min. Our experimental measurements demonstrated that this facile procedure resulted in an immense six-fold increase in photocurrent as well as six times more rapid photoelectrochemical degradation of RhB.

6.2 Experimental

6.2.1 Materials

Solutions were prepared using sulfuric acid (Aldrich, 99.999%) and pure water, which was purified by a Nanopure water system (18.2 MΩ cm). All solutions were deaerated with ultrapure Ar (99.999%) prior to the experiments.

6.2.2 Fabrication and modification of nanoporous TiO_2

The fabrication of highly ordered nanoporous TiO_2 is already discussed in section 3.2.3.2 of chapter 3. A three-electrode cell system was employed for the electrochemical measurements, wherein a Pt coil with a surface area of 10 cm^2 served as the auxiliary electrode, and an Ag/AgCl electrode was used as the reference electrode. The potential quoted in this paper was thus against the Ag/AgCl electrode, whose 0.0 V is equivalent to 0.197 V versus a reversible hydrogen electrode (RHE). The electrochemical (EC) treatment of the nanoporous TiO_2 was performed in a

0.1M H_2SO_4 solution under an applied current of -5 mA cm^{-2} for a different period of time varied from 2.5 to 40 min.

6.2.3 Characterization of the synthesized nanoporous TiO₂

The synthesized nanoporous TiO_2 was characterized by energy dispersive spectroscopy (EDS), field-emission scanning electron microscopy (FE-SEM, Hitachi SU 70), X-ray diffraction (Philips PW 1050-3710 Diffractometer with Cu Kα radiation), cyclic voltammetry (CV), linear voltammetry (LV), and chronamperometry. Mott−Schottky plots were measured in a 0.1M H_2SO_4 solution at a fixed frequency of 500 Hz. An ADAC Systems™ Cure Spot™ 50 was employed for the irradiation of the nanoporous TiO_2. The UV–visible light, with an intensity of 7.4 mW cm^{-2}, was introduced into the cell using a fibre optic cable, which was placed above the electrode, and the distance between the light source and the electrode surface was ~1.0 cm. The electrolyte utilized for the measurement of the photocurrent was 0.1M H_2SO_4, which was bubbled with Ar, prior to, and during the experiments.

6.2.4 Photoelectrocatalytic activity measurements

The photoelectrocatalytic oxidation of RhB (an organic dye pollutant) was investigated to further examine the photoelectrocatalytic activity of the synthesized nanoporous TiO_2 under UV–visible light, solar light and visible light with the applied electrode potential of 1.0 V versus Ag/AgCl. A Small Collimated Beam Solar Simulator (SF150C, Sciencetech Inc) with an intensity of one Sun was employed to introduce solar light into the reactor. The visible light source employed in this study consisted of an Oriel system including a 300 W xenon arc lamp. Meanwhile, infrared light and all light wavelengths below 400 nm were blocked by a water filter and an optical filter (Edmund Optical Co. GG420), respectively. The intensity of resulting light between 400 and 700 nm was measured to be ~2.50 mW cm^{-2} using a Cole-Palmer Instrument (Radiometer Series

9811). A Cary 50 UV/vis spectrophotometer was utilized to record the UV/vis spectra of RhB during the photoelectrochemical oxidation process. The total organic carbon (TOC) of the RhB solution prior to and after the photoelectrochemical degradation was measured using a TOC analyser (TOC-L CPH, Shimadzu).

6.3 Results and discussion

6.3.1 Characterization of nanoporous TiO$_2$

The structure and morphology of the synthesized nanoporous TiO$_2$ were characterized by SEM. As shown in Figure 6.1A, highly ordered nanopores were uniformly generated on the Ti substrate. A higher resolution SEM image is presented in Figure 6.1B, which revealed that the diameter of the nanopores was ~150 nm, and that each nanopore consisted of several smaller nanopores. It was obvious that the lumens of the pores were exposed at the top of the layer. Strong oxygen and titanium peaks with at a ratio of 2:1 were observed in the EDS (Figure 6.2A), which confirmed the formation of the TiO$_2$ nanoporous arrays. In order to determine the crystal structure and possible phase changes during the EC reduction of the nanoporous TiO$_2$, XRD spectra were collected. As is seen in Figure 6.2B, excluding the peaks (marked with asterisks) derived from the Ti substrate, all of the diffraction peaks were attributed to the tetragonal anatase TiO$_2$, which confirmed that the as-prepared TiO$_2$ nanopores exhibited the anatase phase subsequent to heating at 450 °C for 3h. The XRD spectra, prior to (red curve in Figure 6.2B), and following (blue plot in Figure 6.2B) the EC reduction, were practically identical, indicating that there was no alteration in the crystalline structure during the EC treatment.
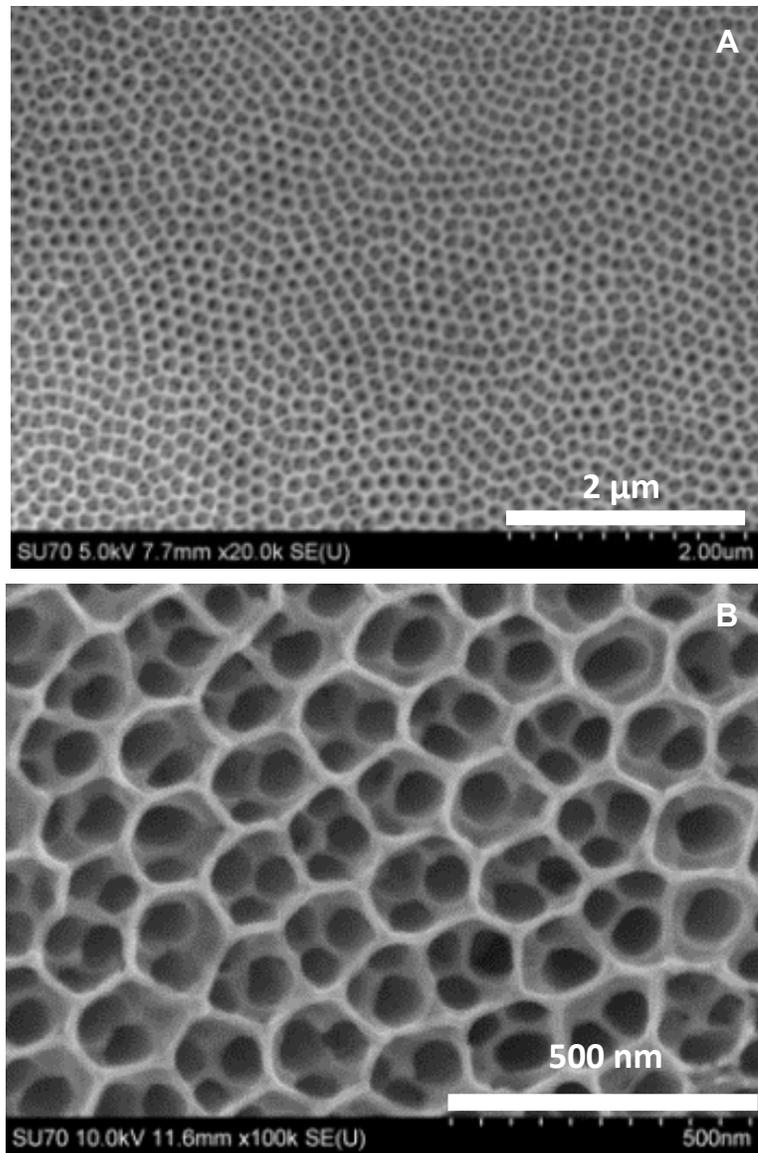
Figure 6.1 (A) and (B) SEM images of the fabricated nanoporous TiO$_2$.
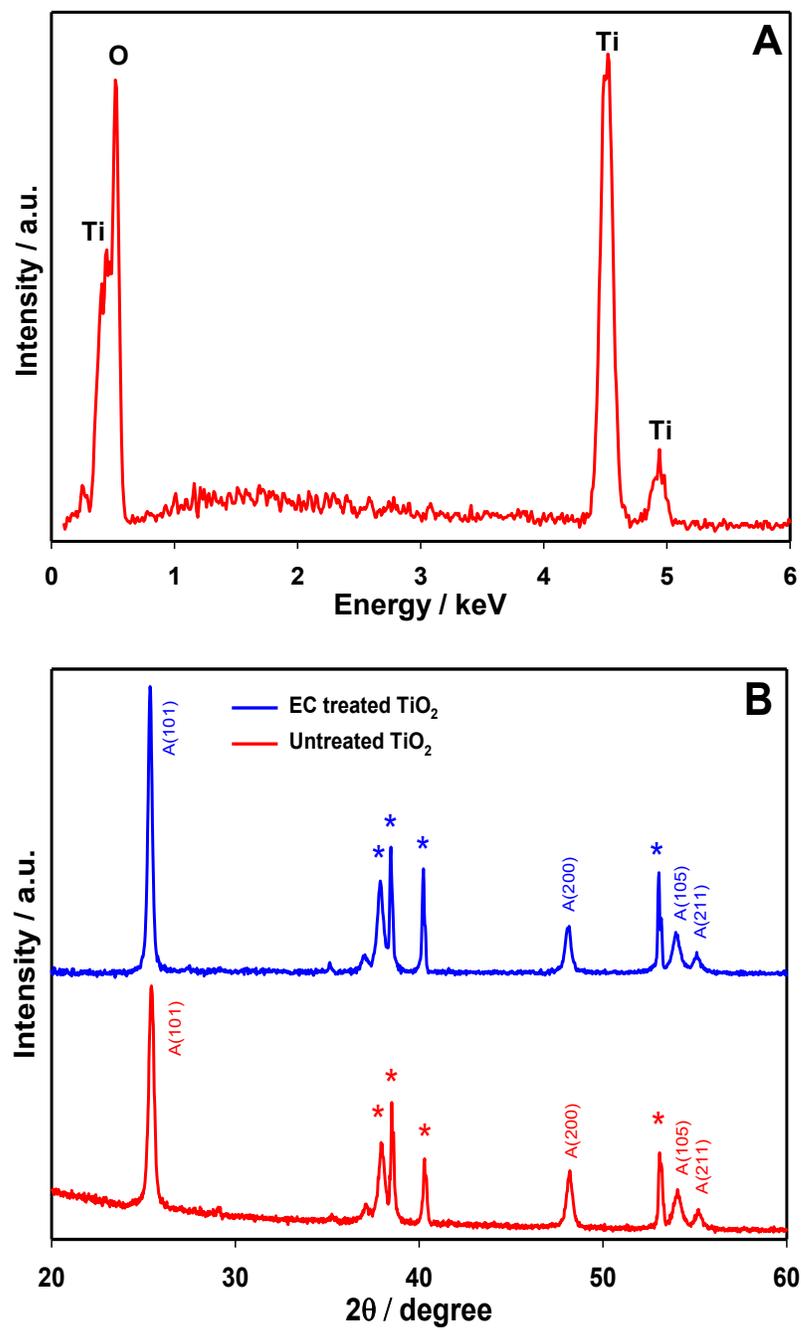
Figure 6.2 (A) EDX and (B) XRD spectra of the formed nanoporous TiO2.
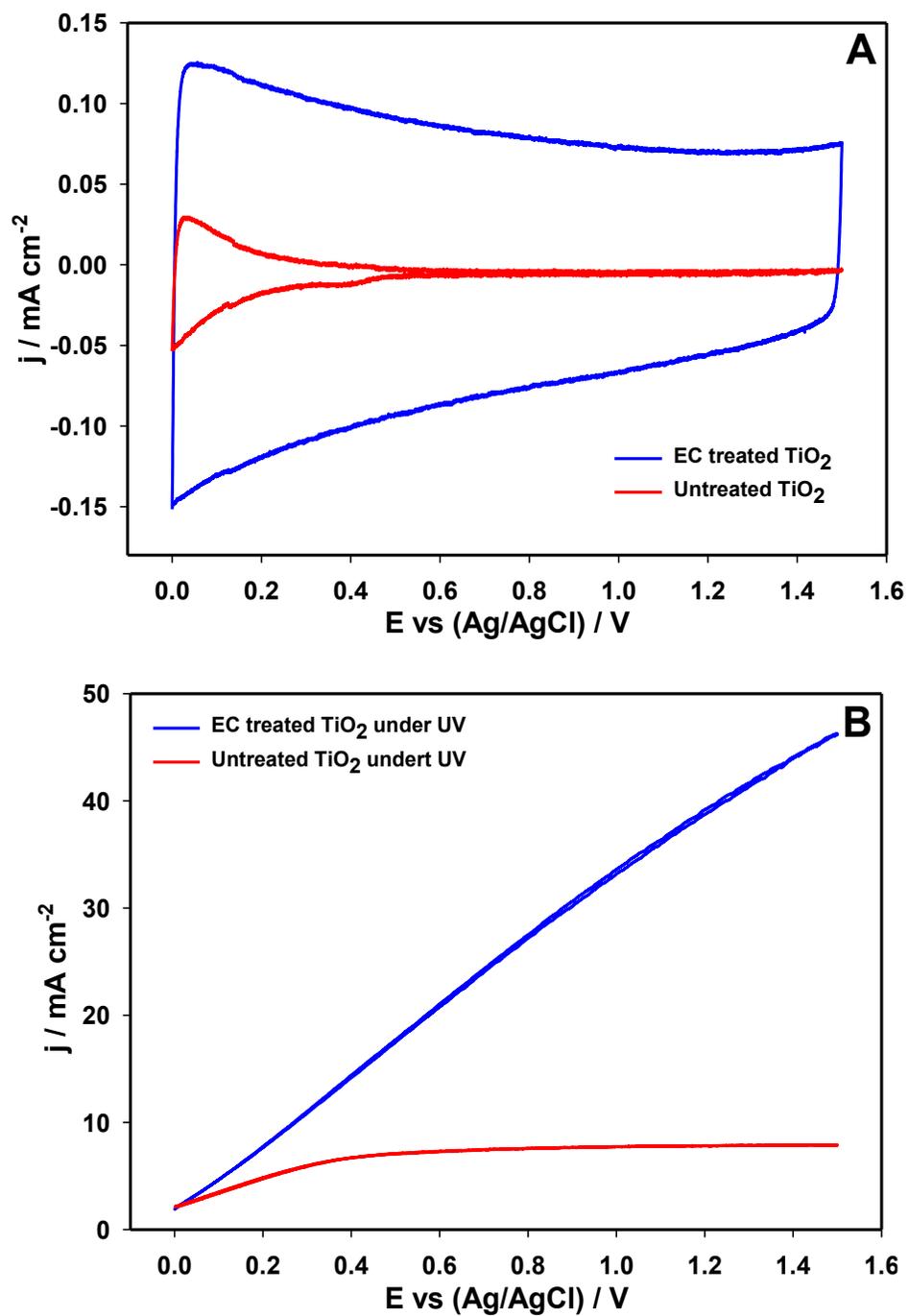
Figure 6.3 CVs of the nanoporous TiO_2 prior to (red), and following the EC treatment in 0.1 M H_2SO_4 (A) in darkness and (B) under UV-visible light. (Scan rate: 20 mV s^{-1})

Figure 6.3A depicts the cyclic voltammograms of the synthesized nanoporous TiO_2, which were recorded in a 0.1M H_2SO_4 solution at a scan rate of 20 mV s^{-1}, prior to (red curve), and following (blue curve) the EC treatment. The CV of the nanoporous TiO_2 prior to the EC reduction was divisible into two distinct regions: (I) an initial stage where hydrogen adsorption/desorption took place, between 0 and 0.35 V; and (II) a double-layer charging region, between 0.35 and 1.5 V. The CV of the nanoporous TiO_2 that underwent the EC treatment was dramatically different from that of the nanoporous TiO_2 without the EC treatment. Aside from the large current increase in Region I, the current in Region II was significantly increased.

Figure 6.3B depicts the CVs of the synthesized nanoporous TiO_2, which were recorded in a 0.1M H_2SO_4 solution at a scan rate of 20 mV s^{-1} under UV–visible light prior to (red curve), and following (blue curve) the EC treatment. The photocurrent of the untreated nanoporous TiO_2 was slowly increased when scanning the electrode potential from 0.0 to 0.8 V, and then maintained at ca. 7.70 mA cm^{-2}, while the photocurrent of the nanoporous TiO_2 that underwent the EC treatment increased continuously in the investigated potential range, attaining 46.23 mA cm^{-2} at 1.5 V, which was ca. six times higher than that of nanoporous TiO_2 without the EC treatment. Moreover, it was interesting to note that the photocurrent of the TiO_2 nanotubes, which were fabricated by the electrochemical oxidation of titanium in dimethyl sulfoxide (DMSO) with 2% HF was only ~0.35 mA cm^{-2} under the same conditions, which was approximately 133 times smaller than that of EC treated nanoporous TiO_2 [39].

Figure 6.4A present the electrode potential versus time plot of the nanoporous TiO_2 electrode recorded during the EC treatment in 0.1 M H_2SO_4 under the applied current density of -5 mA cm^{-2}. The electrode potential was rapidly increased from -0.3 to -1.0 V during the initial three-minute EC treatment, and then decreased to -0.94V, indicating electrochemical reduction
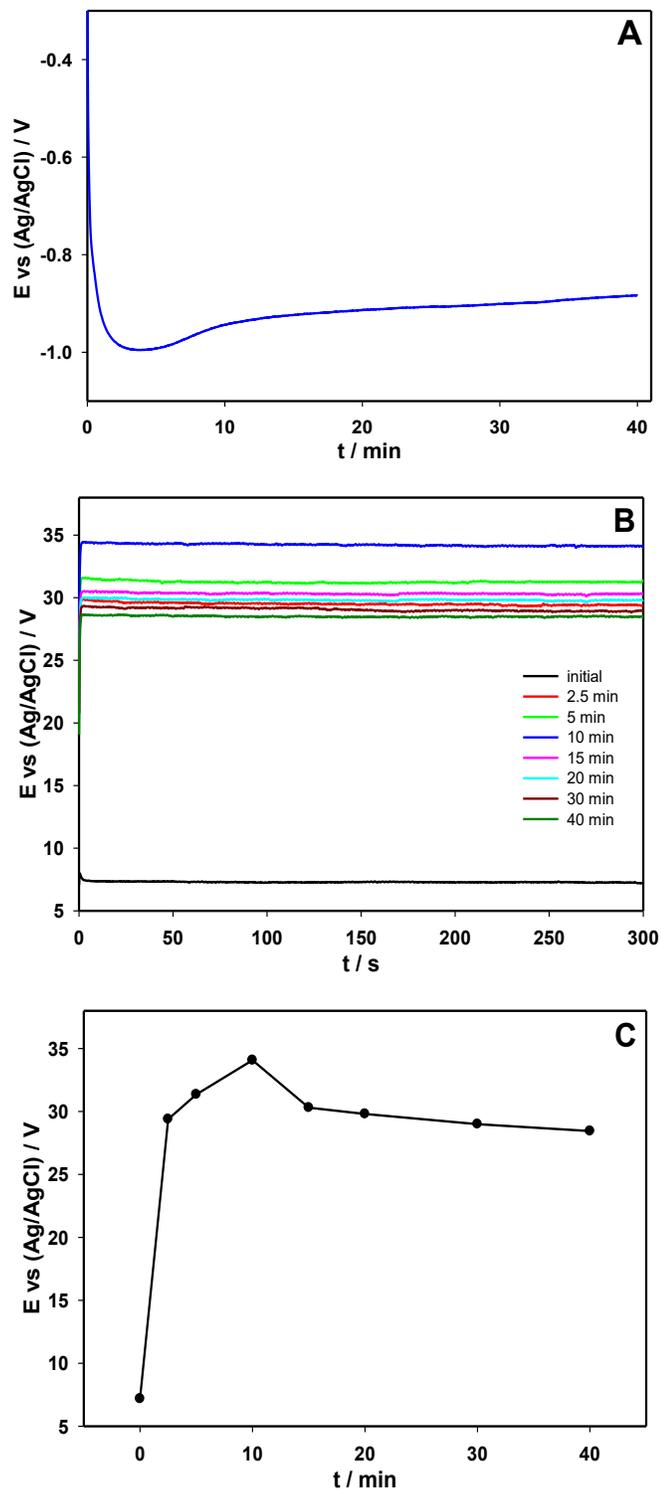
Figure 6.4 (A) Chronopotentiometric curves of the nanoporous TiO$_2$ electrode recorded in 0.1M H$_2$SO$_4$ at −5 mA cm^{-2}, (B) Chronoamperometric curves of the nanoporous TiO$_2$ electrode recorded in 0.1M H$_2$SO$_4$ at 1.0 V prior to, and following EC treatment at −5 mA cm^{-2} for different time periods under UV-visible light, and (C) Plot of the steady-state currents measured at 300 s from the curves presented in panel A versus the time of the EC treatment.

114
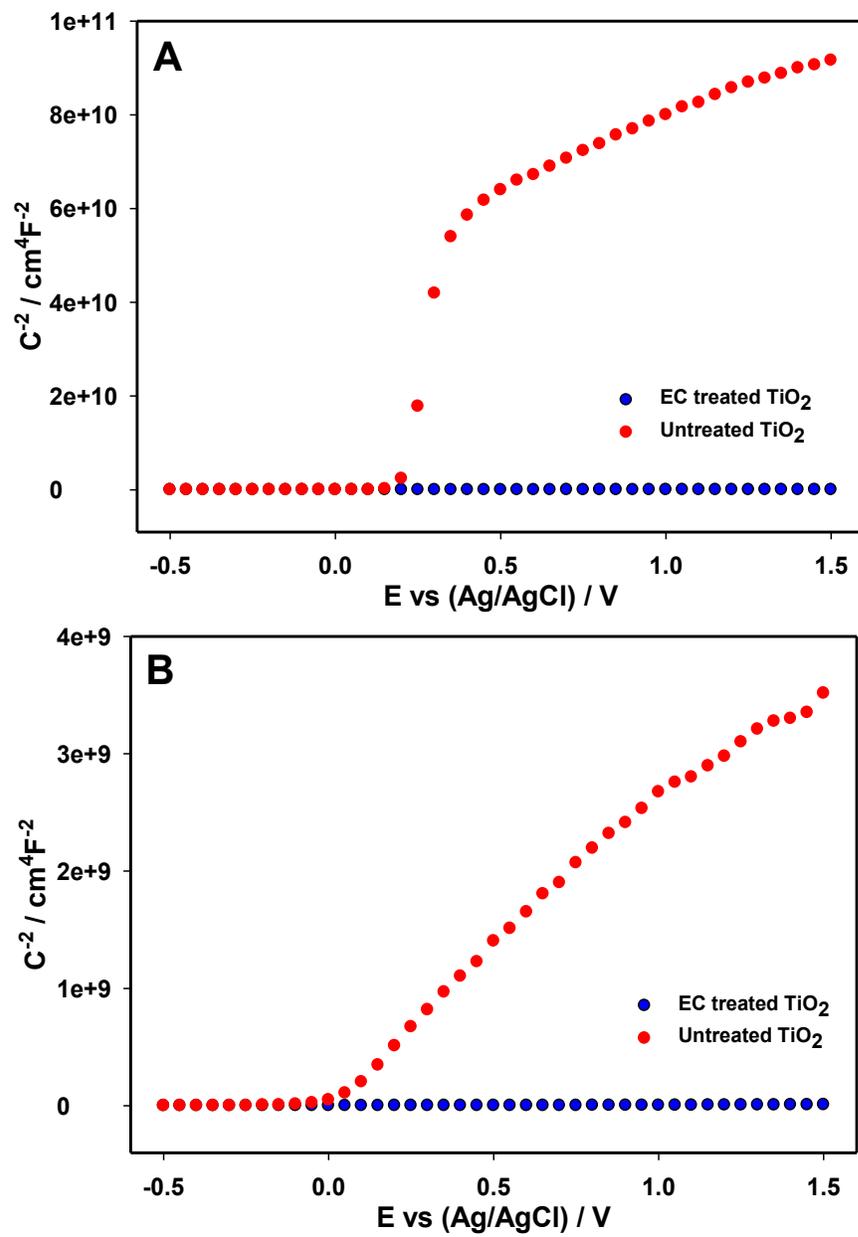
Figure 6.5 Mott-Schotty plots of the nanoporous TiO_2 obtained in 0.1M H_2SO_4 at 500 Hz prior to, and following the treatment (A) in darkness and (B) under UV-visible light.

of TiO_2 chiefly occurred at the beginning of the EC treatment. Significant hydrogen gas evolution was observed on the electrode surface during the EC treatment. Further prolonging the EC treatment time from 10 to 40 min, the electrode potential was gradually decreased from -0.94 to -0.88 V, which might be attributed to the enhancement of conductivity of nanoporous TiO_2 achieved by the EC treatment.

The effect of EC treatment time on the electrochemical activity of the nanoporous TiO_2 was further investigated. Chronoamperometric curves of the nanoporous TiO_2 prior to and following EC treatment at -5 mA cm^{-2} for various durations were recorded in 0.1 M H_2SO_4 under the UV-visible light. As seen in Figure 6.4B, even 2.5 min of EC treatment resulted in a significant increase in the steady-state photocurrent. However, there was no further increase in the photocurrent obtained beyond 10 min (or longer) treatments. Figure 6.4C presents the plot of steady-state current densities that were measured from the chronoamperometric curves (Figure 6.4B) at 300 s. It was obvious that ten-minute EC treatment produced the highest steady-state photocurrent. As seen in Figure 6.4A, there was a significant potential change during the first ten-minute electrochemical reduction; and the electrode potential was slightly decreased in the additional 30-minute treatment. The electrochemical treatment may result in the reduction of the Ti^{4+} to Ti^{3+}, the increase of oxygen vacancies, as well as the disorder of the TiO_2 surface structure caused by the strong hydrogen evolution. These changes could result in the alterations to the electronic and superficial structure of the TiO_2. To some extent the self-doping of Ti^{3+}, the increase of oxygen vacancies and surface disorder are permissible; but if the threshold level is crossed, the photoelectrochemical performance of the treated TiO_2 could be decreased.

To elucidate the insight of this significant enhancement, which was imparted by the EC treatment, the electronic and photoelectronic properties of the nanoporous TiO_2, prior to and

following the EC treatment, were investigated. Mott–Schottky measurements were carried out in a 0.1M H_2SO_4 solution to determine the donor densities (N_D).[42-43] Figure 6.5A and B present the Mott−Schottky plots of the native untreated nanoporous TiO_2 and the electrochemically treated nanoporous TiO_2, both with and without UV–visible light, respectively. There was a good linear relationship between C^{-2} and the potential in the range between 0.15 and 0.40 V vs Ag/AgCl for the untreated, as well as for the electrochemically treated nanoporous TiO_2. It was intriguing to note that the donor density of the nanoporous TiO_2, which underwent the electrochemical treatment (2.4×10^{21} cm^{-3} in darkness, 3.8×10^{22} cm^{-3} under UV–visible light) was almost 54000 times and 9690 times, respectively, larger than that of the nanoporous TiO_2 without the treatment (4.4×10^{16} cm^{-3} in darkness, 3.9×10^{18} cm^{-3} under UV–visible light, respectively).

Figure 6.6A presents the linear voltammograms (LVs) of the TiO_2 nanopores, which were recorded in a 0.1M H_2SO_4 solution at a scan rate of 1 mV s^{-1}, prior to (red curve) and following (blue curve) the EC treatment. The photocurrent transients were observed by switching the UV–visible light on and off. The duration of light pulses was set at 100 s, followed by 100 s of darkness. The photocurrents of the nanoporous TiO_2 with the EC treatment were much higher than those of the untreated nanoporous TiO_2, which was consistent with the results of the cyclic voltammetric measurements shown in Figure 6.3B.

Additionally, the stability of the treated nanoporous TiO_2 was studied in a 0.1 M H_2SO_4 solution at an applied electrode potential of 1.0 V vs. Ag/AgCl under UV–visible light. The steady-state photocurrent and transient photocurrent were recorded by switching the light on for 20 min and then off for 2 min. As seen in Fig. 6B, the responses of the photocurrent under UV–visible light irradiation were rapid and stable, with almost no change over the 800 min test, indicating the prominent stability of the EC treated nanoporous TiO_2. The electrochemical treatment not only

resulted in the formation of Ti^{3+} and oxygen vacancies, but also caused the disorder of the surface structure. The high stability under the long anodic polarization observed in Figure 6.6B can be attributed to the change of the electronic and structure of TiO$_2$ during the EC treatment.
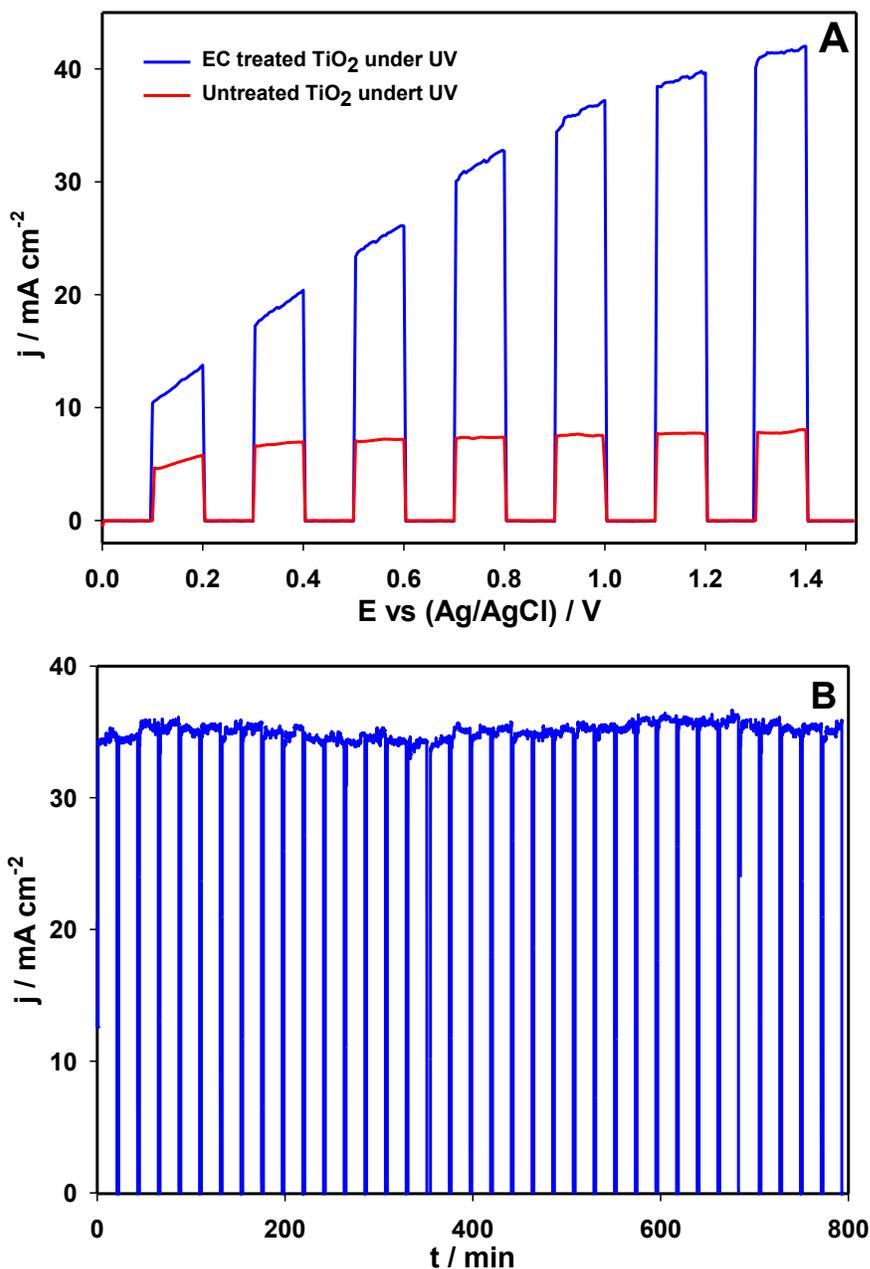
Figure 6.6 (A) LVs of the nanoporous TiO$_2$ prior to (red), and following the EC treatment in 0.1M H$_2$SO$_4$ under the UV-visible light (Scan rate: 1 mV s^{-1}) and (B) Stability test of the EC reduced nanoporous TiO$_2$ carried out in 0.1 M H$_2$SO$_4$ (Applied potential bias: 1.0 V; the duration of light pulses was set at 20 min, followed by dark current measurements for 2 min).
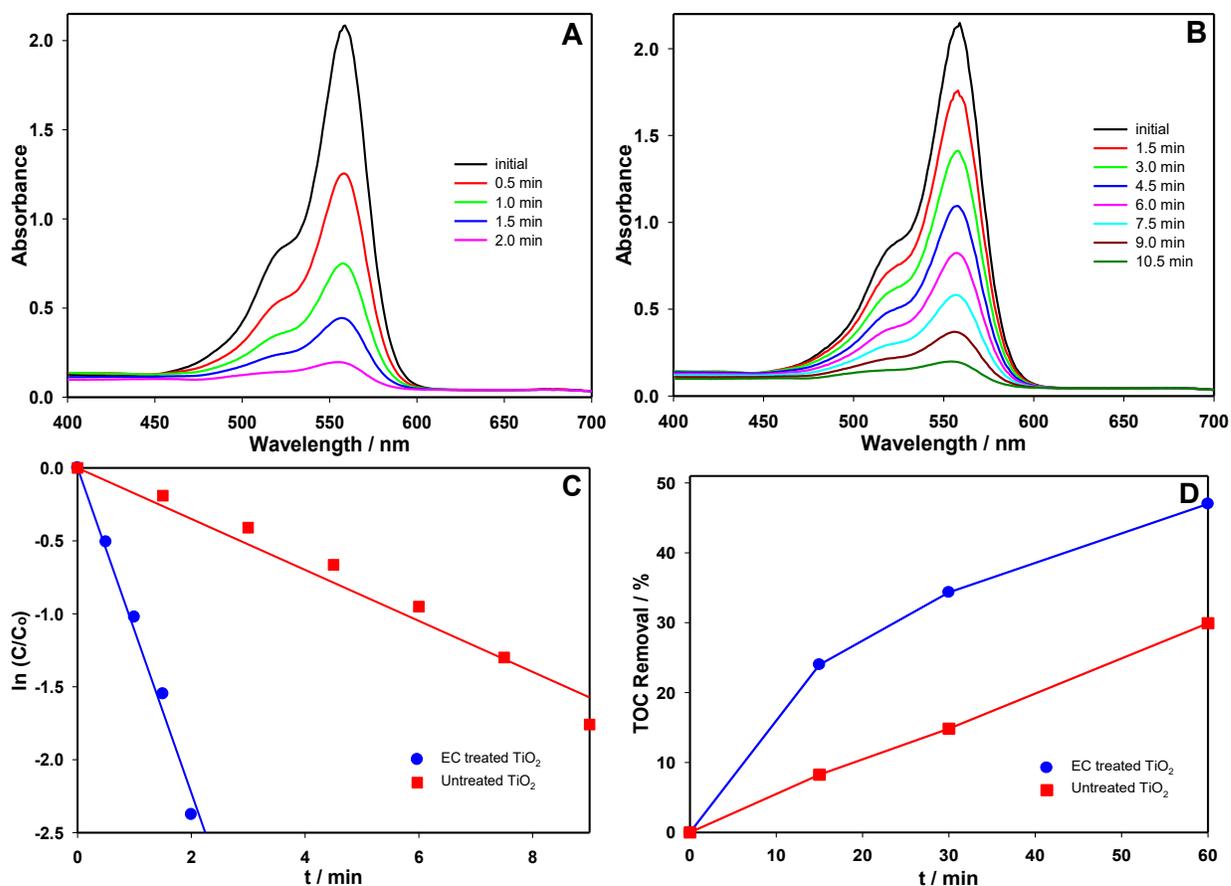
Figure 6.7 Absorbance spectra for the photoelectrochemical oxidation of 25.0 μM Rh B in 0.1 M H_2SO_4 at (A) the electrochemically treated nanoporous TiO_2, and (B) the untreated nanoporous TiO_2 under UV–visible light; (C) Plot of $\ln(C/C_o)$ versus time (Applied potential bias: 1.0 V); and (D) Plot of TOC removal of Rh B solution versus photoelectrochemical oxidation time.

6.3.2 Photoelectrochemical oxidation of Rh B at the nanoporous TiO_2 electrode

We conducted a further investigation into the photoelectrochemical oxidation of Rh B to examine the enhanced photoactivity of the nanoporous TiO_2, subsequent to the EC treatment under UV–visible light, solar light and visible light at an applied potential of 1.0 V. Figure 6.7A shows the time dependence of the spectral absorbance of 25.0μM Rh B in 0.1M H_2SO_4 obtained at 30-second intervals during the photoelectrochemical oxidation process under UV–visible light. The absorbance of Rh B at 558 nm decreased with time and approached 0.19 following only 2 min of photoelectrochemical degradation, which corresponded to a >91% Rh B removal from the solution.

For comparison, the photoelectrochemical oxidation of Rh B was also carried out at native untreated nanoporous TiO_2 (Figure 6.7B), where a similar proportion of Rh B removal from solution was achieved after 10.5 min of the photoelectrochemical degradation. As shown in Figure 6.7C, the photoelectrochemical oxidation of Rh B at the as-prepared nanoporous TiO_2 and the nanoporous TiO_2 that underwent EC treatment may be fitted based on the first-order kinetics. The TOC contents were further analyzed to measure the effectiveness of the photoelectrochemical oxidation of RhB at the untreated and treated nanoporous TiO_2 electrodes. As shown in Figure 6.7D, The TOC removal with the EC treated nanoporous TiO_2 electrode was much quicker, in comparison to the untreated nanoporous TiO_2 electrode under the same photoelectrochemical degradation conditions.

The rate constants for the oxidation of Rh B under the UV-visible irradation at the nanoporous TiO_2, with and without EC treatment, were found to be 1.159 min^{-1} and 0.191 min^{-1}, respectively (Figure 6.8A). It was apparent that the oxidation of Rh B at the electrochemically treated nanoporous TiO_2 was ca. six times more rapid than that of the nanoporous TiO_2 without the EC treatment, indicating a significant enhancement in UV–visible light activity. This was consistent with the photocurrents observed in Figure 6.3.

The solar and visible light photoelectrochemical activity of the nanoporous TiO_2 were further studied. The absorbance spectra for the photoelectrochemical oxidation of 25.0 μM Rh B in 0.1 M H_2SO_4 at a 1.0 V applied potential were recorded at different time intervals during the oxidation process, under solar light and visible light (figures not shown). As expected, the absorbance peak of Rh B at 558 nm also decreased with time at the untreated and treated nanoporous TiO_2 under
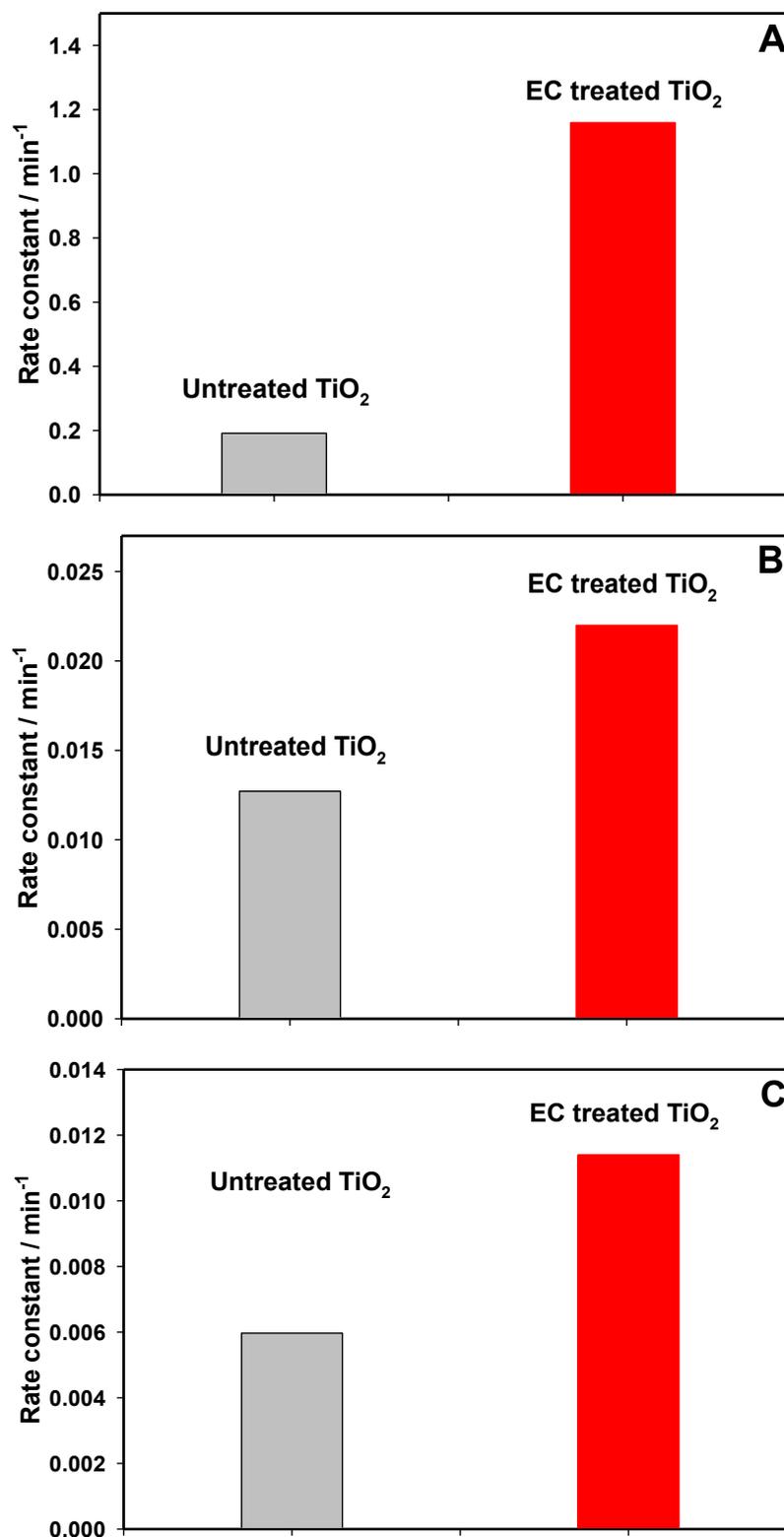
Figure 6.8 Rate constants for the photoelectrochemical oxidation of 25.0 μM Rh B in 0.1 M H$_2$SO$_4$ at the electrochemically treated nanoporous TiO$_2$ and the untreated nanoporous TiO$_2$ under (A) UV-visible light; (B) solar light and (C) visible light (>400 nm) (ApplRhBied potential bias: 1.0 V).

121

both solar light and visible light. However, the nanoporous TiO_2 that underwent the EC treatment exhibited a much shorter time requirement to achieve a similar proportion of Rh B removal. As shown in Figure 6.8B and Figure 6.8C, 73.2% and 90.0% increases of the rate constants of the photoelectrochemical oxidation of Rh B were observed at the electrochemical treated nanoporous TiO_2, in comparison to the untreated electrode under exposure to solar and visible light, respectively. The enhanced activity of the EC treated nanoporous TiO_2 might have been due to an efficient charge separation and increased donor density. As a result of this situation, the tendency for electron-hole recombination was decreased, allowing the photogenerated conduction band electrons and valence band holes were available to drive photoelectrochemical reactions for the degradation of organic pollutants.

6.4 Conclusions

In summary, a novel and simple approach for the significant enhancement of UV–visible light solar and visible light activity of nanoporous TiO_2 has been demonstrated. Using this approach, TiO_2 was in situ electrochemically reduced. The treated nanoporous TiO_2 exhibited remarkable stability under UV–visible light, as well as a six-fold enhancement in photocurrent, which was over 130 times higher than that of the TiO_2 nanotubes fabricated by the electrochemical oxidation of titanium in dimethyl sulfoxide (DMSO) with 2% HF. Moreover, when compared with untreated nanoporous TiO_2, this facile reduction treatment resulted in an extraordinary increase in the donor density of the nanoporous TiO_2 (by approximately four orders of magnitude) and was six times faster for the photoelectrochemical degradation of Rh B. The solar and visible light catalytic activity of nanoporous TiO_2 toward the photoelectrochemical degradation of Rh B were also improved via this facile reduction treatment, which is promising for environmental and energy applications.

References

(1)   Senthilkumar, S.; Basha, C. A.; Perumalsamy, M.; Prabhu, H. *Electrochimica Acta* **2012**, *77*, 171-178.

(2)   Alvarado, L.; Chen, A. *Electrochimica Acta* **2014**, *132*, 583-597.

(3)   Ramos, C.; García, A.; Diez, V. *Water research* **2014**, *67*, 203-215.

(4)   Thind, S. S.; Wu, G.; Chen, A. *Applied Catalysis B: Environmental* **2012**, *111*, 38-45.

(5)   Vakili, M.; Rafatullah, M.; Salamatinia, B.; Abdullah, A. Z.; Ibrahim, M. H.; Tan, K. B.; Gholami, Z.; Amouzgar, P. *Carbohydrate polymers* **2014**, *113*, 115-130.

(6)   Horikoshi, S.; Hojo, F.; Hidaka, H.; Serpone, N. *Environmental science & technology* **2004**, *38*, 2198-2208.

(7)   Fu, H.; Pan, C.; Yao, W.; Zhu, Y. *The Journal of Physical Chemistry B* **2005**, *109*, 22432-22439.

(8)   Zhang, L.; Xu, L.; He, J.; Zhang, J. *Electrochimica Acta* **2014**, *117*, 192-201.

(9)   Adams, B.; Tian, M.; Chen, A. *Electrochimica Acta* **2009**, *54*, 1491-1498.

(10)   Andrade, L. S.; Tasso, T. T.; da Silva, D. L.; Rocha-Filho, R. C.; Bocchi, N.; Biaggio, S. R. *Electrochimica Acta* **2009**, *54*, 2024-2030.

(11)   Yang, Y.; Pignatello, J. J.; Ma, J.; Mitch, W. A. *Environmental science & technology* **2014**, *48*, 2344-2351.

(12)   Tian, M.; Thind, S. S.; Simko, M.; Gao, F.; Chen, A. *The Journal of Physical Chemistry A* **2012**, *116*, 2927-2934.

(13)   Huang, W.; Ji, Y.; Yang, Z.; Feng, X.; Liu, C.; Zhu, Y.; Lu, X. *Industrial & engineering chemistry research* **2010**, *49*, 6243-6249.

(14)   Matouq, M.; Al-Anber, Z.; Susumu, N.; Tagawa, T.; Karapanagioti, H. *Separation and Purification Technology* **2014**, *135*, 42-47.

(15)   Thind, S. S.; Tian, M.; Chen, A. *Electrochemistry Communications* **2014**, *43*, 13-17.

(16)   Chong, M. N.; Jin, B.; Chow, C. W.; Saint, C. *Water research* **2010**, *44*, 2997-3027.

(17)   Chen, A. *Canadian Journal of Chemistry* **2014**, *92*, 581-597.

(18)   Lü, W.; Chen, J.; Wu, Y.; Duan, L.; Yang, Y.; Ge, X. *Nanoscale research letters* **2014**, *9*, 1-7.

(19)   Fujishima, A. *nature* **1972**, *238*, 37-38.

(20)   Cheng, J.; Zhang, M.; Wu, G.; Wang, X.; Zhou, J.; Cen, K. *Environmental science & technology* **2014**, *48*, 7076-7084.

(21)   Hebert, K. R.; Albu, S. P.; Paramasivam, I.; Schmuki, P. *Nature materials* **2012**, *11*, 162-166.

(22)   Su, R.; Tiruvalam, R.; He, Q.; Dimitratos, N.; Kesavan, L.; Hammond, C.; Lopez-Sanchez, J. A.; Bechstein, R.; Kiely, C. J.; Hutchings, G. J. *ACS nano* **2012**, *6*, 6284-6292.

(23)   Chen, X.; Mao, S. S. *Chem. Rev* **2007**, *107*, 2891-2959.

(24)   Hwang, Y. J.; Hahn, C.; Liu, B.; Yang, P. *Acs Nano* **2012**, *6*, 5060-5069.

(25)   Chen, X.; Shen, S.; Guo, L.; Mao, S. S. *Chemical reviews* **2010**, *110*, 6503-6570.

(26)   Lee, W. J.; Lee, J. M.; Kochuveedu, S. T.; Han, T. H.; Jeong, H. Y.; Park, M.; Yun, J. M.; Kwon, J.; No, K.; Kim, D. H. *ACS nano* **2011**, *6*, 935-943.

(27)   Wu, G.; Nishikawa, T.; Ohtani, B.; Chen, A. *Chemistry of Materials* **2007**, *19*, 4530-4537.

(28)   Park, J. H.; Kim, S.; Bard, A. J. *Nano letters* **2006**, *6*, 24-28.

(29)   Wu, G.; Wang, J.; Thomas, D. F.; Chen, A. *Langmuir* **2008**, *24*, 3503-3509.

(30)   Zhang, C.; Li, Y.; Wang, Y.; He, H. *Environmental science & technology* **2014**, *48*, 5816-5822.

(31)   Hoang, S.; Guo, S.; Hahn, N. T.; Bard, A. J.; Mullins, C. B. *Nano letters* **2011**, *12*, 26-32.

(32)   Feilizadeh, M.; Vossoughi, M.; Zakeri, S. M. E.; Rahimi, M. *Industrial & Engineering Chemistry Research* **2014**, *53*, 9578-9586.

(33)   Hoang, S.; Berglund, S. P.; Hahn, N. T.; Bard, A. J.; Mullins, C. B. *Journal of the American Chemical Society* **2012**, *134*, 3659-3662.

(34)   Zuo, F.; Bozhilov, K.; Dillon, R. J.; Wang, L.; Smith, P.; Zhao, X.; Bardeen, C.; Feng, P. *Angewandte Chemie* **2012**, *124*, 6327-6330.

(35)   Zuo, F.; Wang, L.; Wu, T.; Zhang, Z.; Borchardt, D.; Feng, P. *Journal of the American Chemical Society* **2010**, *132*, 11856-11857.

(36)   Chen, X.; Liu, L.; Peter, Y. Y.; Mao, S. S. *Science* **2011**, *331*, 746-750.

(37)   Wang, G.; Wang, H.; Ling, Y.; Tang, Y.; Yang, X.; Fitzmorris, R. C.; Wang, C.; Zhang, J. Z.; Li, Y. *Nano letters* **2011**, *11*, 3026-3033.

(38)   Chang, X.; Thind, S. S.; Chen, A. *ACS Catalysis* **2014**, *4*, 2616-2622.

(39)   Tian, M.; Thind, S. S.; Chen, S.; Matyasovzsky, N.; Chen, A. *Electrochemistry Communications* **2011**, *13*, 1186-1189.

(40)   Gong, J.; Lai, Y.; Lin, C. *Electrochimica Acta* **2010**, *55*, 4776-4782.

(41)   Ye, M.; Xin, X.; Lin, C.; Lin, Z. *Nano letters* **2011**, *11*, 3214-3220.

(42)   Munoz, A. *Electrochimica acta* **2007**, *52*, 4167-4176.

(43)   Gimenez, S.; Dunn, H. K.; Rodenas, P.; Fabregat-Santiago, F.; Miralles, S. G.; Barea, E.
        M.; Trevisan, R.; Guerrero, A.; Bisquert, J. *Journal of Electroanalytical Chemistry* **2012**,
        668, 119-125.

Chapter 7: Highly Active Nanoporous TiO$_2$ Supported Pt-Pb Bifunctional Electrode for Solar-assisted Direct Methanol Fuel Cell

7.1 Introduction

Fuel cells are the electrochemical energy conversion devices that convert the chemical energy stored in reactants into electrical energy.[1] In recent years fuel cells have been extensively researched as they exhibit high system efficiencies, low emissions, and fuel flexibility. They also display rapid electrode kinetics as they may be operated under high temperatures.[2-4] The other most prominent feature of fuel cells is that they can operate using a variety of available fuels, such as natural gas, coal gas, various liquid fuels, etc.[5-7] Although hydrogen is considered to be the best chemical energy carrier, its handling at higher temperatures and its transportation are quite treacherous.[8] Liquid fuels are considered as a promising alternative to hydrogen for portable applications, as they possess high volumetric energy density. There are several different types of liquids that are currently being used as fuels in these fuel cells, with the prominent ones being ethanol, methanol, formic acid, glucose, etc.[9-12]

Methanol is considered as the best fuel for applications that require electrical power below 5 kW, has an energy density that is four times higher than that of hydrogen, and is very easy to handle. In general, methanol gets adsorbed on the surface of the electrode and subsequently gets oxidized. As methanol adsorption takes time, the methanol oxidation is a slow reaction and thus requires multiple active reaction sites.[13-15]

A typical fuel cell consists of three components: anode, cathode, and electrolyte. Various types of electrolytes may be employed in fuel cells depending on the required conditions. For very high temperature the electrolytes may be molten phosphoric acid, molten alkaline carbonate,

conducting ceramic oxide, etc.[16-18] The most important factor which determines the efficiency and usability of a particular fuel cell is the material that is used to make the anode. Therefore, the development of anode materials has taken center stage in the evolution of fuel cells. To date, platinum is considered as the optimal and the most effective electrocatalyst for the oxidation of methanol and formic acid in fuel cells.[19] Despite possessing high activity, Pt still lacks efficient utilization in fuel cells due to multiple drawbacks such as high cost, and short-life durability.

New composite materials are being investigated to increase the activity of Pt under lower potentials, and to make it more durable in the presence of poisonous species. The best method for enhancing the electrocatalytic activity of platinum is to combine it with other active metals to form bimetallic or ternary metal electrocatalysts.[20] Using this approach, the cost of making electrodes may be reduced, as the required quantity of Pt is decreased, and alternative less expensive metals are being added.

Very high activity toward methanol oxidation via PtRu electrodes had been reported by various research groups.[21] Antolini et al. studied the methanol oxidation reaction on platinum alloys using the first row of transition metals.[22-23] It was noted that an increase in methanol oxidation was observed when the Pt was diluted with high quantities of Co and Ni, as they are excellent methanol tolerant catalysts.[24] Ternary PtRuIr catalysts, which were supported on nanotubes were fabricated by Shijun Liao and co-workers with high activity in the oxidation of methanol.[25] A Pt-Pd composite is another combination that is under intensive study by various research groups. However, the high cost of platinum, ruthenium, iridium, and palladium, limits their practical application. In contrast, lead nitrate is inexpensive and could be employed to fabricate Pt-Pb nanocomposites.[26-28]

For the methanol oxidation reaction (MOR), the surface of the electrode material plays a very important role, since with a higher surface area additional active sites are available; hence, a larger volume of methanol may be adsorbed.[29] TiO_2 is one of the most extensively studied semiconductors in materials science. It possess many outstanding properties such as chemical inertness, high efficiency, non-toxicity, environmentally friendly, and low cost. It is the best photocatalyst available in current research, and can also be fabricated with myriad morphologies with various dimensions.[30-32]

Tubular TiO_2 nanostructures grown on a titanium substrate is a promising electrode candidate for electrochemical applications, as they may be easily operated and possess very high surface areas. However, TiO_2 suffers from a major drawback in that it has a large band gap (~3.2 eV), such that it may only be excited upon exposure to UV light. Moreover, as a semiconductor, TiO_2 does not possess good conductivity which prohibits its use as an electrocatalyst.[33-34] Recently researchers have developed various reduction approaches to narrow the band gap and increase the charge transfer of TiO_2 materials. One of the most facile approaches is electrochemical reduction, where the TiO_2 electrode is electrochemically reduced by applying either a negative current or potential. These electrochemically reduced TiO_2 electrodes exhibit a thousand times higher electron donor density in contrast to untreated TiO_2.[35-37] In consideration of this fact, metal catalyst-modified reduced TiO_2 appears to be a promising synthetic electrode material that could simultaneously offer enhanced electronic conductivity and photoelectrocatalytic activity. To the best of our knowledge, very few attempts have been reported regarding investigation of such reduced TiO_2 supported metal catalyst bifunctional electrodes for photo-assisted MOR.

In this study, Pt and Pb nanocomposite materials were deposited on one side of an electrochemically reduced nanoporous TiO_2 electrode for methanol oxidation. Nanoporous TiO_2

electrodes were fabricated via an anodization method, which were then reduced by applying a -5 mA cm^{-2} current density for 10 min. The Pt and Pb nanocomposites were deposited onto the reduced TiO$_2$ through photodeposition. The oxidation of methanol on these electrodes was studied under different experimental conditions. It was concluded that when the PtPb/EC-TiO$_2$ electrode was employed for methanol oxidation under photoelectrochemical conditions (where both solar irradiation and potential bias is applied on the electrode); higher activity was observed as compared to an untreated electrode, or the treated electrode under electrochemical conditions only. The solar light photo-assisted electrochemical oxidation of methanol might facilitate the development of high efficiency DMFC.

7.2 Experimental

7.2.1 Materials

Titanium plates (99.2%) and CH$_3$OH and were purchased from Caledon Laboratories Ltd. Canada and Alfa Aesar, respectively. The remaining chemicals were reagent grade products and were used as received from Sigma Aldrich. The water (18.2 MΩ cm) that was utilized in all experimental solutions was purified by a Nanopure Diamond water system.

7.2.2 Fabrication and treatment of nanoporous TiO$_2$

The fabrication of highly ordered nanoporous TiO$_2$ is already discussed in section 3.2.3.2 of chapter 3. The nanoporous TiO$_2$ was then reduced in 0.1 M H$_2$SO$_4$ at cathodic current density of 5 mA cm^{-2} for 10 min.

For the photochemical deposition of Pt and Pb, 20 microliters from an equimolar solution of 0.1 M Pb(NO$_3$)$_2$ and 0.1 M H$_2$PtCl$_6$ • 6H$_2$O was taken and added into a 5 mL, 50% methanol solution (v/v) with a nanoporous TiO$_2$ electrode suspended within it. This solution was degassed

with continuous flow of argon and then capped and irradiated under UV light for 1 h. For comparison, a Pt deposited TiO_2 electrode was fabricated with 40 microliter 0.1 M $H_2PtCl_6 \cdot 6H_2O$ under identical conditions.

7.2.3 Characterization of the Synthesized Materials.

The synthesized nanoporous TiO_2 were characterized by FE-SEM (Hitachi SU 70) energy dispersive spectroscopy (EDS) to obtain the morphology and composition of the prepared electrodes. To study the crystal structure, XRD (Philips, Model PW 1050-3710 diffractometer with Cu Kα radiation) analysis was used. For electrochemical characterization, a three-electrode cell system was employed where a Pt coil with a 10 cm^2 surface area was utilized as the auxiliary electrode, and an Ag/AgCl electrode was employed as the reference electrode. All of the electrochemical tests were measured with a Voltalab 40 Potentiostat (PGZ301). Mott–Schottky plots were conducted at a fixed frequency (500 Hz). The amplitude of modulation potential for the electrochemical impedance measurements was 10 mV. Nyquist plots were recorded at an electrode potential of 500 mV vs Ag/AgCl.

7.3 Results and Discussion

7.3.1 Characterization of PtPb/EC-TiO₂ and Pt/EC-TiO₂

A bifunctional electrode, as the name suggests, is an electrode that possesses dual functionalities. Recently, researchers have developed bifunctional electrodes where one side of the electrode behaved as an electrocatalyst and the other side as a photocatalyst. Figure 7.1 represents a basic model of the bifunctional electrode that was used in this research work. Nanoporous TiO_2 structures were grown onto the Ti substrate, where one side was used for the deposition of either Pt or Pt-Pb nanoparticles. The metal deposited side served as an electrocatalyst and was activated

by an applied potential, whereas the opposite side acted as a photocatalyst and was activated by an applied irradiation. It has been shown in the literature that due to synergistic effects this type of bifunctional system typically exhibits improved performance over electrocatalysts or photocatalysts that are operated separately.
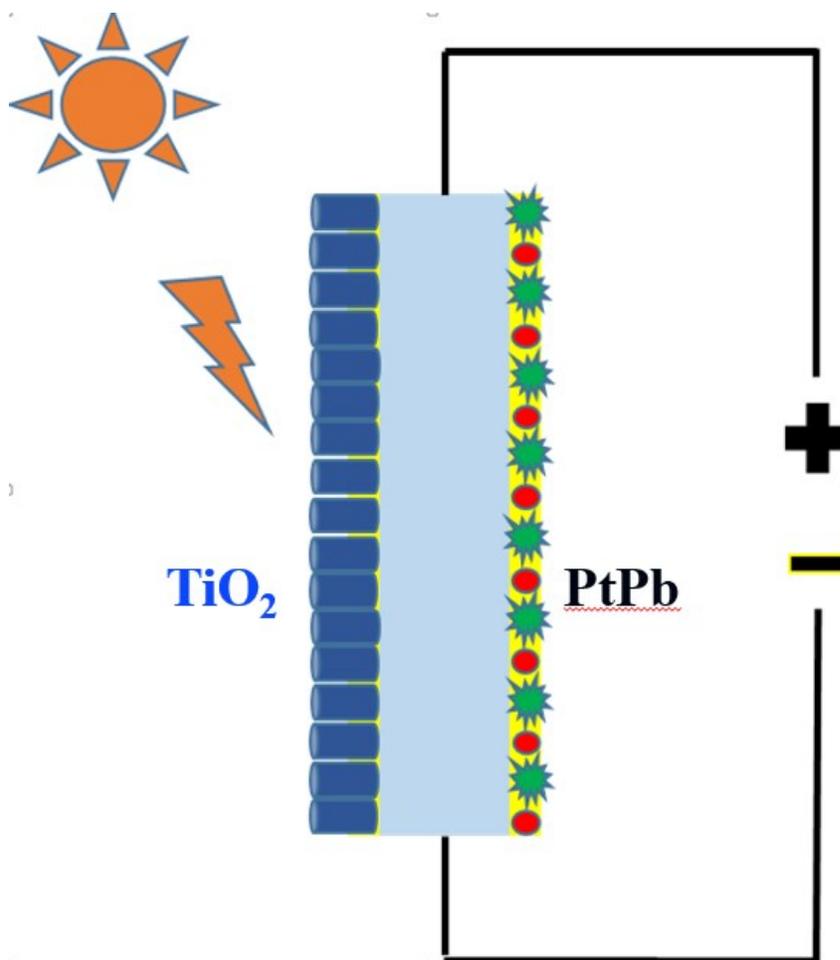

Figure 7.1 Schematic diagram of PtPb/EC-TiO$_2$ bifunctional electrode.

Morphology plays a critical role in the determination of the photocatalytic activity of materials. The more extensive the surface area, the higher the population of photocatalytically active sites that are available where reactions may take place; hence, conveying a higher overall activity of the electrode material. Nanoporous TiO_2 electrodes possess a high surface area as they have variously elongated tube-like grooves present within them. To investigate the morphology of the prepared nanoporous TiO_2 electrode prior to and following the deposition of metal nanoparticles, SEM was utilized, with the respective images presented in Figure 7.2. It can be concluded that very uniform and highly ordered nanoporous structures may be obtained by the anodization fabrication method (Figure 7.2A). With the assistance of high magnification SEM images, the diameters of the fabricated TiO_2 nanoporous were estimated to be ~150 nm (Figure 7.2B). It may also be observed that every pore on the Ti substrate contains several smaller nanopores. This type of morphology provides a very high electrode surface area. Figure 7.2C&D and Figure 7.2E&F present the SEM images of the Pt/EC-TiO_2 and PtPb/EC-TiO_2 electrodes respectively. Figure 7.2C shows that the photodeposition of Pt on the surface of the nanoporous TiO_2 is very effective as uniform deposition may be observed, with no large aggregated clusters of Pt anywhere on the substrate. High magnification images showed very fine and small particulates present at the lumen openings of the nanopores. Similar results were obtained from the SEM images of the PtPb/EC-TiO_2 electrode. The only difference was that with the addition of Pb larger particulates were formed on the substrate. The Pt and Pb composite nanoparticles were also very uniformly deposited over the surface of the electrode.
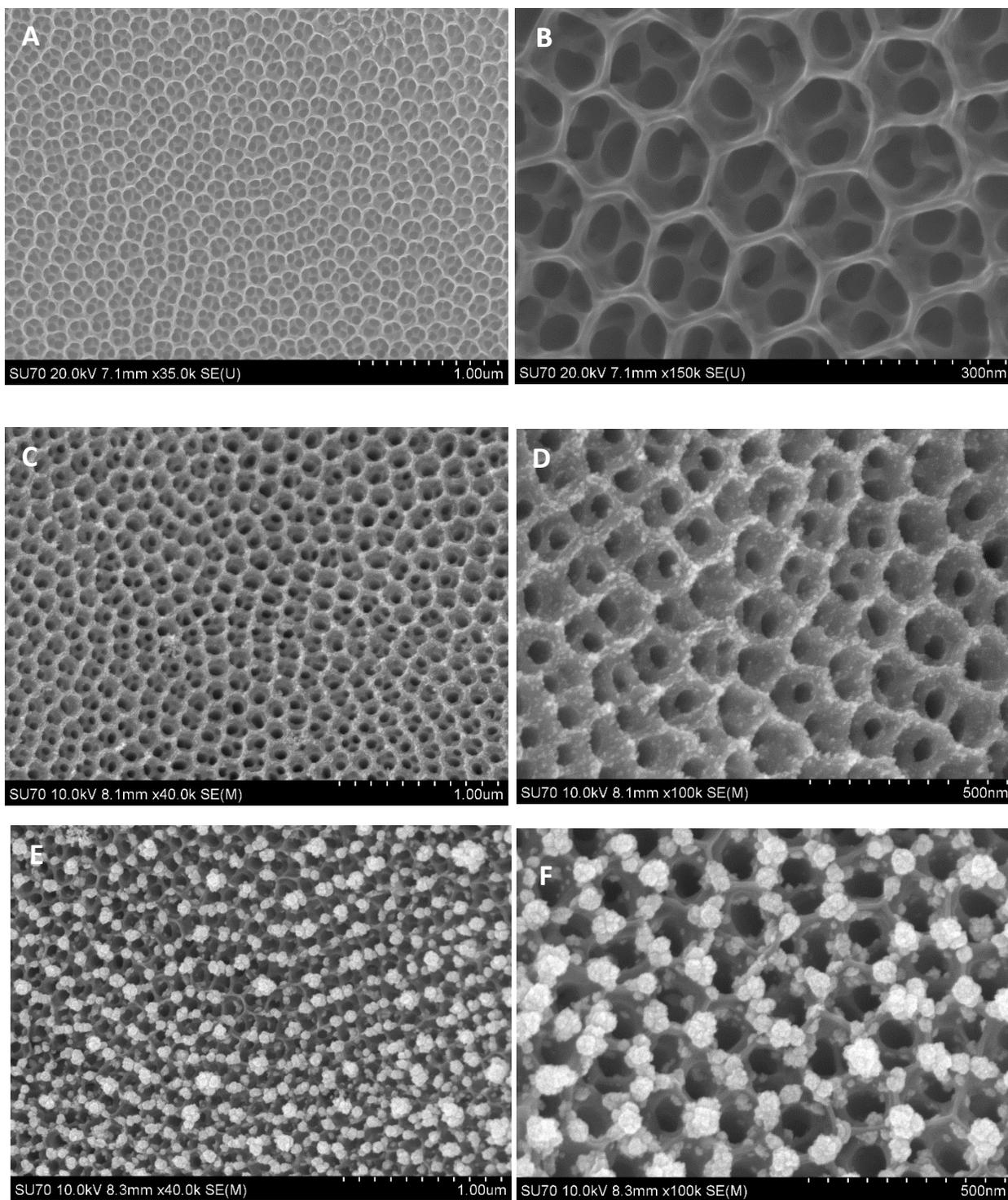
Figure 7.2 SEM images of fabricated (A) (B) nanoporous TiO_2, (C) (D) Pt/EC-TiO_2 electrode and (E) (F) PtPb/EC-TiO_2.
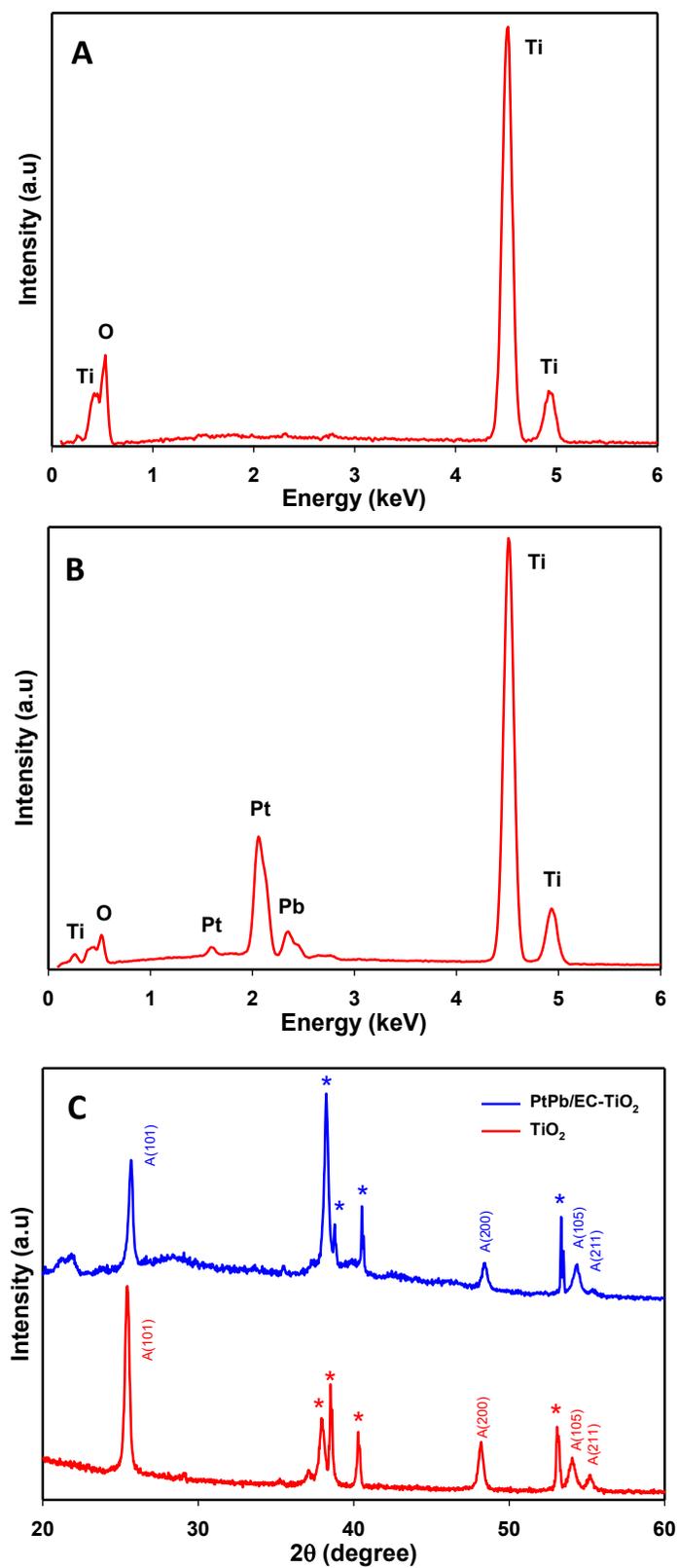
Figure 7.3 EDS spectra of the formed (A) nanoporous TiO_2 and (B) PtPb/EC-TiO_2, and (C) XRD spectra of nanoporous TiO_2 and PtPb/EC-TiO_2.

Figure 7.3 presents the EDS data obtained from the electrodes during the SEM to confirm the composition of the electrodes and to calculate the deposition ratio of the PtPb/EC-TiO₂ electrodes. Strong oxygen and titanium peaks were observed in Figure 7.3A for the TiO_2 sample, with a peak ratio of 2:1 respectively, which confirmed the formation of the nanoporous TiO_2. The EDS spectra of the PtPb/EC-TiO₂ electrode (Figure 7.3B) confirmed the presence of Pt, Pb on the nanoporous TiO_2 surface. Additionally, the Pt:Pb ratio was confirmed as 65:35. XRD data was collected and used to determine the crystal structure of the prepared electrodes, with the results shown in Figure 7.3C. The blue curve, which is the XRD pattern observed for the TiO_2 structure, shows that the TiO_2 is present in its most highly active tetragonal anatase phase. The peaks marked with asterisks are derived from the Ti substrate. The XRD pattern of the PtPb/EC-TiO₂ electrode was not very different than pure TiO_2, and there was no clear peak that could be assigned to Pt or Pb. This was likely because the quantity of the deposited Pt and Pb was very small, and cannot be detected by XRD.

The donor density of the electrode material plays a very important role in the determination of its electronic conductivity. Mott–Schottky measurements were carried out in a 0.1 M H_2SO_4 solution to analyze the donor density of the metal deposited TiO_2 electrodes, with and without the EC treatment. The effect of the solar light irradiation was also evaluated. The Mott–Schottky plot may be employed to estimate the donor density (ND):

$$\frac{1}{C^2} = \frac{2}{\varepsilon\varepsilon_0 e N_D}(E - E_{fb} - \frac{kT}{e})$$

where

C = capacitance of the space charge layer [F·m^{-2}]

ε = average value of the semiconductor dielectric constant (~120 for TiO_2)

ε_0 = permittivity of the free space charge (8.854×10^{-12} F·m^{-1})

e = absolute value of the electron charge (1.602×10^{-19} C).
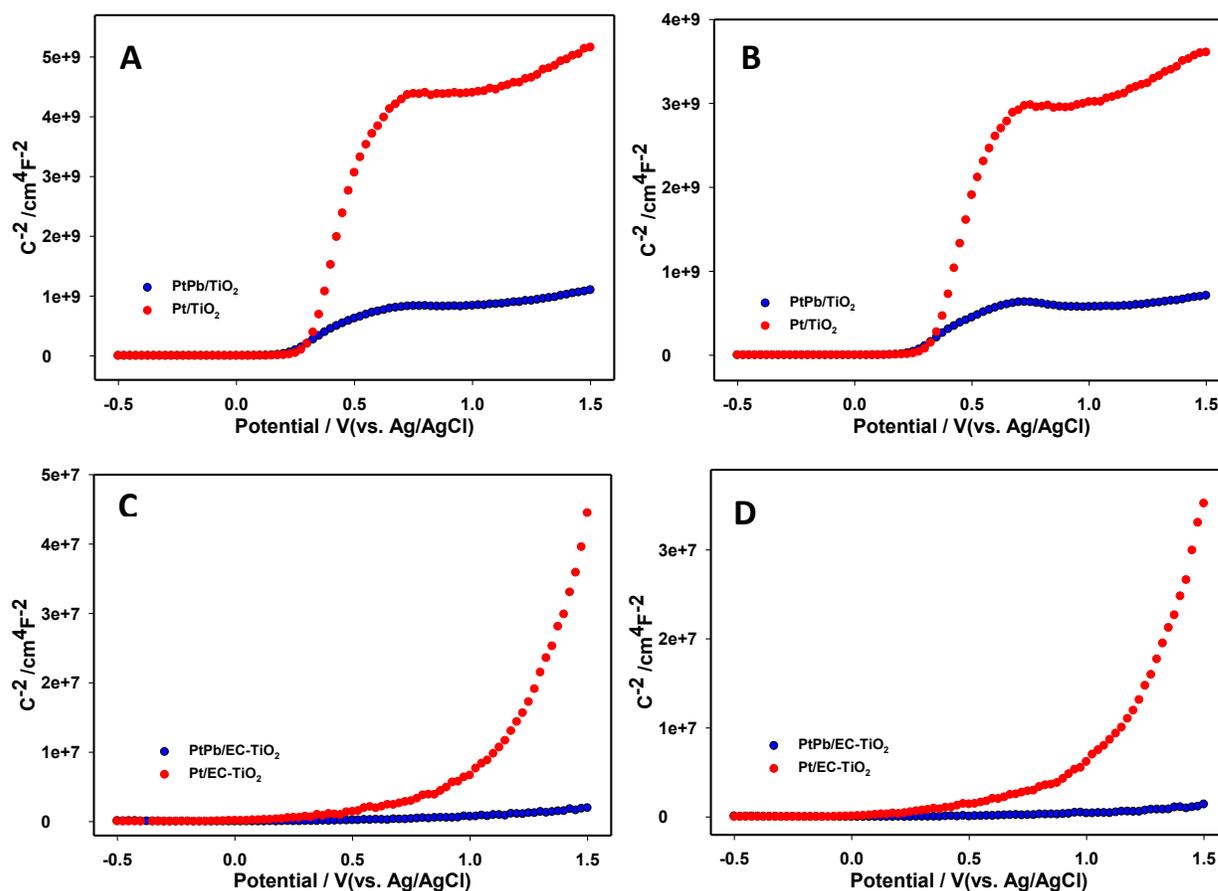
Figure 7.4 Mott-Schottky plots of PtPb/TiO$_2$ and Pt/TiO$_2$ electrodes obtained (A) in dark and (B) under solar light irradiation, Pt/EC-TiO$_2$ and PtPb/EC-TiO$_2$ electrodes obtained (C) in dark and (D) under solar light irradiation in 0.1 M H$_2$SO$_4$ at 500 Hz.

Table 7.1 The donor density data calculated from Figure 7.4.

Electrodes	Donor Density	
	Dark	Solar
PtPb/TiO$_2$	6.56e+18	7.80e+18
Pt/TiO$_2$	8.85e+17	1.25e+18
PtPb/EC-TiO$_2$	1.54e+22	3.16e+22
Pt/EC-TiO$_2$	2.48e+21	2.92e+21

Figure 7.4 shows the Mott–Schottky plots for the PtPb/TiO$_2$, Pt/TiO$_2$, PtPb/EC-TiO$_2$, and Pt/EC-TiO$_2$ electrodes measured with and without solar irradiation. The calculated donor density values are presented in Table 7.1. It may be observed that the PtPb/TiO$_2$ electrode had more than a seven times higher donor density value than that of Pt/TiO$_2$ in the dark. It was interesting to note that when the same measurements were run on the same electrodes with the solar irradiation on the uncovered TiO$_2$ side, an increase in the donor density value was observed. This confirmed the effectiveness of the bifunctional system. It is well known that the electrochemical reduction of TiO$_2$ electrodes results in a dramatic enhancement of electrocatalytic activity. This may also be seen in this case, as following the deposition of same quantity of metal on the EC reduced nanoporous TiO$_2$, both the Pt/EC-TiO$_2$ and PtPb/EC-TiO$_2$ showed more than a 2,000 times increase in the donor density values in the dark. When these EC treated electrodes were operated under solar irradiation, a further increase in the donor density was observed, which showed that these fabricated nanomaterials may be employed and utilized under solar light for various fuel cell applications.

The electrochemical behavior of the prepared samples was further investigated by electrochemical impedance measurements. All of the impedance measurements were performed in 0.1 M H$_2$SO$_4$ at a potential of 500 mV vs Ag/AgCl. All of the results are presented in the Figure 7.5 where the dotted lines represent the experimental data obtained from the measurements, and the solid lines represent the corresponding fitted data, which was acquired by using the circuit presented in the inset of Figure 7.5. Real and imaginary components of the impedance are represented by Z' and Z", respectively. In the circuit, Rs represents the uncompensated solution resistance, Rp denotes the charge transfer resistance, and CPE (defined as CPE-T and CPE-P), represents the constant phase element. All of the values from the Nyquist plots are shown in Table

7.2. The PtPb/EC-TiO$_2$ electrode showed a three times lower charge transfer resistance than that of the Pt/EC-TiO$_2$ electrode in the dark. When these electrodes were exposed to solar light a further decrease in the charge transfer resistance was observed.
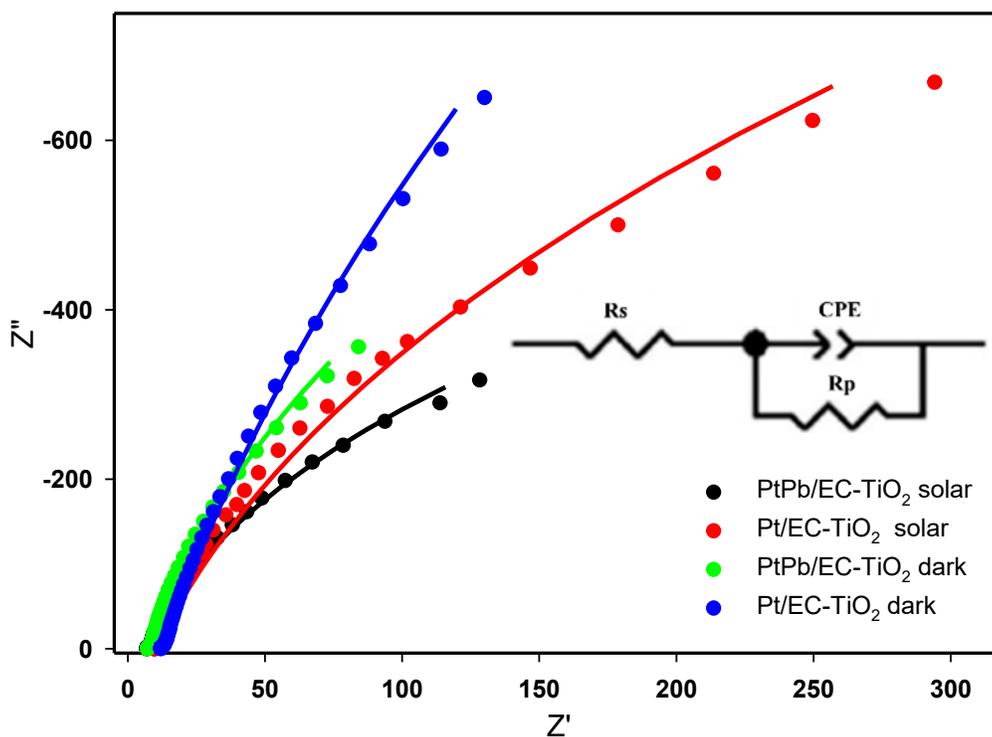
Figure 7.5 Nyquist plots of Pt/EC-TiO$_2$ and PtPb/EC-TiO$_2$ electrodes measured in dark and under solar light irradiation in 0.1 M H$_2$SO$_4$ at a potential of 500 mV. The frequency was altered, from 40 kHz to 100 mHz. The amplitude of modulation potential was 10 mV. The inset is the equivalent circuit, which was used to fit the raw data.

Table 7.2 EIS data obtained from Nyquist plots of Figure 7.5.

Electrodes	Rs (Ω cm^2)		Rp (kΩ cm^2)		CPE-T (μF cm^{-2})		CPE-P	
	Value	Error (%)	Value	Error (%)	Value	Error (%)	Value	Error (%)
PtPb/EC-TiO$_2$ solar	**8.52**	**0.37**	**1470**	**7.34**	**4467.90**	**0.75**	**0.93**	**0.34**
PtPb/EC-TiO$_2$ dark	7.75	0.38	3721	18.39	4419.50	0.76	0.94	0.34
Pt/EC-TiO$_2$ solar	**8.32**	**0.33**	**3347**	**6.53**	**2439.10**	**0.65**	**0.91**	**0.27**
Pt/EC-TiO$_2$ dark	8.63	0.23	11242	17.95	2366.50	0.46	0.93	0.20
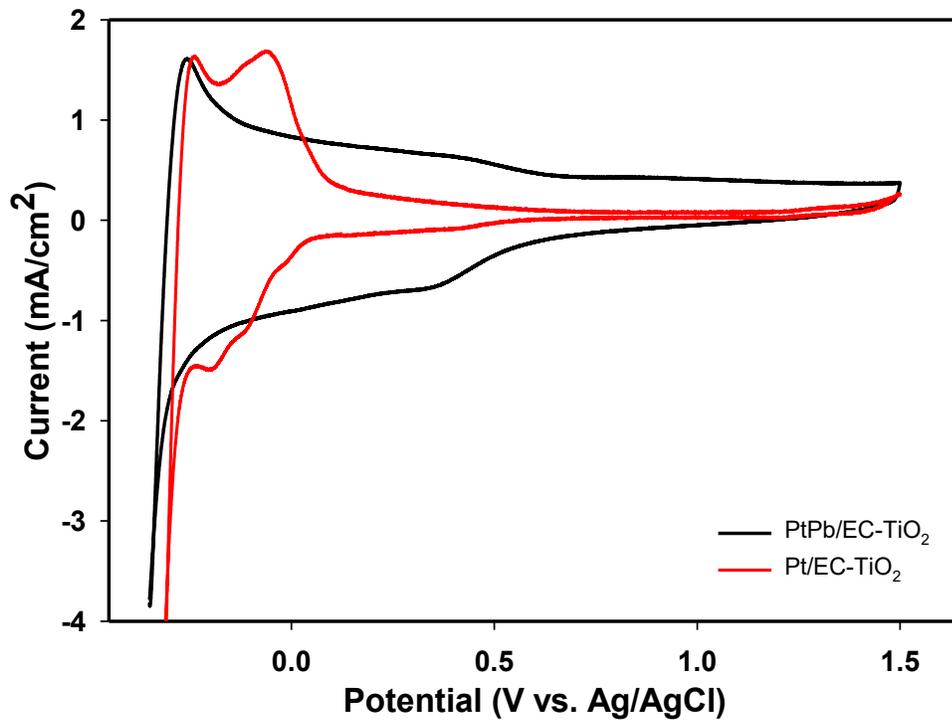
Figure 7.6 CVs of Pt/EC-TiO$_2$ and PtPb/EC-TiO$_2$ electrodes in 0.1 M H$_2$SO$_4$ at a scan rate of 20 mV s^{-1}.
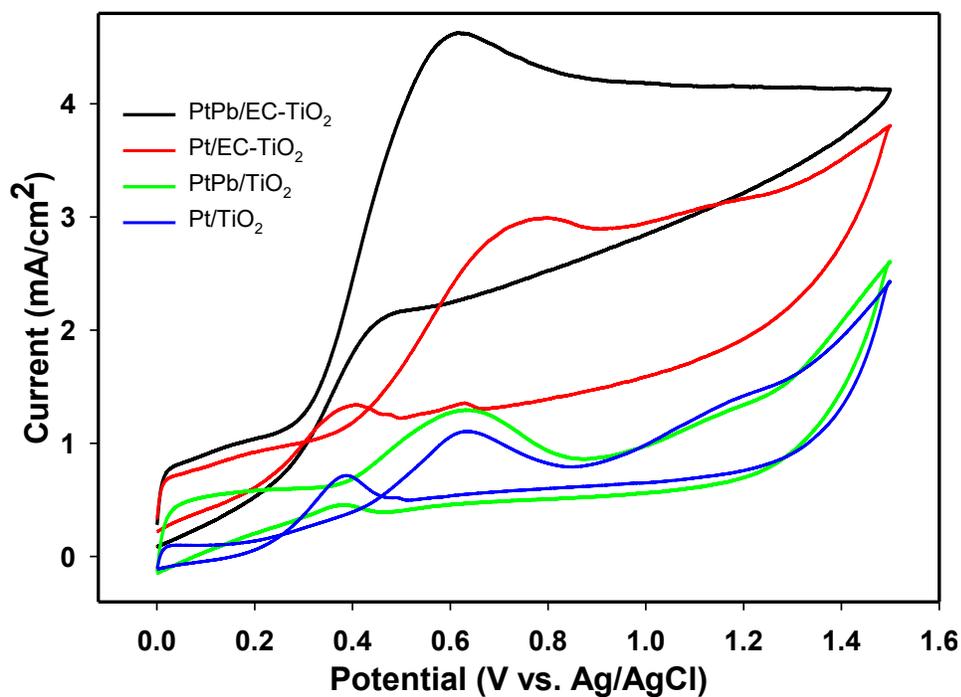
Figure 7.7 CVs of PtPb/EC-TiO$_2$, Pt/EC-TiO$_2$, PtPb/TiO$_2$, and Pt/TiO$_2$ electrodes under solar light irradiation in 0.1 M CH$_3$OH + 0.1 M H$_2$SO$_4$ at a scan rate of 20 mV s^{-1}.

7.3.2 Photoelectrocatalytic performance of PtPb/EC-TiO₂ for MOR

The photoelectrochemical characterization of the prepared electrodes was performed by cyclic voltammetry and chronoamperometry. Figure 7.6 depicts the CVs of the prepared PtPb/EC-TiO$_2$ and Pt/EC-TiO$_2$ electrodes in 0.1 M H$_2$SO$_4$ in the dark. It may be seen that the CVs of these two electrodes can be separated into two regions: (I) -0.35 V to 0.5 V, where hydrogen adsorption/desorption takes place, and (II) the double-layer charging, from 0.5 V to 1.5 V. The hydrogen adsorption/desorption peak was obtained due to the adsorption of the hydrogen on the TiO$_2$ nanopores, and primarily on the Pt nanoparticles. For Pt/EC-TiO$_2$, a very distinguished adsorption desorption peak for hydrogen was observed, as Pt was the main adsorbing material. With the addition of Pb, the PtPb/EC-TiO$_2$ electrode showed a broad peak in this region, which was due to the hindrance in hydrogen adsorption provided by the Pb molecules on the Pt surface. The PtPb/EC-TiO$_2$ electrode also showed a higher double layer, which revealed that this electrode was more conductive than the TiO$_2$-Pt electrode.

Figure 7.7 shows the CVs of methanol oxidation with various electrodes under solar irradiation. The solution was 0.1 M CH$_3$OH + 0.1 M H$_2$SO$_4$ and the scan rate was 20 mV/s. For the Pt/TiO$_2$ electrode a typical methanol oxidation curve was observed, which exhibited two typical peaks; one located at 0.64 V in the forward scan, and the other centered at 0.39 V in the reverse scan. For the PtPb/TiO$_2$ electrode, the methanol oxidation was very similar to that on the Pt/TiO$_2$ electrode with a slight increase in the current. When the methanol oxidation was performed on the electrodes that underwent the EC reduction under solar irradiation, a very significant increase in the current was observed. This increase in the activity may be attributed to the high conductivity of the TiO$_2$ electrode that resulted from the EC reduction. It can also be concluded that the PtPb/EC-TiO$_2$ electrode demonstrated much better activity than Pt/EC-TiO$_2$ electrode.
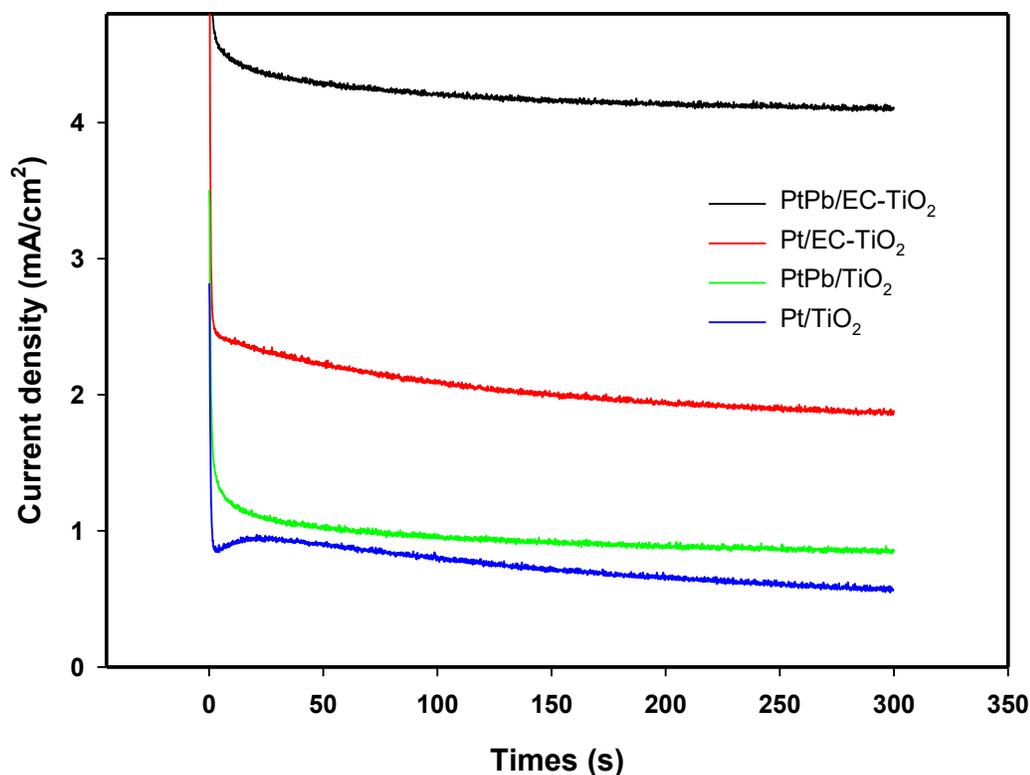
Figure 7.8 Chronopotentiometric curves of PtPb/EC-TiO$_2$, Pt/EC-TiO$_2$, PtPb/TiO$_2$, and Pt/TiO$_2$ electrodes with solar light irradiation in 0.1 M CH$_3$OH + 0.1 M NaOH at an applied potential of 500 mV.

To further characterize the samples, chronoamperommetry was carried out, with the results shown in the Figure 7.8. The current density was measured under solar light irradiation and a constant applied bias of 0.5 V in 0.1 M CH$_3$OH + 0.1 M H$_2$SO$_4$. For the Pt/TiO$_2$ electrode the current density after 200 sec was ca. 0.65 mA/cm^2, whereas for PtPb/TiO$_2$ electrode it was ca. 0.90 mA/cm^2. However, with the help of the EC reduction, the Pt/EC-TiO$_2$ and PtPb/EC-TiO$_2$ electrodes showed a 1.95 mA/cm^2 and 4.14 mA/cm^2 current density, respectively. These results are consistent with the CV measurements.

7.4 Conclusion

In this work a bifunctional strategy was employed for the oxidation of methanol under simultaneous applied potential and solar irradiation. For the electrode material, a highly organized nanoporous TiO_2 structure was successfully grown via an anodization technique. A very facile electrochemical method was used to reduce and enhance the activity of the nanoporous TiO_2 electrode. Pt and Pb metal nanoparticles were photochemically deposited on the TiO_2 substrate. SEM images revealed that Pt and Pb nanoparticles were very uniformly deposited over the nanoporous TiO_2 electrode, and no aggregated clusters of metal nanoparticles were found. Cyclic voltammetry and chronoamperommetry studies indicated that the $PtPb/EC-TiO_2$ electrode, under the irradiation of solar light and applied potential, showed much higher activity toward methanol oxidation. Under solar irradiation, the calculated electron donor density of the $PtPb/EC-TiO_2$ electrode was almost 11 times higher than that of the $Pt/EC-TiO_2$ electrode. The impedance studies also showed that the bifunctional $PtPb/EC-TiO_2$ electrode had the least charge transfer resistance, which makes it an efficient electrode for methanol fuel cell applications.

References

(1)   Qu, L.; Liu, Y.; Baek, J.-B.; Dai, L. *ACS nano* **2010**, *4*, 1321-1326.

(2)   Debe, M. K. *Nature* **2012**, *486*, 43-51.

(3)   Wang, Y.; Chen, K. S.; Mishler, J.; Cho, S. C.; Adroher, X. C. *Applied Energy* **2011**, *88*, 981-1007.

(4)   Suntivich, J.; Gasteiger, H. A.; Yabuuchi, N.; Nakanishi, H.; Goodenough, J. B.; Shao-Horn, Y. *Nature chemistry* **2011**, *3*, 546-550.

(5)   Peighambardoust, S. J.; Rowshanzamir, S.; Amjadi, M. *International Journal of Hydrogen Energy* **2010**, *35*, 9349-9384.

(6)   Merle, G.; Wessling, M.; Nijmeijer, K. *Journal of Membrane Science* **2011**, *377*, 1-35.

(7)   Wang, Y.-J.; Zhao, N.; Fang, B.; Li, H.; Bi, X. T.; Wang, H. *Chemical reviews* **2015**, *115*, 3433-3467.

(8)   Zou, X.; Zhang, Y. *Chemical Society Reviews* **2015**, *44*, 5148-5180.

(9)   Shen, S.; Zhao, T.; Xu, J.; Li, Y. *Journal of Power Sources* **2010**, *195*, 1001-1006.

(10)   Kakati, N.; Maiti, J.; Lee, S. H.; Jee, S. H.; Viswanathan, B.; Yoon, Y. S. *Chemical reviews* **2014**, *114*, 12397-12429.

(11)   Matos, J.; Borodzinski, A.; Zychora, A. M.; Kedzierzawski, P.; Mierzwa, B.; Juchniewicz, K.; Mazurkiewicz, M.; Hernández-Garrido, J. C. *Applied Catalysis B: Environmental* **2015**, *163*, 167-178.

(12)   Ci, S.; Wen, Z.; Mao, S.; Hou, Y.; Cui, S.; He, Z.; Chen, J. *Chemical Communications* **2015**, *51*, 9354-9357.

(13)   Zhang, J.; Liu, H. *Electrocatalysis of direct methanol fuel cells: from fundamentals to applications*; John Wiley & Sons, 2009.

(14)   Koenigsmann, C.; Wong, S. S. *Energy & Environmental Science* **2011**, *4*, 1161-1176.

(15)   Liu, H.; Song, C.; Zhang, L.; Zhang, J.; Wang, H.; Wilkinson, D. P. *Journal of Power Sources* **2006**, *155*, 95-110.

(16)   Li, J.; Wu, N. *Catalysis Science & Technology* **2015**, *5*, 1360-1384.

(17)   Pinar, F. J.; Cañizares, P.; Rodrigo, M. A.; Úbeda, D.; Lobato, J. *Journal of Power Sources* **2015**, *274*, 177-185.

(18)   Zeis, R. *Beilstein journal of nanotechnology* **2015**, *6*, 68-83.

(19)   Li, L.; Hu, L.; Li, J.; Wei, Z. *Nano Research* **2015**, *8*, 418-440.

(20)   Patel, P. P.; Datta, M. K.; Jampani, P. H.; Hong, D.; Poston, J. A.; Manivannan, A.; Kumta, P. N. *Journal of Power Sources* **2015**, *293*, 437-446.

(21)   Feng, L.; Li, K.; Chang, J.; Liu, C.; Xing, W. *Nano Energy* **2015**, *15*, 462-469.

(22)   Antolini, E. *Journal of Power Sources* **2007**, *170*, 1-12.

(23)   Antolini, E.; Salgado, J. R.; Gonzalez, E. R. *Journal of Power Sources* **2006**, *160*, 957-968.

(24)   Su, F.; Poh, C. K.; Zeng, J.; Zhong, Z.; Liu, Z.; Lin, J. *Journal of Power Sources* **2012**, *205*, 136-144.

(25)   Liao, S.; Holmes, K.-A.; Tsaprailis, H.; Birss, V. I. *Journal of the American Chemical Society* **2006**, *128*, 3504-3505.

(26)   Gunji, T.; Tanabe, T.; Jeevagan, A. J.; Usui, S.; Tsuda, T.; Kaneko, S.; Saravanan, G.; Abe, H.; Matsumoto, F. *Journal of Power Sources* **2015**, *273*, 990-998.

(27)   Huang, Y.; Cai, J.; Guo, Y. *international journal of hydrogen energy* **2012**, *37*, 1263-1271.

(28)   Huang, Y.; Zheng, S.; Lin, X.; Su, L.; Guo, Y. *Electrochimica Acta* **2012**, *63*, 346-353.

(29)   Zhao, X.; Yin, M.; Ma, L.; Liang, L.; Liu, C.; Liao, J.; Lu, T.; Xing, W. *Energy & Environmental Science* **2011**, *4*, 2736-2753.

(30)   Chen, X.; Mao, S. S. *Chem. Rev* **2007**, *107*, 2891-2959.

(31)   Chen, X.; Liu, L.; Huang, F. *Chemical Society Reviews* **2015**, *44*, 1861-1885.

(32)   Roy, P.; Berger, S.; Schmuki, P. *Angewandte Chemie International Edition* **2011**, *50*, 2904-2939.

(33)   Chang, X.; Thind, S. S.; Chen, A. *ACS Catalysis* **2014**, *4*, 2616-2622.

(34)   Tiido, K.; Alexeyeva, N.; Couillard, M.; Bock, C.; MacDougall, B. R.; Tammeveski, K. *Electrochimica Acta* **2013**, *107*, 509-517.

(35)   Chen, X.; Liu, L.; Peter, Y. Y.; Mao, S. S. *Science* **2011**, *331*, 746-750.

(36)   Chang, X.; Thind, S. S.; Tian, M.; Hossain, M. M.; Chen, A. *Electrochimica Acta* **2015**, *173*, 728-735.

(37)   Xu, C.; Song, Y.; Lu, L.; Cheng, C.; Liu, D.; Fang, X.; Chen, X.; Zhu, X.; Li, D. *Nanoscale research letters* **2013**, *8*, 1.

Chapter 8: Concluding remarks and future work

8.1 Conclusions

As environmental contamination is posing an ever larger threat to ecosystems, new catalysts are urgently required to promote potential technologies for environmental remediation applications. This thesis is dedicated to the development of new, economical and efficient nanostructured TiO_2 based materials for utilization in catalytic processes. The cost effectiveness of a process plays a critical role in the assessment of whether it will be scalable or not. TiO_2 is an inexpensive material that has demonstrated strong potential to play a central role in newly emerging technologies. In this work a very simple anodization method was employed in the fabrication of nanostructured TiO_2 materials. This method is very straightforward, easy to control and does not require expensive materials or instrumentation. A very facile EC reduction method was also developed in this work, which likely provided the most cost effective method for increasing the photo and electrocatalytic activity of the TiO_2 based nanomaterials. Brief summaries and key conclusions of the work presented are as follows.

8.1.1 TiO_2 nanotubes as an electrocatalyst

TiO_2 nanotubes were successfully grown on Ti plates utilizing anodization oxidation in a two-electrode cell with DMSO and 2% HF as an electrolyte under an applied potential of 40 V for 7 hours. The prepared TiO_2 nanotubes were annealed at 450 ^{o}C to obtain the anatase phase, which is the most catalytically active phase of TiO_2. The SEM of the fabricated electrodes revealed that the TiO_2 nanotubes had very uniform growth throughout the Ti substrate and had a pore diameter of ca. 100 nm at the top of the layer. As TiO_2 is a semiconductor oxide, it has very low conductivity when a bias is applied through it.

To increase the electrocatalytic activity of the TiO_2 nanotubes, a very facile and efficient EC reduction method was developed in this research work. In this EC reduction method, TiO_2 nanotubes were treated in 0.1 M H_2SO_4 under different cathodic current densities. In order to elucidate the optimal EC reduction conditions, the effects of applied current and time on the electrochemical activity of the TiO_2 nanotubes were examined with different applied current densities, spanning -2.5, -5, -7.5, and -10 mA cm^{-2} over different timelines, respectively. It was concluded that the EC treatment under -5.0 mA cm^{-2} resulted in the highest steady-state current.

The XPS results revealed that three different peaks centered at 459.11, 457.90, and 456.81 eV were observed for Ti, which corresponded to Ti^{4+}, Ti^{3+}, and Ti^{2+}, respectively. It was observed that the quantity of Ti^{4+} decreased following the EC reduction, whereby the Ti^{3+} and Ti^{2+} were increased. This indicated that during the EC reduction process, some portion of the Ti^{4+} underwent conversion to Ti^{3+} and Ti^{2+}. Additionally, an increase in oxygen vacancies was also observed, as the level of O(II) decreased from 86.39% to 78.97% after 10 min. of reduction. This increase in the oxygen vacancies also contributed to the increase of the electrochemical activity of the TiO_2 nanotubes.

Lignin, which is the second most abundant biopolymer on Earth, is an amorphous, aromatic polyphenolic macromolecule composed of phenyl propane units that are linked together by C-C and C-O bonds. In this work an effort was made to fabricate very efficient and economical electrodes for the oxidation of lignin. TiO_2 nanotubes were prepared by an anodization method, and the lengths of the fabricated TiO_2 nanotubes demonstrated a very significant effect on their electrocatalytic activity toward the oxidation of lignin.

Electrodes with different lengths of TiO_2 nanotubes grown onto them were fabricated by anodizing the titanium substrate over different time periods. These electrodes were then

electrochemically reduced by applying -5 mA cm^{-2} for 10 min. SEM analysis was employed to calculate the lengths of the grown TiO$_2$ nanotubes, and the results showed that nanotubes with lengths of ca. 4, 8, 10, 13, and 15 μm were correlated with 4, 8, 12, 16, and 20 H of anodization, respectively. This increase in nanotube lengths had a noticeable effect on the electrochemical properties of TiO$_2$, as with increases in the lengths of the nanotubes, a broader double layer charging and discharging figure was obtained through CV.

It was also concluded from electrochemical impedance studies that the electrode, which was fabricated under 16 h of anodization, resulted in the least charge transfer resistance in contrast to the electrodes that were prepared under 4, 8, 12, and 20 H. For the oxidation of the lignin, the 16 H electrode also exhibited the most rapid kinetics, and within three hours a very significant quantity of lignin was oxidized. The rate constant observed for the electrochemical oxidation of the lignin under 16 H of treatment was 11 times higher in comparison to the pure Pt electrode. This fabricated electrode demonstrated a very high rate of stability as various cycles of lignin oxidation were run on the same electrode without any decrease in activity. Hence, this electrochemical approach for lignin oxidation to various value-added products might facilitate the commercial scale fabrication of numerous organic compounds.

8.1.2 Nanoporous TiO$_2$ as photoelectrocatalyst

Highly ordered nanoporous TiO$_2$ were grown on a titanium substrate using a three-step anodization process in a one compartment two-electrode cell that contained ethylene glycol + 0.3 wt% NH$_4$F + 2 wt% H$_2$O, with a Ti plate as the anode, and a Pt coil as the cathode. Following the first and second anodization, the grown TiO$_2$ layers were peeled off and a fresh anodization was done to obtain a final TiO$_2$ layer. This layer consisted of very uniform nanoporous TiO$_2$, which had much higher photocatalytic activity in contrast to the TiO$_2$ nanotubes that were grown by a

one-step anodization method. It was concluded that subsequent to EC reduction the nanoporous TiO$_2$ possessed approximately 130 times more photocurrent as compared to the TiO$_2$ nanotubes. A very significant increase in the electron donor density of the nanoporous TiO$_2$ was observed following the EC reduction. The treated TiO$_2$ nanoporous material showed a six times more rapid photoelectrochemical degradation of Rh B. A significant increase in the solar and visible light catalytic activity of nanoporous TiO$_2$ was also observed following the EC reduction. These highly photoactive nanoporous electrodes showed strong potential for environmental and energy applications.

 Hydrogen is considered as a fuel of the future and is garnering most of the attention of the research community; however, methanol is an alternative that possesses an energy density, which is four times higher than that of hydrogen, and it is very easy to handle. The primary issue with methanol fuel cells is that methanol adsorption is sluggish, therefore making methanol oxidation a very slow reaction that requires multiple active sites. During my PhD study, a bifunctional approach was used for the oxidation of methanol where an applied bias and photon energy was simultaneously employed at the electrode.

Electrochemically reduced and very uniform nanoporous TiO$_2$ was used as a substrate to provide an extensive surface area for the deposition of metal nanoparticles. Platinum, which is the best available catalyst for the oxidation of methanol, was used in conjunction with lead nanoparticles. With the addition of Pb the quantity of Pt may be reduced, thus decreasing the cost of electrode fabrication, as Pt is a very expensive element. The addition of Pb also lowered the occurrence of Pt fouling. SEM images revealed that the Pt and Pb nanoparticles were very uniformly deposited over the TiO$_2$ nanoporous materials, and no clusters of metal nanoparticles were observed. It was revealed that a PtPb/EC-TiO$_2$ electrode under solar light irradiation and an

applied potential showed much higher activity toward the oxidation of methanol. Electron donor density calculations also verified that when solar irradiation is applied onto the PtPb/EC-TiO$_2$ electrode, it was ca. 11 times higher than that of Pt/EC-TiO$_2$ electrode. This indicated that the PtPb nanocomposite electrode had improved electronic properties in contrast to the solely Pt containing electrode. Impedance studies also showed that the bifunctional PtPb/EC-TiO$_2$ electrode had the least charge transfer resistance, which makes it an efficient electrode for methanol fuel cell applications.

8.2 Future Work

In this PhD research, I successfully developed a very facile and efficient EC reduction method to significantly enhance both the electrocatalytic and photocatalytic activities of TiO$_2$ nanomaterials. This approach is very simple and showed very promising future applications, thus I strongly believe that the research work accomplished for this thesis will contribute to the development of highly efficient nanomaterials in the future for use in various beneficial environmental applications.

The electrochemically treated TiO$_2$ nanotubes and nanoporous electrodes exhibited very high activity in this work toward the oxidation of SA, Rh B, methanol, and lignin. It is suggested that this high electrocatalytic activity of treated materials should be explored further for various applications such as DSSC, water splitting, electrochromic devices, etc.. Researchers have been exploring novel and efficient materials for dye sensitized solar cells. DSSC comprise a third generation photovoltaic (solar) cell that converts visible light into electrical energy, which may then be employed for the provision of energy in the support of various human activities. DSSC are gaining much needed attention, as they are also referred to as imbuing artificial photosynthesis in that they mimic the absorption of visible light energy by plants. In a general DSSC setup, solar

light is irradiated on the dye, which results in the excitation of electrons. These excited electrons are then injected into TiO_2, which conducts it away and the movement of these electrons creates the energy that is stored within a rechargeable battery, or other electronic devices.

As TiO_2 plays a very important role in DSSC, conductive TiO_2 nanomaterials are required to be efficiently utilized in this type of application. The electrochemically reduced TiO_2 prepared in this research work should be a good alternative, as it exhibits a much higher level of electron donor density and demonstrates very promising electrocatalytic properties. In the future, treated TiO_2 should be explored in DSSC applications.

Treated TiO_2 should also be explored for utilization in electrochromic devices, which comprise a type of electrochromic cell. Electrochromic devices consist primarily of two electrochromic layers that are separated by an electrolytic layer. An external voltage is applied to both conducting electrodes, which are used on the sides of both electrochromic layers. Treated TiO_2 has potential, and should be explored to be employed as the electrode material for electrochromic device applications.

In this thesis work, TiO_2 nanostructured materials with extensive surface areas served as substrates for the deposition of PtPb nanocomposites. Highly active reduced TiO_2 materials might be explored even more vigorously for the deposition of metal atoms or metal oxides on their surfaces. Highly active materials such as Au, Pd, IrO_2, Ni, RuO_2, Co etc. should be tested with various combinations to fabricate electrodes that could be used in fuel cell applications. Different fuels including methanol, formic acid, glucose, etc. might be employed for oxidation on these highly active TiO_2 based nanomaterials.

Hydrogen storage is also a very promising application where these highly active reduced TiO_2 materials may be employed. There are a number of studies in the literature where TiO_2 was

used as a substrate for the deposition of Pd based nanomaterials for hydrogen storage applications. It would be interesting to learn whether the employment of these electrochemically reduced TiO_2 electrodes might further increase hydrogen storage capacities.

Bifunctional electrodes are also garnering significant attention presently, where photocatalysts and electrocatalysts are applied together in a single system. Light irradiation is used to activate the photocatalysts, whereas an applied potential is employed to activate the electrocatalysts. In further studies, reduced TiO_2 based electrodes should be further explored for wastewater treatment and other applications. As reduced TiO_2 exhibits much higher photocatalytic and electrocatalytic activity, it will be the best suited for a bifunctional electrode system.

This EC reduction method might also be used on other oxide materials to evaluate changes in their activity toward the photochemical and electrochemical oxidation of pollutant molecules in natural water systems. WO_3 comprises an additional semiconductor oxide material that is being extensively utilized for various applications such as photocatalysis, DSSC, electrochemical devices, and in various sensing applications. WO_3 electrodes and nanomaterials should be electrochemically reduced to learn whether enhancements in activity might be similar to that observed for TiO_2.

Publications

Xin Chang, Sapanbir S. Thind, and Aicheng Chen. "Electrocatalytic enhancement of salicylic acid oxidation at electrochemically reduced TiO_2 nanotubes." *ACS Catalysis* 4 (2014): 2616-2622.

Xin Chang, Sapanbir S. Thind, Min Tian, Md. Motasser Hossain and Aicheng Chen. "Significant enhancement of the photoelectrochemical activity of nanoporous TiO_2 for environmental applications." *Electrochimica Acta* 173 (2015): 728-735.

Zhaoyang Zhang, **Xin Chang**, and Aicheng Chen. "Determination of chemical oxygen demand based on photoelectrocatalysis of nanoporous TiO_2 electrodes." *Sensors and Actuators B: Chemical* 223 (2016): 664-670.

Sapanbir S. Thind, **Xin Chang**, Jordan S. Wentzell, and Aicheng Chen. "High-performance supercapacitor based on tantalum iridium oxides supported on tungsten oxide nanoplatelets." *Electrochemistry Communications* 67 (2016): 1-5.

Guohong Xie, **Xin Chang**, Bal Ram Adhikari, Sapanbir S. Thind, and Aicheng Chen. "Photoelectrochemical degradation of acetaminophen and valacyclovir using nanoporous titanium dioxide." *Chinese Journal of Catalysis* 37 (2016): 1062-1069.